

<sup>1</sup>  
Impact of PØD $\nu_\mu$  and  $\bar{\nu}_\mu$  Samples in BANFF

<sup>2</sup>  
Hogan, Matthew<sup>1</sup> and Toki, Walter<sup>1</sup>

<sup>3</sup>  
June 18, 2019

<sup>4</sup>  
<sup>1</sup> *Colorado State University, Fort Collins, USA*

<sup>5</sup>  
**Abstract**

<sup>6</sup>  
This is the abstract

# 7 **Contents**

8	<b>1 Introduction</b>	<b>10</b>
9	1.1 ND280 . . . . .	10
10	1.1.1 The PØD . . . . .	11
11	1.2 Usage of ND280 Psyche Software . . . . .	12
12	<b>2 ND280 Binned Likelihood</b>	<b>14</b>
13	2.1 Motivation . . . . .	14
14	2.2 Introduction to Conditional PDFs and Likelihoods . . . . .	15
15	2.3 BANFF Fit Test Statistic . . . . .	16
16	2.3.1 Flux, Cross Section, and Detector Systematics . . . . .	20
17	<b>3 PØD Selections and Data Samples</b>	<b>24</b>
18	3.1 Global Reconstruction . . . . .	24
19	3.2 PØD Selection Cuts . . . . .	26
20	3.2.1 Pre-Selection Cuts . . . . .	26
21	3.2.2 $\nu_\mu$ CC Inclusive in FHC Cut . . . . .	29
22	3.2.3 $\bar{\nu}_\mu$ CC Inclusive in RHC Cuts . . . . .	29
23	3.2.4 $\nu_\mu$ Background CC Inclusive in RHC Cuts . . . . .	31
24	3.3 Sample Kinematics and Validation . . . . .	31
25	3.4 PØD Water-Out Samples . . . . .	32
26	3.4.1 CC Inclusive . . . . .	33
27	3.4.1.1 $\nu_\mu$ Selection in FHC Mode: . . . . .	33
28	3.4.1.2 $\bar{\nu}_\mu$ Selection in RHC Mode: . . . . .	40
29	3.4.1.3 $\nu_\mu$ Background Selection in RHC Mode: . . . . .	47
30	3.4.2 CC 1-Track (CCQE Enhanced) . . . . .	54

31	3.4.2.1	$\nu_\mu$ Selection in FHC Mode:	54
32	3.4.2.2	$\bar{\nu}_\mu$ Selection in RHC Mode:	61
33	3.4.2.3	$\nu_\mu$ Background Selection in RHC Mode:	68
34	3.4.3	CC N-Tracks (CCnQE Enhanced)	68
35	3.4.3.1	$\nu_\mu$ Selection in FHC Mode:	68
36	3.4.3.2	$\bar{\nu}_\mu$ Selection in RHC Mode:	75
37	3.4.3.3	$\nu_\mu$ Background Selection in RHC Mode:	82
38	3.5	PØD Water-In Samples	82
39	3.5.1	CC Inclusive	83
40	3.5.1.1	$\nu_\mu$ Selection in FHC Mode:	83
41	3.5.1.2	$\bar{\nu}_\mu$ Selection in RHC Mode:	90
42	3.5.1.3	$\nu_\mu$ Background Selection in RHC Mode:	97
43	3.5.2	CC 1-Track (CCQE Enhanced)	97
44	3.5.2.1	$\nu_\mu$ Selection in FHC Mode:	97
45	3.5.2.2	$\bar{\nu}_\mu$ Selection in RHC Mode:	104
46	3.5.2.3	$\nu_\mu$ Background Selection in RHC Mode:	111
47	3.5.3	CC N-Tracks (CCnQE Enhanced)	111
48	3.5.3.1	$\nu_\mu$ Selection in FHC Mode:	111
49	3.5.3.2	$\bar{\nu}_\mu$ Selection in RHC Mode:	112
50	3.5.3.3	$\nu_\mu$ Background Selection in RHC Mode:	112
51	3.5.4	Differences Between Water-Out and Water-In Samples	112
52	<b>4</b>	<b>PØD-Only BANFF Parameterization</b>	<b>113</b>
53	4.1	PØD Samples Fit Binning	113
54	4.1.1	Fit Binning Determination	114
55	<b>5</b>	<b>Detector Systematics</b>	<b>117</b>

56	5.1 Detector Systematic Uncertainties . . . . .	117
57	5.1.1 Efficiency-like Systematics . . . . .	117
58	5.1.2 Observable Variation Systematics . . . . .	118
59	5.1.3 Normalization Systematics . . . . .	118
60	<b>6 Fitter Validation</b>	<b>120</b>
61	<b>7 PØD-Only Fitter Results</b>	<b>121</b>
62	<b>8 FGD-P0D Comparisons</b>	<b>122</b>
63	<b>9 Discussion</b>	<b>122</b>
64	<b>References</b>	<b>123</b>
65	<b>Nomenclature</b>	<b>125</b>

66 **List of Figures**

67	1.1	Exploded view of the off-axis detectors of ND280 . . . . .	10
68	1.2	Cartoon of the PØD . . . . .	11
69	1.3	Cartoon of an Individual PØDule . . . . .	12
70	1.4	Fluxing Tuning Histogram for FHC Events . . . . .	13
71	2.1	BANFF Pre-fit Flux Covariance Matrix . . . . .	20
72	2.2	BANFF ND280 NuMu and ANuMu Flux Binning Parameters . . . . .	21
73	2.3	Cross Section Parameters Pre-fit Correlation Matrix . . . . .	21
74	3.1	PØD Air FHC $\nu_\mu$ CC Inc. Lepton Cand. Reco. Momentum by True Particle	34
75	3.2	PØD Air FHC $\nu_\mu$ CC Inc. Lepton Cand. Reco. $\cos\theta$ by True Particle . . .	35
76	3.3	PØD Air FHC $\nu_\mu$ CC Inc. Lepton Cand. Reco. Momentum by NEUT Mode	36
77	3.4	PØD Air FHC $\nu_\mu$ CC Inc. Lepton Cand. Reco. $\cos\theta$ by NEUT Mode . . .	37
78	3.5	PØD Air FHC $\nu_\mu$ CC Inc. Lepton Cand. Reco. Momentum by True Topology	38
79	3.6	PØD Air FHC $\nu_\mu$ CC Inc. Lepton Cand. Reco. $\cos\theta$ by True Topology . . .	39
80	3.7	PØD Air FHC $\nu_\mu$ CC Inc. Lepton Cand. True $E_\nu$ by NEUT Mode . . . .	40
81	3.8	PØD Air RHC $\bar{\nu}_\mu$ CC Inc. Lepton Cand. Reco. Momentum by True Particle	41
82	3.9	PØD Air RHC $\bar{\nu}_\mu$ CC Inc. Lepton Cand. Reco. $\cos\theta$ by True Particle . . .	42
83	3.10	PØD Air RHC $\bar{\nu}_\mu$ CC Inc. Lepton Cand. Reco. Momentum by NEUT Mode	43
84	3.11	PØD Air RHC $\bar{\nu}_\mu$ CC Inc. Lepton Cand. Reco. $\cos\theta$ by NEUT Mode . . .	44
85	3.12	PØD Air RHC $\bar{\nu}_\mu$ CC Inc. Lepton Cand. Reco. Momentum by True Topology	45
86	3.13	PØD Air RHC $\bar{\nu}_\mu$ CC Inc. Lepton Cand. Reco. $\cos\theta$ by True Topology . . .	46
87	3.14	PØD Air FHC $\bar{\nu}_\mu$ CC Inc. Lepton Cand. True $E_\nu$ by NEUT Mode . . . .	47
88	3.15	PØD Air RHC $\nu_\mu$ CC Inc. Lepton Cand. Reco. Momentum by True Particle	48
89	3.16	PØD Air RHC $\nu_\mu$ CC Inc. Lepton Cand. Reco. $\cos\theta$ by True Particle . . .	49
90	3.17	PØD Air FHC $\nu_\mu$ CC Inc. Lepton Cand. Reco. Momentum by NEUT Mode	50

91	3.18 PØD Air FHC $\nu_\mu$ CC Inc. Lepton Cand. Reco. $\cos\theta$ by NEUT Mode . . . . .	51
92	3.19 PØD Air FHC $\nu_\mu$ CC Inc. Lepton Cand. Reco. Momentum by True Topology . . . . .	52
93	3.20 PØD Air FHC $\nu_\mu$ CC Inc. Lepton Cand. Reco. $\cos\theta$ by True Topology . . . . .	53
94	3.21 PØD Air FHC $\nu_\mu$ CC Inc. Lepton Cand. True $E_\nu$ by NEUT Mode . . . . .	54
95	3.22 PØD Air FHC $\nu_\mu$ CC Inc. Lepton Cand. Reco. Momentum by True Particle . . . . .	55
96	3.23 PØD Air FHC $\nu_\mu$ CC Inc. Lepton Cand. Reco. $\cos\theta$ by True Particle . . . . .	56
97	3.24 PØD Air FHC $\nu_\mu$ CC Inc. Lepton Cand. Reco. Momentum by NEUT Mode . . . . .	57
98	3.25 PØD Air FHC $\nu_\mu$ CC Inc. Lepton Cand. Reco. $\cos\theta$ by NEUT Mode . . . . .	58
99	3.26 PØD Air FHC $\nu_\mu$ CC Inc. Lepton Cand. Reco. Momentum by True Topology . . . . .	59
100	3.27 PØD Air FHC $\nu_\mu$ CC Inc. Lepton Cand. Reco. $\cos\theta$ by True Topology . . . . .	60
101	3.28 PØD Air FHC $\nu_\mu$ CC Inc. Lepton Cand. True $E_\nu$ by NEUT Mode . . . . .	61
102	3.29 PØD Air RHC $\bar{\nu}_\mu$ CC Inc. Lepton Cand. Reco. Momentum by True Particle . . . . .	62
103	3.30 PØD Air RHC $\bar{\nu}_\mu$ CC Inc. Lepton Cand. Reco. $\cos\theta$ by True Particle . . . . .	63
104	3.31 PØD Air RHC $\bar{\nu}_\mu$ CC Inc. Lepton Cand. Reco. Momentum by NEUT Mode . . . . .	64
105	3.32 PØD Air RHC $\bar{\nu}_\mu$ CC Inc. Lepton Cand. Reco. $\cos\theta$ by NEUT Mode . . . . .	65
106	3.33 PØD Air RHC $\bar{\nu}_\mu$ CC Inc. Lepton Cand. Reco. Momentum by True Topology . . . . .	66
107	3.34 PØD Air RHC $\bar{\nu}_\mu$ CC Inc. Lepton Cand. Reco. $\cos\theta$ by True Topology . . . . .	67
108	3.35 PØD Air FHC $\bar{\nu}_\mu$ CC Inc. Lepton Cand. True $E_\nu$ by NEUT Mode . . . . .	68
109	3.36 PØD Air FHC $\nu_\mu$ CC N-Tracks Lepton Cand. Reco. Momentum by True	
110	Particle . . . . .	69
111	3.37 PØD Air FHC $\nu_\mu$ CC N-Tracks Lepton Cand. Reco. $\cos\theta$ by True Particle . . . . .	70
112	3.38 PØD Air FHC $\nu_\mu$ CC N-Tracks Lepton Cand. Reco. Momentum by NEUT	
113	Mode . . . . .	71
114	3.39 PØD Air FHC $\nu_\mu$ CC N-Tracks Lepton Cand. Reco. $\cos\theta$ by NEUT Mode . . . . .	72
115	3.40 PØD Air FHC $\nu_\mu$ CC N-Tracks Lepton Cand. Reco. Momentum by True	
116	Topology . . . . .	73

117	3.41 PØD Air FHC $\nu_\mu$ CC N-Tracks Lepton Cand. Reco. $\cos\theta$ by True Topology	74
118	3.42 PØD Air FHC $\nu_\mu$ CC N-Tracks Lepton Cand. True $E_\nu$ by NEUT Mode . . .	75
119	3.43 PØD Air RHC $\bar{\nu}_\mu$ CC N-Tracks Lepton Cand. Reco. Momentum by True	
120	Particle . . . . .	76
121	3.44 PØD Air RHC $\bar{\nu}_\mu$ CC N-Tracks Lepton Cand. Reco. $\cos\theta$ by True Particle .	77
122	3.45 PØD Air RHC $\bar{\nu}_\mu$ CC N-Tracks Lepton Cand. Reco. Momentum by NEUT	
123	Mode . . . . .	78
124	3.46 PØD Air RHC $\bar{\nu}_\mu$ CC N-Tracks Lepton Cand. Reco. $\cos\theta$ by NEUT Mode .	79
125	3.47 PØD Air RHC $\bar{\nu}_\mu$ CC N-Tracks Lepton Cand. Reco. Momentum by True	
126	Topology . . . . .	80
127	3.48 PØD Air RHC $\bar{\nu}_\mu$ CC N-Tracks Lepton Cand. Reco. $\cos\theta$ by True Topology	81
128	3.49 PØD Air FHC $\bar{\nu}_\mu$ CC N-Tracks Lepton Cand. True $E_\nu$ by NEUT Mode . .	82
129	3.50 PØD Water FHC $\nu_\mu$ CC Inc. Lepton Cand. Reco. Momentum by True Particle	84
130	3.51 PØD Water FHC $\nu_\mu$ CC Inc. Lepton Cand. Reco. $\cos\theta$ by True Particle .	85
131	3.52 PØD Water FHC $\nu_\mu$ CC Inc. Lepton Cand. Reco. Momentum by NEUT Mode	86
132	3.53 PØD Water FHC $\nu_\mu$ CC Inc. Lepton Cand. Reco. $\cos\theta$ by NEUT Mode .	87
133	3.54 PØD Water FHC $\nu_\mu$ CC Inc. Lepton Cand. Reco. Momentum by True Topology	88
134	3.55 PØD Water FHC $\nu_\mu$ CC Inc. Lepton Cand. Reco. $\cos\theta$ by True Topology .	89
135	3.56 PØD Water FHC $\nu_\mu$ CC Inc. Lepton Cand. True $E_\nu$ by NEUT Mode . . .	90
136	3.57 PØD Water RHC $\bar{\nu}_\mu$ CC Inc. Lepton Cand. Reco. Momentum by True Particle	91
137	3.58 PØD Water RHC $\bar{\nu}_\mu$ CC Inc. Lepton Cand. Reco. $\cos\theta$ by True Particle .	92
138	3.59 PØD Water RHC $\bar{\nu}_\mu$ CC Inc. Lepton Cand. Reco. Momentum by NEUT Mode	93
139	3.60 PØD Water RHC $\bar{\nu}_\mu$ CC Inc. Lepton Cand. Reco. $\cos\theta$ by NEUT Mode .	94
140	3.61 PØD Water RHC $\bar{\nu}_\mu$ CC Inc. Lepton Cand. Reco. Momentum by True	
141	Topology . . . . .	95
142	3.62 PØD Water RHC $\bar{\nu}_\mu$ CC Inc. Lepton Cand. Reco. $\cos\theta$ by True Topology .	96

143	3.63 PØD Water FHC $\bar{\nu}_\mu$ CC Inc. Lepton Cand. True $E_\nu$ by NEUT Mode . . . . .	97
144	3.64 PØD Water FHC $\nu_\mu$ CC 1-Track Lepton Cand. Reco. Momentum by True	
145	Particle . . . . .	98
146	3.65 PØD Water FHC $\nu_\mu$ CC 1-Track Lepton Cand. Reco. $\cos\theta$ by True Particle	99
147	3.66 PØD Water FHC $\nu_\mu$ CC 1-Track Lepton Cand. Reco. Momentum by NEUT	
148	Mode . . . . .	100
149	3.67 PØD Water FHC $\nu_\mu$ CC 1-Track Lepton Cand. Reco. $\cos\theta$ by NEUT Mode	101
150	3.68 PØD Water FHC $\nu_\mu$ CC 1-Track Lepton Cand. Reco. Momentum by True	
151	Topology . . . . .	102
152	3.69 PØD Water FHC $\nu_\mu$ CC 1-Track Lepton Cand. Reco. $\cos\theta$ by True Topology	103
153	3.70 PØD Water FHC $\nu_\mu$ CC 1-Track Lepton Cand. True $E_\nu$ by NEUT Mode . .	104
154	3.71 PØD Water RHC $\bar{\nu}_\mu$ CC Inc. Lepton Cand. Reco. Momentum by True Particle	105
155	3.72 PØD Water RHC $\bar{\nu}_\mu$ CC Inc. Lepton Cand. Reco. $\cos\theta$ by True Particle . .	106
156	3.73 PØD Water RHC $\bar{\nu}_\mu$ CC Inc. Lepton Cand. Reco. Momentum by NEUT Mode	107
157	3.74 PØD Water RHC $\bar{\nu}_\mu$ CC Inc. Lepton Cand. Reco. $\cos\theta$ by NEUT Mode . .	108
158	3.75 PØD Water RHC $\bar{\nu}_\mu$ CC Inc. Lepton Cand. Reco. Momentum by True	
159	Topology . . . . .	109
160	3.76 PØD Water RHC $\bar{\nu}_\mu$ CC Inc. Lepton Cand. Reco. $\cos\theta$ by True Topology .	110
161	3.77 PØD Water FHC $\bar{\nu}_\mu$ CC Inc. Lepton Cand. True $E_\nu$ by NEUT Mode . . . .	111
162	4.1 PØD Momenta Resolutions Used for Fit Binning . . . . .	115
163	4.2 PØD Angular Residuals Used for Fit Binning . . . . .	116

<sup>164</sup> **List of Tables**

<sup>165</sup> 3.1	PØD WT FV and Corridor Definition . . . . .	28
<sup>166</sup> 3.2	POT Used in This Analysis . . . . .	32
<sup>167</sup> 5.1	[2] . . . . .	119

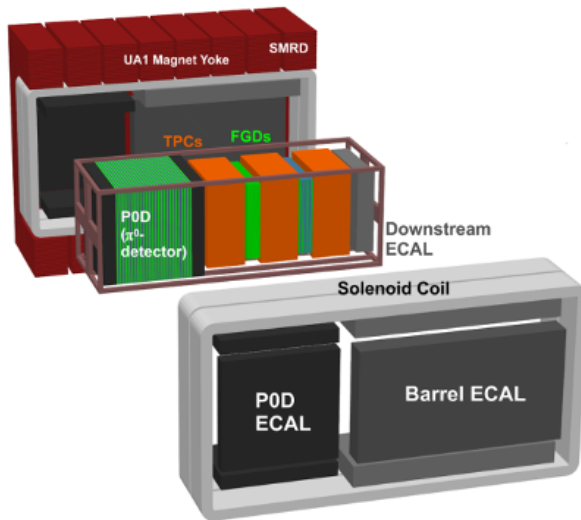


Figure 1.1: Exploded view of the off-axis detectors of ND280. The neutrino beam is directed from left to right along the figure.

## **1 Introduction**

The primary goal of an oscillation experiment is to measure the parameters in a neutrino mixing matrix. All other parameters, with some having some theoretical importance to fundamental physics, are nuisance parameters. To understand the methodology of Beam and Near detector Flux task Force (BANFF) fit, it is relevant to understand how likelihood fitting works.

### **1.1 ND280**

The T2K near detector (ND) complex consists of on-axis and off-axis detectors at 280m away from the secondary beamline proton target. The off-axis detector is used in this analysis which consists of several subdetectors housed inside the UA1/NOMAD magnet yoke as shown in figure 1.1. A similar analysis was also performed with the on-axis detector and is available in T2K-TN-335[14]. . The magnet provides a 0.2T magnetic field which is designed to provide momentum and particle identification for the tracker region.

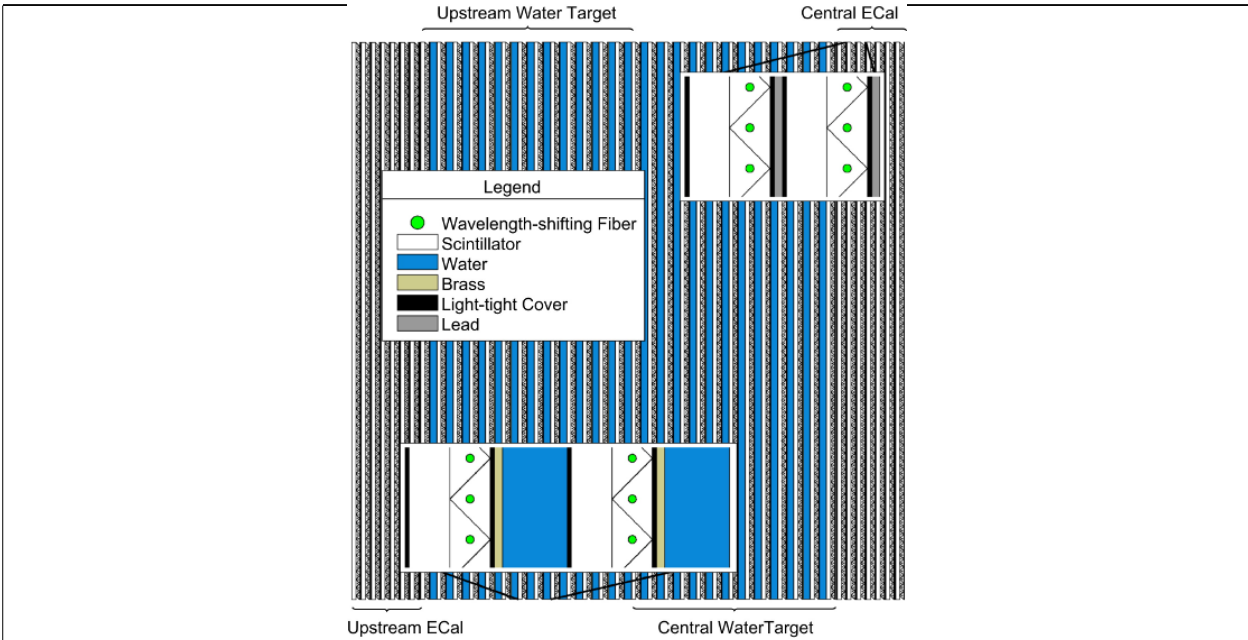


Figure 1.2: This cartoon illustrates the concept design of the PØD where the neutrino beam is approaching from the left.

### **1.1.1 The PØD**

The PØD, short for  $\pi^0$  Detector, is a plastic scintillator based tracking calorimeter inside the ND280 basket. The PØD is constructed as many sandwiches of active and inactive materials designed to fully contain  $\pi^0$  decay photons. The four primary regions inside the PØD in order of upstream to downstream of the neutrino beam are the upstream ECal (USECal), upstream water target (WT), central WT, and central ECal (CECal). A representation of the entire PØD can be seen in Figure 1.2. Each active module, also called a PØDule, consists of two orthogonally oriented sheets of triangular, scintillator-doped plastic bars as shown in

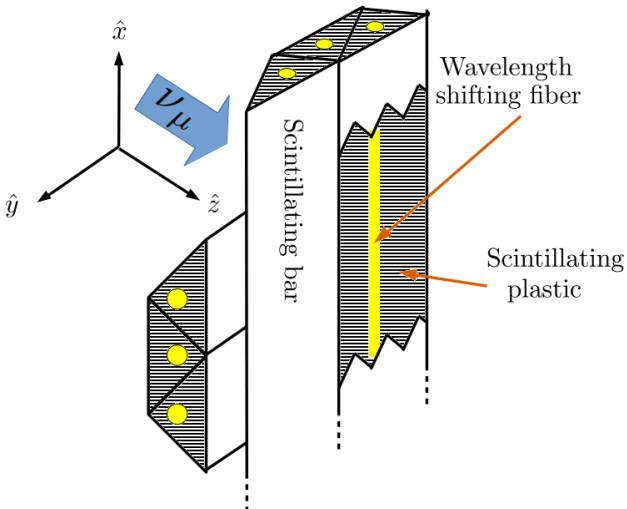


Figure 1.3: This cartoon illustrates the design of a PØDule with orthogonal layers of scintillating, triangular bars. When a charged particle travels through the bar such as a muon from CC interaction, the scintillation light is captured and wavelength shifted inside a fiber bored in the center of each bar. The wavelength shifted light is later observed by a photon counter.

189     Figure 1.3. The ECal regions are designed to contain decay photons inside the PØD by  
 190    alternating the scintillator planes with lead sheets. The WT regions, as compared to the lead  
 191    sheets in the ECals, alternate a thin brass sheet and water filled bags between the PØDules.  
 192    A unique feature of the PØD is that the water can be drained out resulting in two detector  
 193    configurations: water-in and water-out.

## 194    1.2 Usage of ND280 Psyche Software

195    Psyche is a general framework for data handling, event selections, and systematic evaluations  
 196    with toy experiments. Psyche is a “lean” package from the perspective of analyzing MC  
 197    events since that functionality is built heavily into Highland2. The analysis performed in  
 198    this technical note required making additions to psyche in order replicate features available  
 199    in Highland2. It would be wise for future analyses to build a selection in Highland2 and  
 200    migrate that psyche once mature.

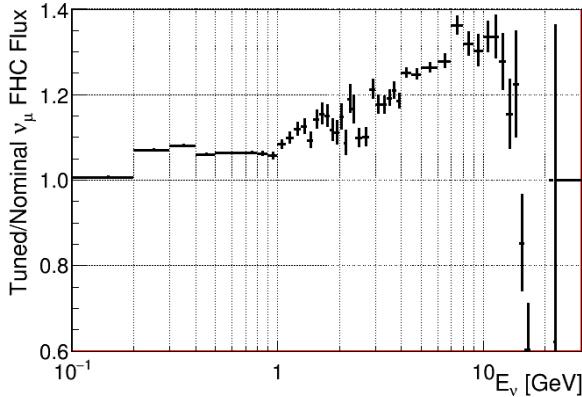


Figure 1.4: Fluxing tuning histogram for  $\nu_\mu$  FHC events taken from the 13av3 flux release.

BANFF uses a psyche package called psycheSteering that interfaces with all the psyche tools to manage the migration of samples into its analysis code. New PØD selections were added to the psycheSelections package and validated using the psycheSteering AnalysisManager class. The AnalysisManager provides the functionality to get the true and reconstructed detector observables from each reconstructed event along with the flux tuning and detector systematic weights.

Flux tuning is the process of applying an event weight based on the true neutrino energy, flavor, and run period. Since the ND280 MC uses a series of models to describe the expected neutrino flux, it cannot perfectly model the true flux nor know the beam conditions at run time. The beam group is responsible for releasing the expected and measured neutrino flux in order to account for these differences. To flux tune an event, the relevant neutrino flavor flux histogram must be referenced. The weight is extracted by taking the ratio of the tuned flux to the nominal flux in the MC for a given neutrino energy. As an example Figure 1.4 shows the flux tuning weights for true  $\nu_\mu$  FHC events.

215 **2 ND280 Binned Likelihood**

216 The BANFF likelihood maximization procedure is a binned likelihood maximization of the  
217 ND280 data. In a ND280 and Super-Kamiokande (SK) joint fit, the measurements from both  
218 detectors are considered along with their respective nuisance parameters. This approach  
219 is more computationally expensive compared to the Markov Chain Monte Carlo analysis  
220 (MaCh3) which will not be explained here. The BANFF likelihood maximization, hitherto  
221 referred to as the “BANFF-fit”, includes nuisance parameters that affect the measurement of  
222 the oscillation parameters, but are not physics goals of the T2K experiment. The BANFF-  
223 fit parameters and their respective covariances are then used as inputs in the oscillation  
224 analysis. This “divide-and-conquer” approach allows for more rapidly completed studies  
225 on the effects of model parameters and biases present. Also this approach should provide  
226 the same result with a joint ND280 and SK analysis as is performed in MaCh3. However,  
227 information encoded in the ND280 measurements for shared nuisance parameters like the  
228 neutrino flux is inevitably lost in the BANFF-fit.

229 The modern BANFF-fit likelihood is described in detail in TN-220[11]. It uses a fre-  
230 quentist approach to find the best nuisance parameter set to maximize a binned likelihood.  
231 Subsequent updates to the BANFF analysis[12, 5, 4] increase the sample sizes and systematic  
232 parameterizations.

233 **2.1 Motivation**

234 Curve fitting is commonly found in the particle physics community literature due to the  
235 need to compare two models or constrain unknown model parameters using one or more  
236 histograms. For the first case, this involves two competing models,  $H_0$  and  $H_1$ , in order to  
237 establish if the data supports new Physics ( $H_1$ ) not predicted in the Standard Model ( $H_0$ ).  
238 The second case finds the “best” set of the model predictions,  $\theta$ , that match the data as is the

239 case for the BANFF-fit. In both cases, chi-squared tests are performed to provide goodness  
240 of fit, parameter estimation (also referred to as “best fit parameters”), and error/confidence  
241 estimation.

## 242 2.2 Introduction to Conditional PDFs and Likelihoods

243 Consider the problem of extracting physics parameters  $\vec{y}$  given some data vector  $\vec{N}$ . The  
244 conditional probability density function (PDF)  $\mathcal{P}$  to measure these parameters is given as

$$\mathcal{P}(\vec{y}|\vec{N}) = \frac{\mathcal{L}(\vec{N}|\vec{y})\mathcal{P}(\vec{y})}{\int \mathcal{L}(\vec{N}|\vec{x})\mathcal{P}(\vec{x})d\vec{x}}, \quad (2.1)$$

245 where anything right of a vertical line represents a condition on the probability,  $\mathcal{L}(\vec{N}|\vec{y})$   
246 is the likelihood of the model with parameters  $\vec{y}$ ,  $\mathcal{P}(\vec{y})$  is the probability for the model,  
247 and the denominator is the normalization over all possible constraints on the observations.  
248 A frequentist interpretation of a PDF is a proportion of outcomes of repeated trials or  
249 experiments. A likelihood function is an expression of the probability of observing data as a  
250 function of the model parameters in their appropriate ranges.

251 One arrives at (2.1) by using the definition of compound probabilities

$$\mathcal{P}(A, B) = \mathcal{P}(B|A)\mathcal{P}(A) \quad (2.2)$$

252 to evaluate  $\mathcal{P}(\vec{y}|\vec{N})$  as

$$\mathcal{P}\left(\underbrace{\vec{y}}_B \middle| \underbrace{\vec{N}}_A\right) = \frac{\mathcal{P}(\vec{N}, \vec{y})}{\mathcal{P}(\vec{N})} \quad (2.3)$$

253 with the denominator here is recognized as the normalization of the PDF. The compound

254 PDF  $\mathcal{P}(\vec{N}, \vec{y})$  can expanded using Bayes' theorem which states

$$\mathcal{P}(A|B)\mathcal{P}(B) = \mathcal{P}(B|A)\mathcal{P}(A), \quad (2.4)$$

255 and combined with (2.2) yielding

$$\mathcal{P}\left(\underbrace{\vec{N}}_A, \underbrace{\vec{y}}_B\right) = \mathcal{P}(\vec{N}|\vec{y}) \times \mathcal{P}(\vec{y}), \quad (2.5)$$

256 where the PDFs to the left and right of the  $\times$  operator are recognized as the likelihoods and  
257 priors, respectively. Combining resulting in (2.3) and (2.5) reproduces the original expression  
258 of (2.1).

### 259 2.3 BANFF Fit Test Statistic

260 For the BANFF fit, one considers the problem of trying to maximize the agreement between  
261 measured and predicted data histograms. This is equivalent to maximizing a binned likeli-  
262 hood function  $\mathcal{L}$  of the data given the a set of parameters that predict the measured rate.  
263 The use of likelihood functions in fits to histogram is explained further in reference [3] and  
264 the PDG review on Statistics. By invoking Wilks' theorem, also known as the likelihood ratio  
265 theorem, the likelihood maximization procedure is converted into a minimization problem  
266 involving a test statistic denoted as a chi-squared. Below is an explanation of the BANFF  
267 test statistic,  $\Delta\chi^2$ , and its systematic model terms.

268 Consider many binned samples that select different charged current topologies. A conve-  
269 nient choice of observables for all the samples are the outgoing charged lepton  $l$  momentum  $P_l$   
270 and angle  $\cos\theta_l$  as measured in ND280. Much of this is also documented in TN-220[11] where  
271 additional details can be found. For each  $(P_l, \cos\theta_l)$  analysis bin  $i = 1, 2, \dots, M - 1, M$ , the

272 likelihood is given by

$$\mathcal{L}(\vec{N}^d | \vec{N}^p) = \left( \prod_{i=1}^M \left( \vec{N}_i^p \right)^{\vec{N}_i^d} \frac{e^{-\vec{N}_i^p}}{\vec{N}_i^p!} \right) \quad (2.6)$$

273 where  $\vec{N}_i^d$  is the number of observed data events in the  $i$ th bin and  $\vec{N}_i^p$  is the number of  
 274 predicted events as a function of nuisance parameters in the  $i$ th bin. One recognizes the  
 275 likelihood function in (2.6) as a product of Poisson distributions with each corresponding  
 276 to bins  $i = 1, 2, \dots, M - 1, M$ . The sets of dependent nuisance parameters, also sometimes  
 277 called systematics, that affect the predicted event rate are

- 278 • cross section physics models, labeled as “xsec”,
- 279 • neutrino flux, and
- 280 • detector biases and inefficiencies.

281 Given these three sets of systematics, the number of predicted CC events from any neutrino  
 282 flavor  $\nu_l$  at ND280 is calculated using the general formula

$$N_{\nu_l} = \Phi_{\nu_l} \sum_t (\sigma_{\nu_l}^t M_t) \epsilon_{\nu_l}, \quad (2.7)$$

283 where  $\Phi_{\nu_l}$  is the flux of  $l$  flavor neutrinos,  $\sigma_{\nu_l}^t$  is the cross section of the interaction for  
 284 neutrino flavor  $l$  on target  $t$ ,  $M_t$  is the number of  $t$  targets, and  $\epsilon_{\nu_l}$  is the total efficiency  
 285 to reconstruct and properly identify the event as  $\nu_l$ CC interactions. Each term in (2.7) is  
 286 modeled carefully and the efficiency term is estimated using Monte Carlo (MC) simulations  
 287 and control samples. The number of predicted events from the MC for a given analysis bin  
 288  $i$  is given by

$$\vec{N}_i^p(\vec{b}, \vec{x}, \vec{d}) = w_i^{\text{POT}} (\vec{d})_i^{\text{Det}} \sum_{j=1}^{N_i^{\text{MC}}} \left[ \sum_{k=1}^{N^{\text{Flux}}} \left( \delta_{j,k}^{\text{Flux}} (\vec{b})_k^{\text{Flux}} \right) \prod_{l=1}^{N^{\text{xSyst}}} w_{j,l}((\vec{x})_l^{\text{xsec}}) \right]. \quad (2.8)$$

289 Here  $w_i^{\text{POT}}$  is the protons on target (POT) weight for the  $i$ th analysis which normalizes  
 290 the MC statistics to expected data statistics. To account for the detector inefficiencies, the  
 291  $(\vec{d})_i^{\text{Det}}$  parameters are normalization parameters that vary the total number of predicted  
 292 events in the  $i$ th bin. Each  $(\vec{d})_i^{\text{Det}}$  is determined prior to the fit by surveying over a large  
 293 number of toy experiments with the detector systematics varied in each. The sum over  
 294  $j = 1, 2, \dots, N_i^{\text{MC}} - 1, N_i^{\text{MC}}$  considers the contribution of all MC events in the  $i$ th analysis  
 295 bin. The  $(\vec{b})_k^{\text{Flux}}$  parameters, out of a total of  $N^{\text{Flux}}$ , are flux normalization systematics  
 296 for each flux bin. Since the flux bins are categorized not only by neutrino energy, but also  
 297 by flavor and horn current, the  $\delta_{j,k}^{\text{Flux}}$  term in the sum over  $k$  selects the correct flux bin.  
 298 The parameters  $w_{j,l}$  are pre-calculated weights as a function for the  $l$ th cross section model,  
 299  $(\vec{x})_l^{\text{xsec}}$ , with a total of  $N^{\text{xSyst}}$  cross section model terms. Different  $t$  target materials have  
 300 separate cross section parameters. Also the number of targets  $M_t$  can vary via detector  
 301 systematics.

302 Using the likelihood ratio test theorem, a test statistic is defined as taking -2 times the  
 303 natural logarithm of the ratio of predicted to observed likelihoods

$$\Delta\chi_{\text{LLR}}^2 = -2 \log \frac{\mathcal{L}(\vec{N}^d | \vec{N}^p)}{\mathcal{L}(\vec{N}^d | \vec{N}^d)}, \quad (2.9)$$

304 where this test statistic  $\Delta\chi_{\text{LLR}}^2$  obeys a true chi-squared distribution for asymptotically  
 305 large statistics and the likelihood functions are of the form (2.6). The denominator in (2.9)  
 306 is the MC predicted probability which assumes the best maximum likelihood estimate is  
 307 the number of observed events. Penalty terms from the cross section, flux, and detector  
 308 systematics are included in order to prevent overfitting of the data. The new test statistic

309 for all of ND280,  $\Delta\chi^2_{\text{ND280}}$ , is given by

$$\begin{aligned}\Delta\chi^2_{\text{ND280}} &= \Delta\chi^2_{\text{LLR}} + \Delta\chi^2_{\text{xsec}} + \Delta\chi^2_{\text{Flux}} + \Delta\chi^2_{\text{Det}} \\ &\quad - 2 \left( \log \frac{\mathcal{L}(\vec{N}^d | \vec{N}^p)}{\mathcal{L}(\vec{N}^d | \vec{N}^d)} + \underbrace{\log \pi(\vec{x})}_{\text{xsec}} + \underbrace{\log \pi(\vec{b})}_{\text{Flux}} + \underbrace{\log \pi(\vec{d})}_{\text{Det}} \right),\end{aligned}\quad (2.10)$$

310 where each of the PDFs  $\pi(\vec{y} = \vec{x}, \vec{b}, \vec{d})$  are assumed multivariate normal distributions

$$\pi(\vec{y}) = C_y e^{\left(-\frac{1}{2} \Delta \vec{y} \cdot V_y^{-1} \cdot \Delta \vec{y}^T\right)}, \quad (2.11)$$

311  $\Delta \vec{y}$  is a vector with the difference between the current/explored and nominal set of vector  
312 parameters  $\vec{y}$ ,  $T$  corresponds to the transpose operator, and the normalization is given by

$$C_y = ((2\pi)^{k_y} \det(V_y))^{-\frac{1}{2}} \quad (2.12)$$

313 with  $V_y$  being the covariance matrix for a vector  $\vec{y}$  with  $k_y$  rows. The expanded form of the  
314 test statistic  $\Delta\chi^2_{\text{ND280}}$  is given by

$$\begin{aligned}\Delta\chi^2_{\text{ND280}} &= 2 \sum_{i=1}^M \left[ \vec{N}_i^p - \vec{N}_i^d + \vec{N}_i^d \log \left( \frac{\vec{N}_i^d}{\vec{N}_i^p} \right) \right] \\ &\quad + \Delta \vec{x} \cdot (V_x^{-1}) \cdot \Delta \vec{x}^T + \Delta \vec{b} \cdot (V_b^{-1}) \cdot \Delta \vec{b}^T + \Delta \vec{d} \cdot (V_d^{-1}) \cdot \Delta \vec{d}^T\end{aligned}\quad (2.13)$$

315 where the “ $\cdot$ ” is the matrix multiplication operator. It must be stated that the test statistic  
316 (2.13) purposefully *excludes normalization terms*. Once the global minimum of the test  
317 statistic is found, the postfit covariance matrix  $V$  is calculated as the inverse of the Hessian  
318 matrix  $H$

$$V_{i,j}(\hat{\vec{y}}) = (H_{i,j})^{-1} = \left( \frac{\partial^2}{\partial y_i \partial y_j} (\Delta\chi^2_{\text{ND280}}) \Big|_{\vec{y}=\hat{\vec{y}}} \right)^{-1} \quad (2.14)$$

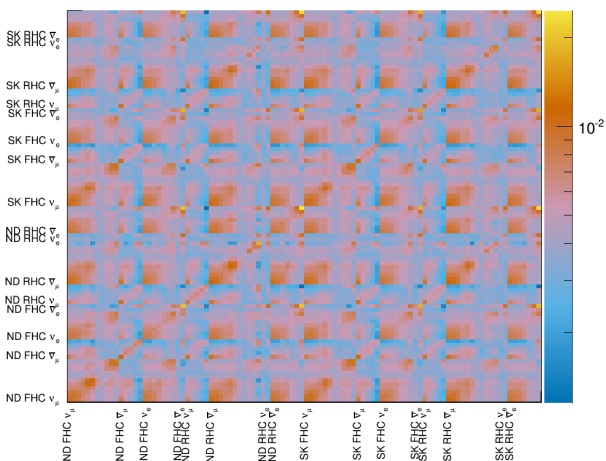


Figure 2.1: BANFF pre-fit flux covariance matrix shown with respective detector, horn current, and neutrino flavor.

319 where  $y_i, y_j \in \vec{y}$  and  $\hat{y}$  is the maximum likelihood estimate for the parameters  $\vec{y}$ .

### 320 2.3.1 Flux, Cross Section, and Detector Systematics

321 Below is a description for each of the systematics in the BANFF likelihood and test statistic  
 322 penalty terms. First is a description of flux, followed by the cross section, and finally the  
 323 detector systematics.

324 **Flux:** The flux weight is binned as a function of neutrino energy, horn current/polarity  
 325 (FHC and RHC), and neutrino flavor ( $\nu_\mu$ ,  $\bar{\nu}_\mu$ ,  $\nu_e$ , and  $\bar{\nu}_e$ ). There are 50 ND280 and 50 SK  
 326 parameters with an associated covariance matrix as shown in Figure 2.1. The binning and  
 327 covariance matrix is provided by the T2K flux group prior to the BANFF analysis. Each  
 328 flux bin is assigned a normalization parameter with initial value of one (1) for all events in  
 329 that neutrino energy bin. A value of 1.1 indicates that any event in that energy bin has an  
 330 additional weight of 1.1, or 10% increase in events. An example of the flux normalizations  
 331 and uncertainties used in the 2017 analysis are shown in Figure 2.2.

332 **Cross Section:** There are a number of cross section model systematics implemented in  
 333 BANFF to account for the uncertainties in cross section measurements. The cross section

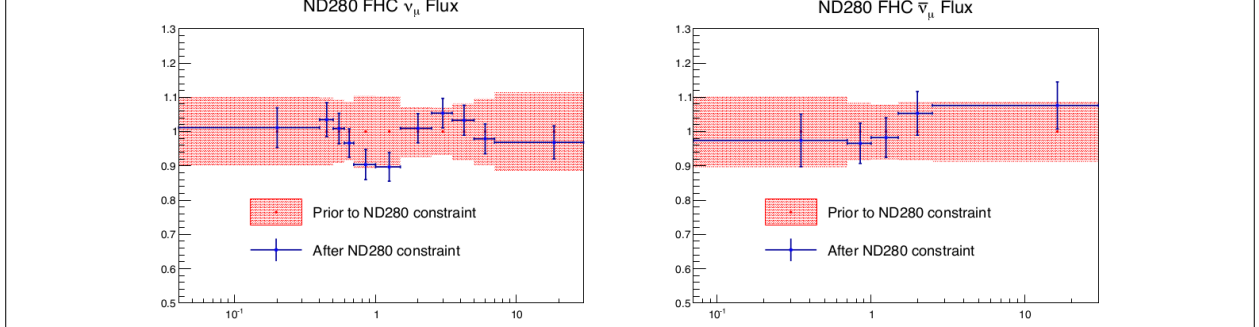


Figure 2.2: BANFF ND280 flux  $\nu_\mu$  and  $\bar{\nu}_\mu$  binning parameters from T2K-TN-324 data post-fit results. The uncertainties are extracted from the pre-fit and post-fit covariance matrices.

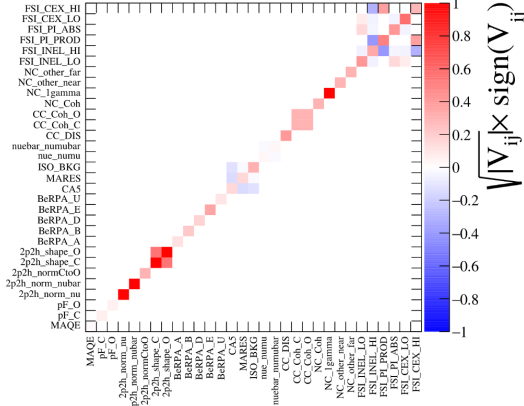


Figure 2.3: Cross section parameters pre-fit correlation matrix from the 2017 BANFF analysis.

models used in this analysis are the 2017 Neutrino Interactions Working Group (NIWG) parameterization, which is a canonical set of parameters and covariance matrix shared among all analyses in T2K. A technical description of the 2017 parameterization is given in TN-315[6] and TN-307[15]. There are a total of 25 cross section parameters for interactions like meson exchange current that affect the shape and normalization of the cross section. The cross section correlation matrix is shown in Figure 2.3[5].

**Detector Systematic Errors:** Detector systematics are implemented in BANFF to account for uncertainties in detector efficiencies. Since neutrino interaction events can migrate from sample-to-sample, bin-to-bin, or both depending on the relevant systematics, numerous toy experiments are performed by varying parameters that model known detector

344 systematics.

345 After many toy experiments, a covariance matrix among the bins is constructed con-  
346 sidering correlations and statistical errors. This detector covariance matrix is fractional to  
347 be consistent with the definitions for the flux and cross section covariance matrices. The  
348 detector covariance matrix,  $\sigma_{\text{Det}}^2$ , between bins  $x$  and  $y$  given explicitly as

$$\sigma_{\text{Det}}^2(x, y) = \frac{1}{x_{\text{Nom}}} \frac{1}{y_{\text{Nom}}} (\sigma_{\text{Cov}}^2(x, y) + \sigma_{\text{Stat}}^2(x, y)), \quad (2.15)$$

349 where ‘‘Nom’’, ‘‘Cov’’, and ‘‘Stat’’ refer to the nominal MC prediction, covariance, and sta-  
350 tistical uncertainties for bins  $x$  and  $y$ , respectively. The nominal bin expectation for bin  $x$   
351 is

$$x_{\text{Nom}} = \sum_{k=1}^{N_x^{\text{MC}}} w_k, \quad (2.16)$$

352 where  $N_x^{\text{MC}}$  being the number of predicted MC events in the bin and  $w_k$  being the product  
353 of all the weights applied to the  $k$ th event (see (2.8) for all possible weights). The covariance  
354 and statistical terms are given by

$$\begin{aligned} \sigma_{\text{Cov}}^2(x, y) &= \frac{1}{N_{\text{Toy}}} \sum_{t=1}^{N_{\text{Toy}}} (x_t - \bar{x})(y_t - \bar{y}) \\ \sigma_{\text{Stat}}^2(x, y) &= \delta(x, y) \sum_{k=1}^{N_x^{\text{MC}}} w_k^2, \end{aligned} \quad (2.17)$$

355 where  $N_{\text{Toy}}$  is the number of toy experiments,  $\bar{x}$  is the mean of the all the toy experiments  
356 in bin  $x$ , and  $\delta(x, y)$  is the Kronecker delta function. Additional uncertainties like fake data  
357 contributions are added to the covariance in quadrature.

358 While there could be one detector systematic normalization for each analysis bin, also  
359 called a observable normalization, a single one can be assigned to multiple analysis bins to  
360 reduce the number of fit parameters. This procedure requires careful consideration of the

361 shared detector systematics among analysis bins. A considerable drawback to designing nor-  
362 malizations in this way is that not all detector systematics are Gaussian with respect to the  
363 observables ( $P_l, \cos \theta_l$ ), and so the covariance matrix may not be an accurate representation  
364 of the detector systematics.

365 **3 PØD Selections and Data Samples**

366 This section describes the development of  $\nu_\mu$  and  $\bar{\nu}_\mu$  CC Inclusive selections in both FHC  
367 and RHC beam configuration for PØD-based analyses. These selections are the continuation  
368 of previous works that developed  $\nu_\mu$  CC Inclusive selections between the PØD and TPC1.  
369 The first such analyses were T2K-TN-80 and T2K-TN-100 which described the  $\nu_\mu$  CC In-  
370 clusive event selection and, later, cross-section analysis using ND280 Production 5 software,  
371 respectively[8, 9]. These analyzes relied on each sub-detector’s reconstruction software and  
372 developed a track matching algorithm since the ND280 “Global” reconstruction matching  
373 was problematic in Production 5. As the inter-detector matching reconstruction improved in  
374 “Global”, two CC-0 $\pi$  cross section analyzes, T2K-TN-258 and T2K-TN-328, were developed  
375 that also used the CC Inclusive selection as pre-selection cuts[17, 7]. The selections described  
376 in this technical note also employ the same pre-selection cuts. What follows from here in  
377 this section is a layout of the following topic discussions.

378 The first topic discussed in this section is a description of the  $\pi^0$  Detector (PØD). The  
379 next topic is the event reconstruction using the “Global” reconstruction software. Following  
380 that is the pre-selection cut flow. With the pre-selection cuts established, each of the three  
381 CC Inclusive selection’s cut flow is described. Concluding this section is a discussion of the  
382 three samples in the following order:  $\nu_\mu$  in FHC mode,  $\bar{\nu}_\mu$  in RHC, and  $\nu_\mu$  background in  
383 RHC.

384 **3.1 Global Reconstruction**

385 The task of the Global reconstruction is to combine all the ND280 information into a com-  
386 bined reconstructed object. It was originally designed to analyze “CCQE-like” events in the  
387 Tracker region and has been extended to operate with all of ND280. A brief description  
388 of the Global reconstruction is described below. First the specific detector technologies and

389 electronics of ND280 are explained. That is followed by the calibration procedure to properly  
390 tune each detector's response. And finally a general outline of the reconstruction algorithms  
391 to form tracks and vertices in ND280 is presented.

392 ND280 events are first collected in the form of electronic signals from either multipixel  
393 photon counters (MPPCs) in the scintillator-based sub-detectors or charge collection planes  
394 of the time projection chambers (TPCs). MPPCs were chosen for the scintillator-based sub-  
395 detectors since they are insensitive to the strong 0.2T magnetic field present in ND280. The  
396 PØD, ECals, and SMRD all share the same “Trip-T” frontend board (TFB) electronics of  
397 which collect the photoelectrons released when photons interact with a pixel in the MPPCs.  
398 The FGDs operate with the same MPPC technology while using different frontend electron-  
399 ics. The TPCs utilize a locally strong electric field to collect ionization electrons from an  
400 Argon-based gas. Collected charge in the TPCs are collected and enhanced using micromega  
401 technology[1]. With the collected information from each sub-detector, the next step is the  
402 data calibration.

403 Data calibration in ND280 is the process where the charge and timing information col-  
404 lected from each sub-detector is adjusted to match with expected parameters. This is an  
405 important process that takes into account environmental changes, aging effects, and other  
406 behavior that might be present. Calibration data is collected frequently before and during  
407 operational runtime and is stored in a database for later use. A common calibration is to  
408 measure the detector's cosmic ray response since most cosmic rays deposit the same energy  
409 per unit length. After the data has been calibrated, reconstruction algorithms now attempt  
410 to find charged particle tracks in the data.

411 The Global reconstruction is a software package that attempts to recognize patterns of  
412 data to form tracks and find vertices for those tracks. Particle shower reconstruction in  
413 Global will not be discussed in this TN since no shower objects are used. Each sub-detector  
414 reconstruction is run to seeds Global's track matching algorithms. Global attempts to then

415 re-fit sub-detector tracks using a Kalman filter while correcting for particle energy loss as a  
416 function of length ( $dE/dx$ ) and multi-scattering processes. A vertex is then associated with  
417 the re-fit track using another Kalman filter algorithm. A further detailed description of the  
418 track matching and vertex finding algorithms for Global is described in T2K-TN-46[16].

419 **3.2 PØD Selection Cuts**

420 The selection of CC Inclusive events use a series of cuts to select the primary lepton. The  
421 pre-selection cuts (“precuts”) are applied first to extract events that start in the PØD FV.  
422 A MIP is more likely to reach TPC1 from the PØD FV since the PØD is constructed out  
423 of heavy materials especially in the CECal. So the main track each selection is designed to  
424 select a muon.

425 This following sections will describe the precuts common to all CC Inclusive selections  
426 and the branching of different cuts, after the precuts, to select the main track.

427 **3.2.1 Pre-Selection Cuts**

428 The pre-selection (“precuts”) were initially developed to select  $\nu_\mu$ CC Inclusive using the PØD  
429 and TPC sub-detector reconstruction softwares separately[8]. They were then used with the  
430 Global reconstruction software for the  $\nu_\mu$ CC-0 $\pi$  selection in the FHC beam configuration as  
431 described in technical note T2K-TN-258[17]. The description and flow of the precuts are  
432 described here as well since there is an incomplete description of the selection precuts.

433 The precuts are performed on each bunch per beam spill as follows

- 434 1. The event has a “good” data quality flag.
  - 435 • An event is rejected if any sub-detector or electronics in ND280 reported as “bad”  
436 during that bunch.
- 437 2. There is at least one (1) track reconstructed in TPC1.

- 438     • There are no restrictions on the number of tracks fully contained in the PØD or  
439            exiting into other sub-detectors.

440     3. The track in TPC1 must have more than 18 nodes.

- 441     • The TPC reconstruction gathers vertical and horizontal hits into clusters of hits.  
442         The charge distribution of the cluster is used to get a vertical (horizontal) position  
443         that is more accurate than the individual readout pads. A node is constructed  
444         out of each cluster with associated track state information. The set of nodes are  
445         used to fit the track helix[13].

446     4. The reconstructed vertex is within the PØD WT FV.

- 447     • The PØD FV is defined to include as much as the WT regions as possible. Its  
448         X and Y borders are 25 cm away from the PØDule edges while its Z borders  
449         intersect the last and first half downstream PØDule in the USECal and CECal,  
450         respectively. The enumerated volume edges are shown in table 3.1. This volume,  
451         while used for track-based analyzes in the past, was optimized for  $\pi^0$  and  $\nu_e$   
452         analyzes[10].

453     5. All tracks that enter TPC1 pass the veto cut

- 454     • An event is rejected if any PØD track enters TPC1 from outside the “corridor”  
455         volume. This cut was designed to eliminate broken tracks between the PØD and  
456         TPC1 when the separate sub-detector reconstructions were used[8]. In practice,  
457         this cut ensures that Global tracks entering TPC1 away from its X and Y edges.  
458         The corridor definition is the same as defined in T2K-TN-208 and shown in Ta-  
459         ble 3.1.

PØD WT FV			Corridor Volume		
-836	< X <	764	-988	< X <	910
-871	< Y <	869	-1020	< Y <	1010
-2969	< Z <	1264	-3139	< Z <	-900

Table 3.1: The PØD WT FV (left) and veto corridor volume (right) in the ND280 coordinate system. The corridor spans from the 5th (8th) to 40th (80th) PØDule (scintillator layer). All the units are given in millimeters.

460 After passing all the precuts, a single, global track, which is observed in TPC1, is assigned  
461 as the lepton candidate or “main track” of a selection.

462 The momentum of the main track,  $P$ , is sum of its momentum in the TPC,  $P_{\text{TPC}}$ , with  
463 the estimate momentum lost in the PØD,  $\Delta P_{\text{PØD}}$

$$P = P_{\text{TPC}} + \Delta P_{\text{PØD}}. \quad (3.1)$$

464 Momentum lost in the PØD is estimated by summing the energy loss ( $dT/dx$ ) in along the  
465 track path  $dx$

$$\Delta T = \int \left( \frac{dT}{dx} \right) dx. \quad (3.2)$$

466 Using the chain rule, we can convert the energy loss into momentum loss

$$\begin{aligned} \frac{dT}{dx} &= \left( \frac{dT}{dP} \right) \left( \frac{dP}{dx} \right) \\ &= \left( \frac{Pc^2}{E} \right) \left( \frac{dP}{dx} \right) \\ &= \beta c \left( \frac{dP}{dx} \right), \end{aligned} \quad (3.3)$$

467 where  $\beta$  is the particle velocity as a ratio of the speed of light  $c$ . The fundamental theorem

468 of Calculus permits the us to write the energy loss now as a momentum loss

$$\Delta P_{\text{P}\emptyset\text{D}} = \int \left( \frac{dP}{dx} \right) dx = \frac{1}{c} \int \left[ \left( \frac{dT}{dx} \right) \frac{1}{\beta} \right] dx.$$

469 Since we cannot take infinitesimally small steps along the track, we must replace the integral  
470 with a sum and  $dx \rightarrow \Delta x$  to arrive at the expression of the momentum loss estimate in the  
471 P $\emptyset$ D

$$P = P_{\text{TPC}} + \frac{1}{c} \sum_t \left[ \left( \frac{dT}{dx} \right) \left( \frac{\Delta x}{\beta} \right) \right]_t. \quad (3.4)$$

472 For most tracks entering the TPC, they will be highly relativistic in the P $\emptyset$ D ( $\beta(x) \approx 1$ ),  
473 and (3.4) becomes

$$P = P_{\text{TPC}} + \frac{1}{c} \sum_t \left[ \left( \frac{dT}{dx} \right) \Delta x \right]_t \quad (3.5)$$

474 The next sections describe the selection cuts. irst in FHC mode and then RHC mode.

### 475 **$\nu_\mu$ CC Inclusive in FHC Cut**

- 476 • The highest momentum negatively charged track (HMNT) is the lepton candidate

477 As discussed in Section section 3.2.1 on page 26, this selection is the basis for the  $\nu_\mu$  CC-0 $\pi$   
478 P $\emptyset$ D+TPC1 analysis. In FHC mode, the vast majority of neutrino interactions are  $\nu_\mu$ CC  
479 events producing an outgoing, negatively charged muon. So if there is no negatively charged  
480 track in the TPC, the event is rejected.

### 481 **$\bar{\nu}_\mu$ CC Inclusive in RHC Cuts**

- 482 • The highest momentum positively charged track (HMPT) is the lepton candidate  
483 • The HMPT must be the highest momentum track (HMT)

484 In RHC, the majority of neutrinos in the beam is  $\bar{\nu}_\mu$  since the horn focuses negatively charged  
485 pions. To select  $\bar{\nu}_\mu$  CC interaction events by selecting positively charged muons, the lepton

candidate is the HMPT in the TPC. The event is rejected if there is no positively charged track. However, since the RHC mode beam is not as  $\bar{\nu}_\mu$  pure as the FHC beam, another cut was added to reduce this effect.

Since RHC neutrino beam can be described as a  $\bar{\nu}_\mu$ -enhanced beam, the HMPT must also be the HMT due to the significant “wrong-sign”  $\nu_\mu$  background. This effect is two fold due to the nature of the neutrino source and the cross section between neutrinos and antineutrinos.

Firstly the neutrino flux is larger in RHC mode due to neutrino production at the target. The source of neutrinos are from protons, which have positive charge, on a graphite target. This method is more likely to produce positively charged pions in the target than negatively charged one. While the horns are designed to select the negatively charged pions in RHC mode, the excess amount of positively charged pions will penetrate the horns’ filter. Therefore there are many more  $\pi^+ \rightarrow \mu^+ + \nu_\mu$  decays in RHC compared to FHC mode.

Secondly, antineutrino interactions on matter are suppressed compared to neutrinos due to helicity considerations. Consider neutrino-electron scattering, the cross section for  $\nu_e + e^-$  is given by

$$\frac{d\sigma}{d\Omega} = \left( \frac{G \hbar c}{2\pi} \right)^2 s, \quad (3.6)$$

where  $G$  is the Fermi constant and  $s$  is the center of mass energy squared. The outgoing particles are isotropic since the initial and final spin state of the system is  $J = 0$ . Compare (3.6) with the cross section for  $\bar{\nu}_e + e^-$

$$\frac{d\sigma}{d\Omega} = \left( \frac{G \hbar c}{4\pi} \right)^2 (1 - \cos \theta)^2 s, \quad (3.7)$$

where  $\theta$  is the observed scattering angle of the electron. Since the total spin of the  $\bar{\nu}_e + e^-$  system is  $J = 1$  with the  $J_z = 1$ , the antineutrino is preferentially forward scattered.

507 Integrating over all angles, the cross sections come out to

$$\sigma(\bar{\nu}_e + e^-) = \frac{1}{3}\sigma(\nu_e + e^-).$$

508 The factor 1/3 arises from the fact that angular momentum conservation forbids the  $J_z = -1$   
509 and 0 states for  $\bar{\nu}_e + e^-$  scattering. The same 1/3 factor arises with  $e^-$  replaced with quarks.  
510 Therefore the cross sections for neutrinos are larger than antineutrinos.

### 511 **$\nu_\mu$ Background CC Inclusive in RHC Cuts**

- 512 • The highest momentum negative track (HMNT) is the lepton candidate  
513 • The HMNT must be the highest momentum track (HMT)

514 As discussed in section 3.2.3 on page 29, the RHC neutrino beam has a significant wrong-  
515 sign  $\nu_\mu$  background. The selection of the HMNT is designed to select the negatively charged  
516 muons. To prevent selecting the antineutrino events, the HMNT must also be the HMT.  
517 The event is rejected if there is no negatively charged track. If there are both positively and  
518 negatively charged tracks, the HMT cut discriminates if the event originates from a  $\nu_\mu$  or  
519  $\bar{\nu}_\mu$ .

## 520 **3.3 Sample Kinematics and Validation**

521 This section examines the kinematics for each of selections while differentiating between  
522 water-in and water-out mode. The selection cuts were implemented in Psyche which is the  
523 software interface that BANFF uses to select events. An analysis of the kinematics are care-  
524 fully cross validated with the same selection cuts in the T2K high level analysis framework  
525 called Highland. Comparing the results between Highland and Psyche is important since  
526 they are complementary frameworks within T2K. The data sets used in this analysis are

Run Period	Horn Current	PØD Status	Data POT ( $\times 10^{20}$ )	MC POT ( $\times 10^{20}$ )
2	+250 kA	Water	0.4339	12.03
		Air	0.3591	9.239
3b	+205 kA		0.2172	4.478
3c	+250 kA		1.364	26.32
4			1.782	34.99
		Water	1.642	34.97
5c	-250 kA		0.4346	22.77
6b		Air	1.288	14.17
6c			0.5058	5.275
6d			0.7753	6.884
6e			0.8479	8.594
7b		Water	2.436	33.70
8	+250 kA		1.580	26.46
		Air	4.148	36.06
Sand	FHC		-	11.19
Sand	RHC		-	12.92
2, 3b, 3c, 4, 8	FHC	Air	7.872	79.18
		Water	3.657	73.47
6b, 6c, 6d, 6e	RHC	Air	3.417	34.92
		Water	2.871	56.48

Table 3.2: T2K MC and data POT divided by run periods. The bottom four rows are the aggregated periods grouped by horn current and PØD status which is how the data analysis is performed.

527 runs 2-8 in both PØD water-in and water-out (air) modes as shown in Table 3.2.

### 528 3.4 PØD Water-Out Samples

529 This section shows the kinematic distributions for the PØD water-out samples. First an  
 530 examination of the CC Inclusive samples and the effects of the systematic weights will be  
 531 explored. The samples are then examined as CC 1-track and CC N-tracks.

532 **3.4.1 CC Inclusive**

533 The CC Inclusive sample cuts are discussed 3.2.1. Since both flux and systematic weights  
534 are applied to all MC events in BANFF, it is important to validate the event weights. Using  
535 neither set of weights is referred to as the nominal MC.

536 **3.4.1.1  $\nu_\mu$  Selection in FHC Mode:** Shown in Figures 3.1 to 3.7 are the momentum  
537 and  $\cos\theta$  distributions for  $\nu_\mu$ CC Inclusive events in FHC mode. There are three pairs of  
538  $P, \theta$  figures with the same truth information break down accompanied by one of neutrino  
539 energy. The truth information categories are lepton candidate particle, NEUT reaction, and  
540 topology. Each figure consists of a set of four sub-figures which illustrate the application of  
541 flux and detector systematic weights.

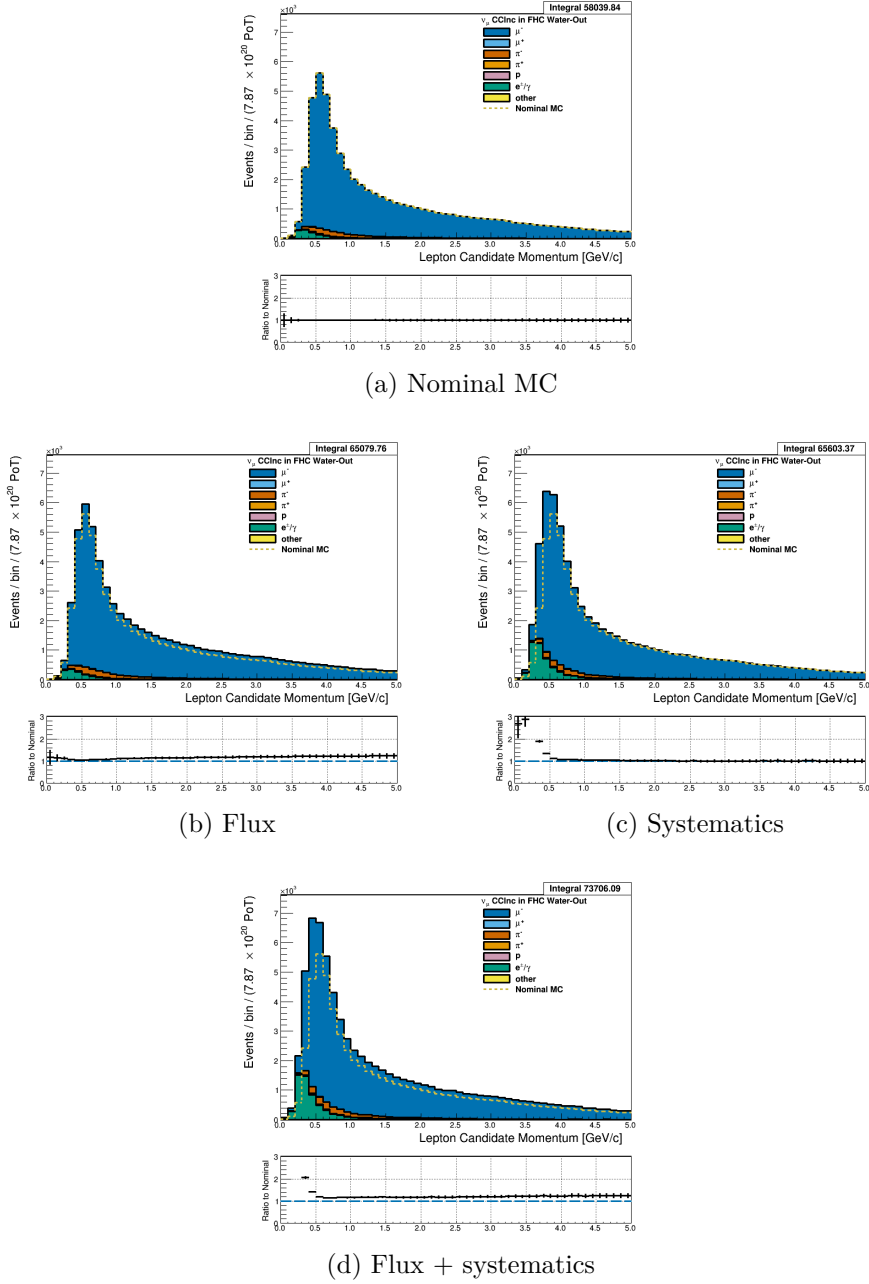


Figure 3.1: Reconstructed lepton candidate momentum separated by true particle species for FHC  $\nu_\mu$  CC Inc. events occurring in the PØD in water-out mode. (a) The nominal MC prediction without any weights applied. (b) The flux tuning are applied. (c) The systematic weighting are applied. (d) Both flux and systematic weighting are applied.

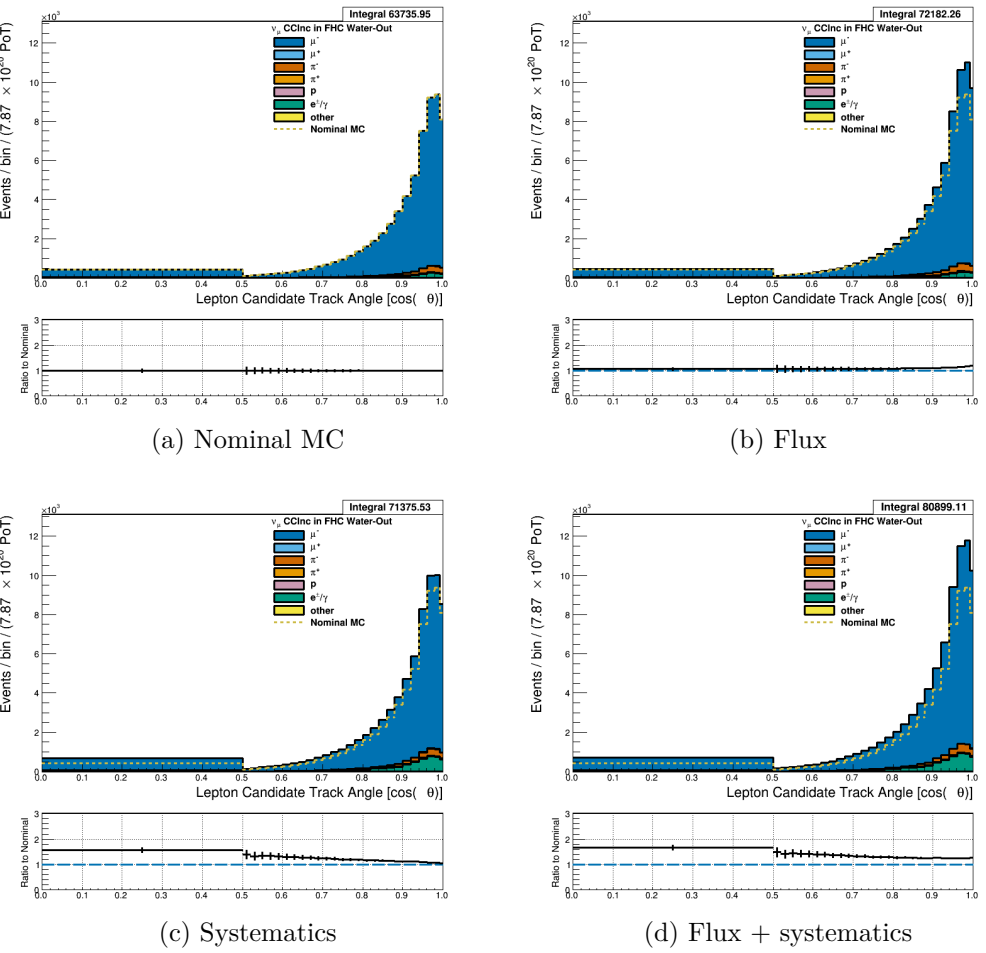


Figure 3.2: Reconstructed lepton candidate angle separated by true particle species for FHC  $\nu_\mu$  CC Inc. events occurring in the PØD in water-out mode. (a) The nominal MC prediction without any weights applied. (b) The flux tuning are applied. (c) The systematic weighting are applied. (d) Both flux and systematic weighting are applied.

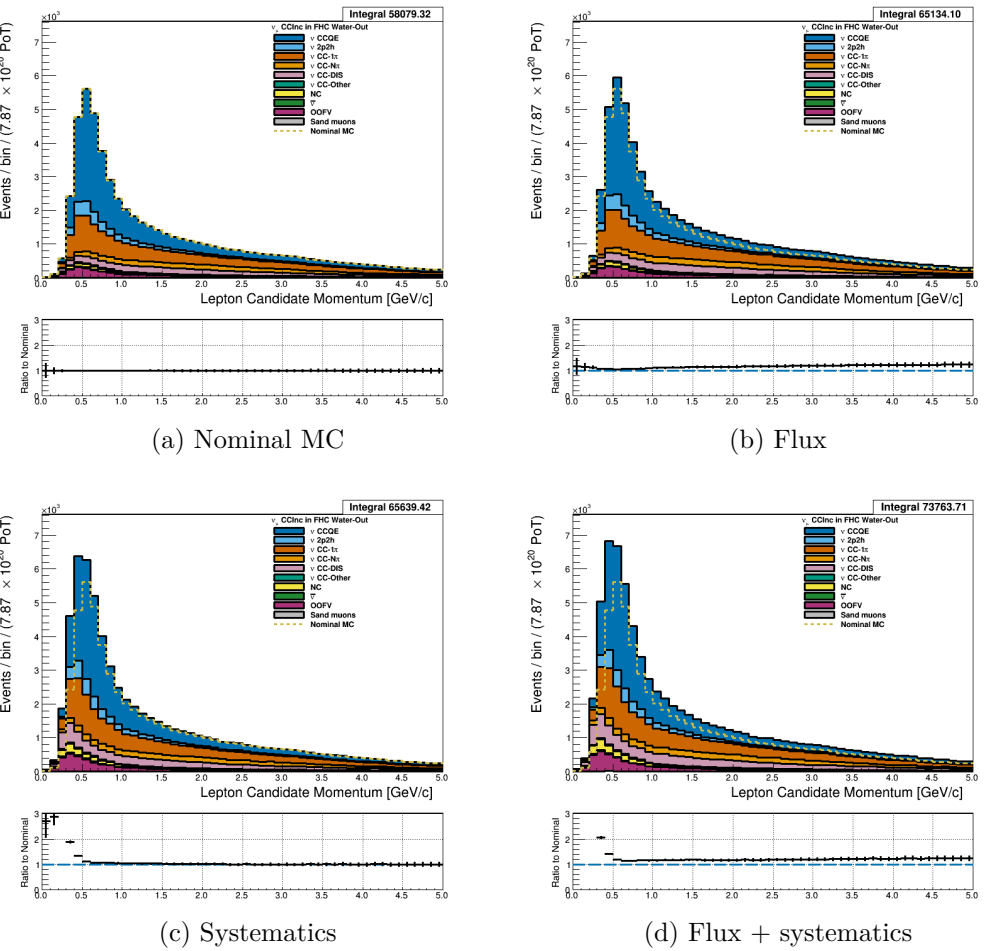


Figure 3.3: Reconstructed lepton candidate momentum separated by NEUT model interaction mode for FHC  $\nu_\mu$  CC Inc. events occurring in the PØD in water-out mode. (a) The nominal MC prediction without any weights applied. (b) The flux tuning are applied. (c) The systematic weighting are applied. (d) Both flux and systematic weighting are applied.

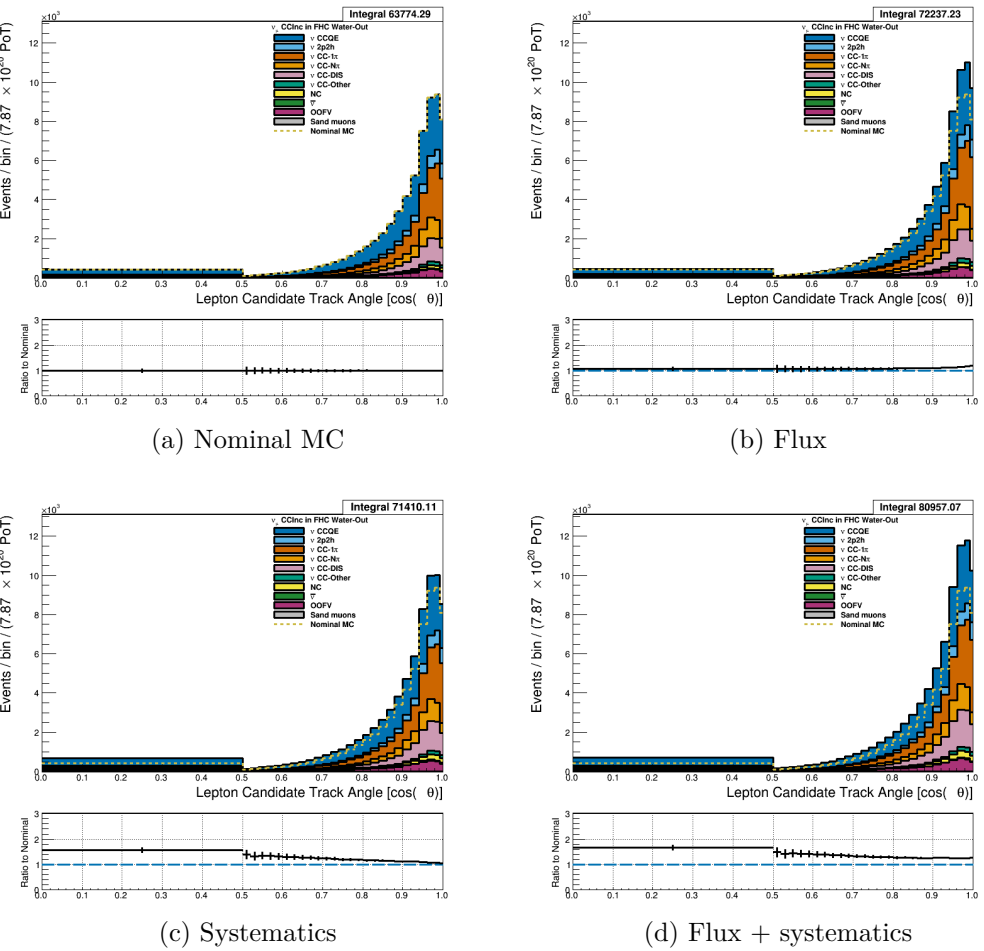


Figure 3.4: Reconstructed lepton candidate  $\cos\theta$  separated by NEUT model interaction mode for FHC  $\nu_\mu$  CC Inc. events occurring in the PØD in water-out mode. (a) The nominal MC prediction without any weights applied. (b) The flux tuning are applied. (c) The systematic weighting are applied. (d) Both flux and systematic weighting are applied.

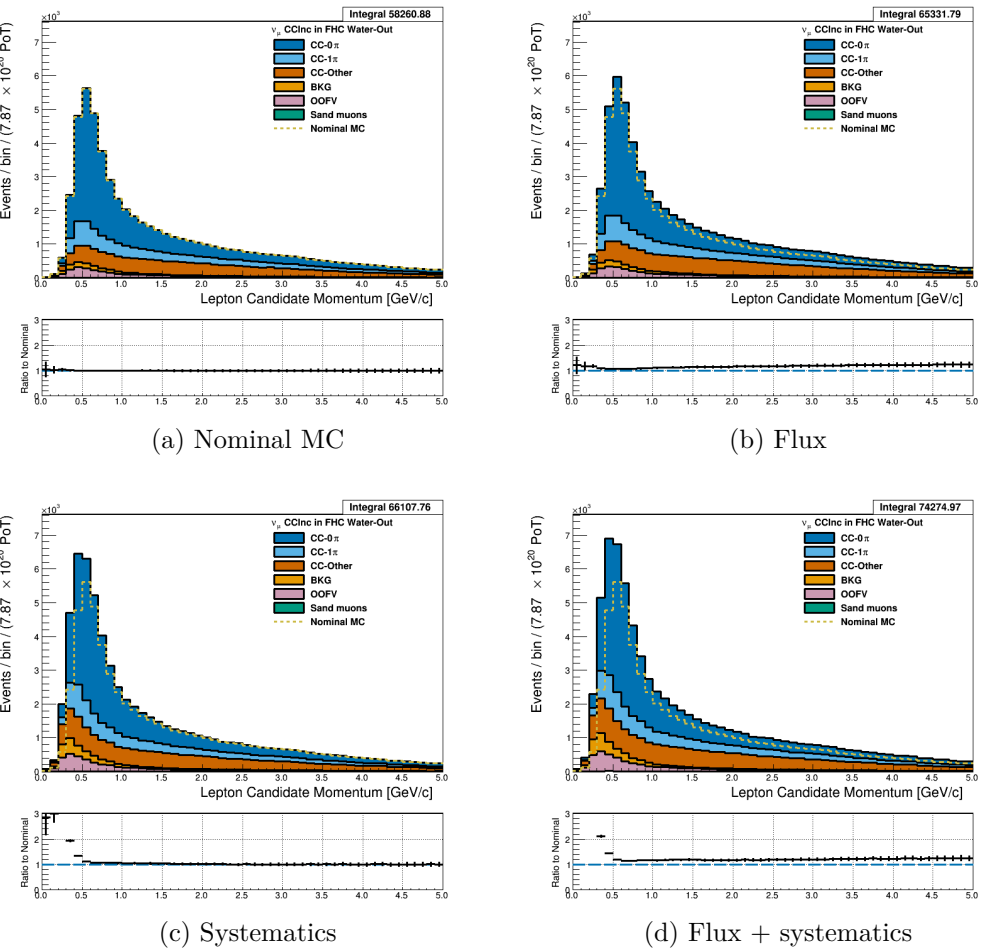


Figure 3.5: Reconstructed lepton candidate momentum separated by topology for FHC  $\nu_\mu$  CC Inc. events occurring in the PØD in water-out mode. (a) The nominal MC prediction without any weights applied. (b) The flux tuning are applied. (c) The systematic weighting are applied. (d) Both flux and systematic weighting are applied.

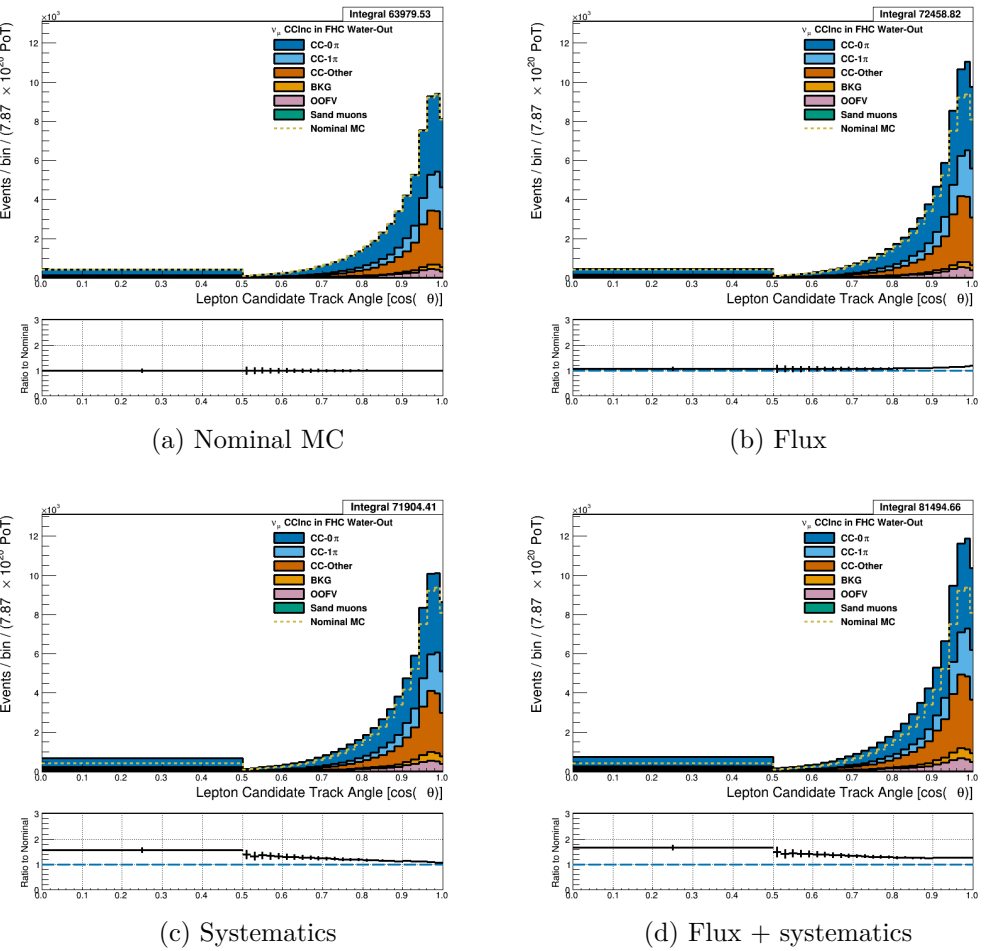


Figure 3.6: Reconstructed lepton candidate  $\cos \theta$  separated by topology for FHC  $\nu_\mu$  CC Inc. events occurring in the PØD in water-out mode. (a) The nominal MC prediction without any weights applied. (b) The flux tuning are applied. (c) The systematic weighting are applied. (d) Both flux and systematic weighting are applied.

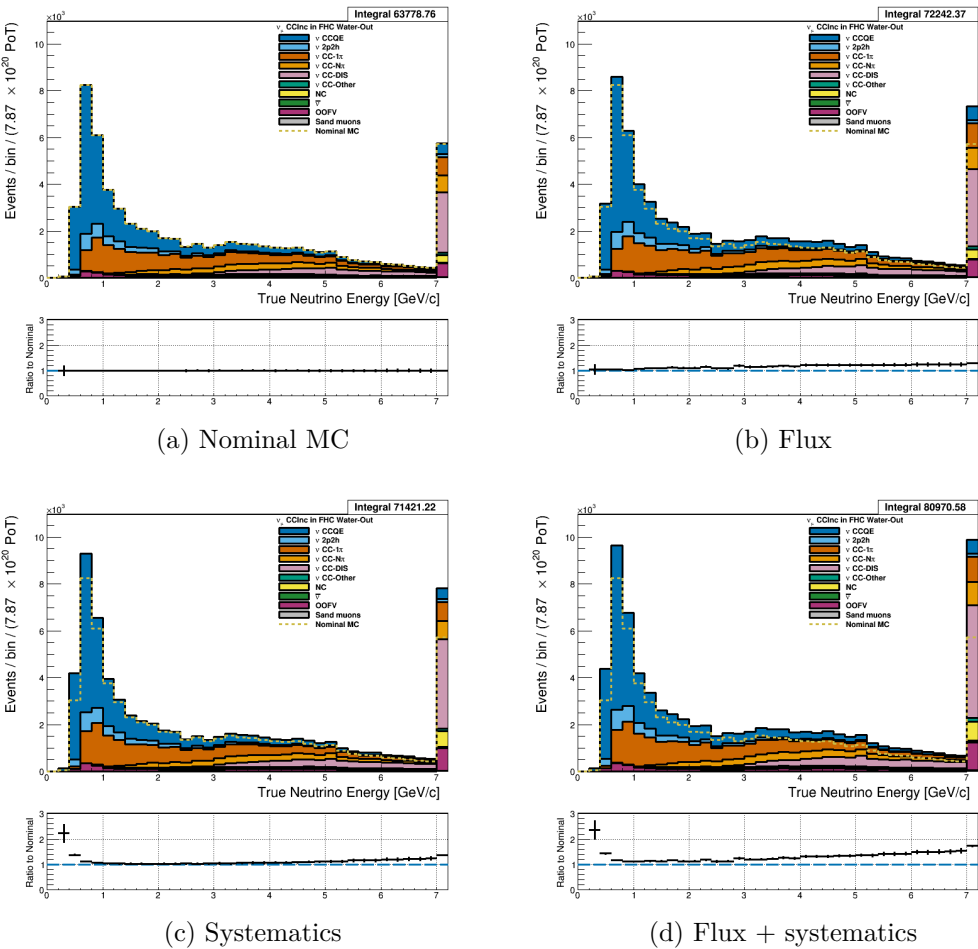


Figure 3.7: True neutrino energy associated with the lepton candidate separated by NEUT model interaction mode for FHC  $\nu_\mu$  CC Inc. events occurring in the PØD in water-out mode. (a) The nominal MC prediction without any weights applied. (b) The flux tuning are applied. (c) The systematic weighting are applied. (d) Both flux and systematic weighting are applied.

**3.4.1.2  $\bar{\nu}_\mu$  Selection in RHC Mode:** Shown in Figures 3.8 to 3.14 for  $\bar{\nu}_\mu$ CC Inclusive events in RHC mode. There are three pairs of  $P, \theta$  figures with the same truth information break down accompanied by one of neutrino energy. The truth information categories are lepton candidate particle, NEUT reaction, and topology. Each figure consists of a set of four sub-figures which illustrate the application of flux and detector systematic weights.

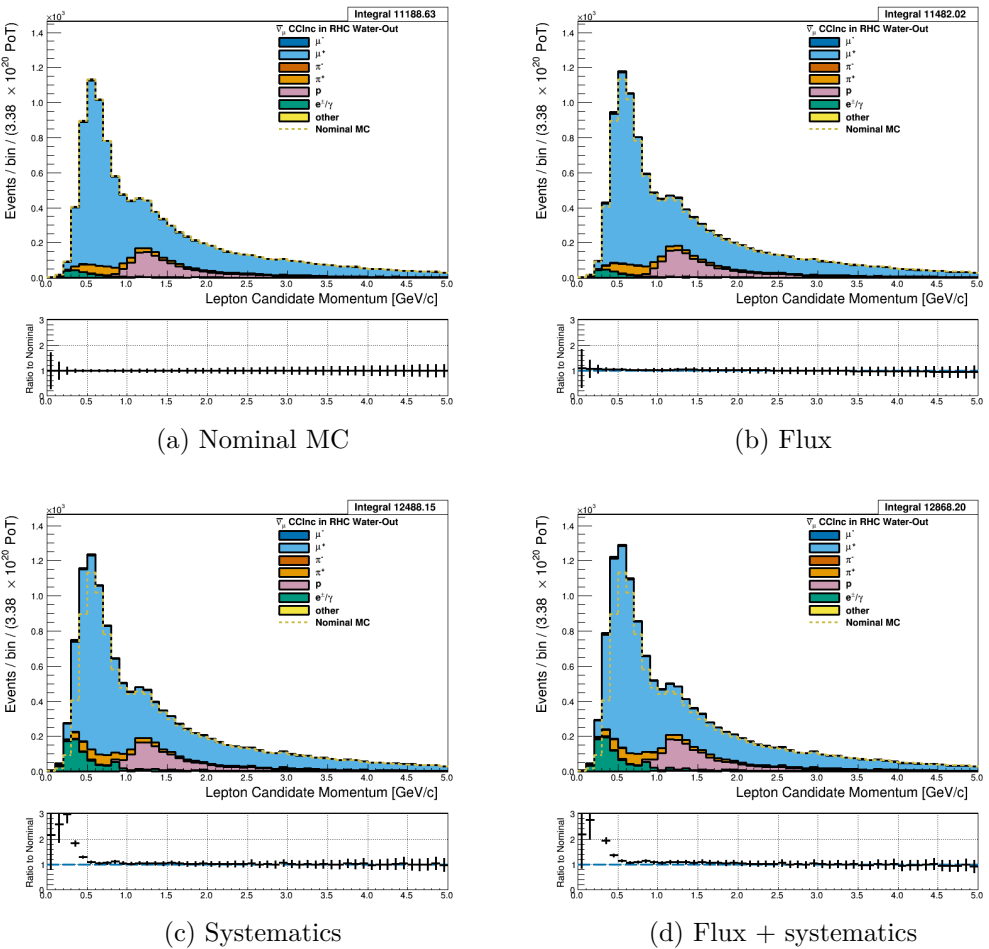


Figure 3.8: Reconstructed lepton candidate momentum separated by true particle species for RHC  $\bar{\nu}_\mu$  CC Inc. events occurring in the PØD in water-out mode. Reconstructed lepton candidate angle separated by true particle species for RHC  $\bar{\nu}_\mu$  CC Inc. events occurring in the PØD in water-in mode. (a) The nominal MC prediction without any weights applied. (b) The flux tuning are applied. (c) The systematic weighting are applied. (d) Both flux and systematic weighting are applied.

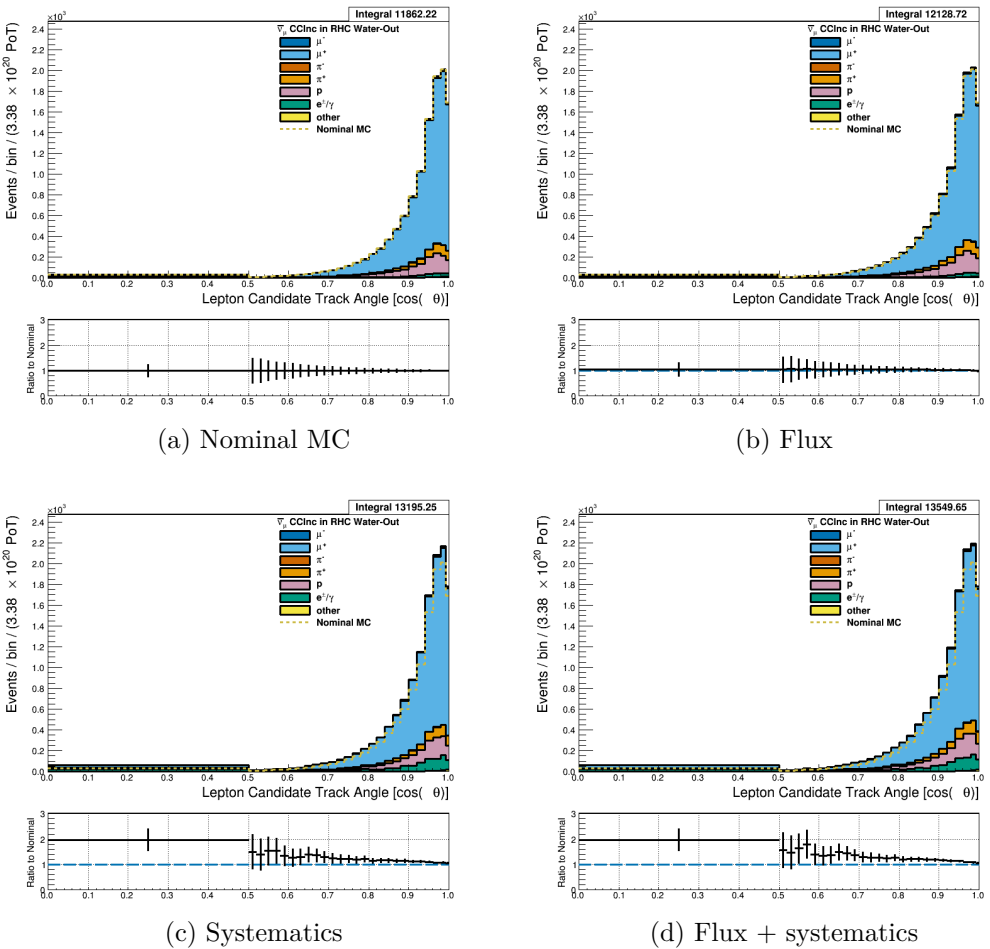


Figure 3.9: Reconstructed lepton candidate angle separated by true particle species for RHC  $\bar{\nu}_\mu$  CC Inc. events occurring in the PØD in water-out mode. (a) The nominal MC prediction without any weights applied. (b) The flux tuning are applied. (c) The systematic weighting are applied. (d) Both flux and systematic weighting are applied.

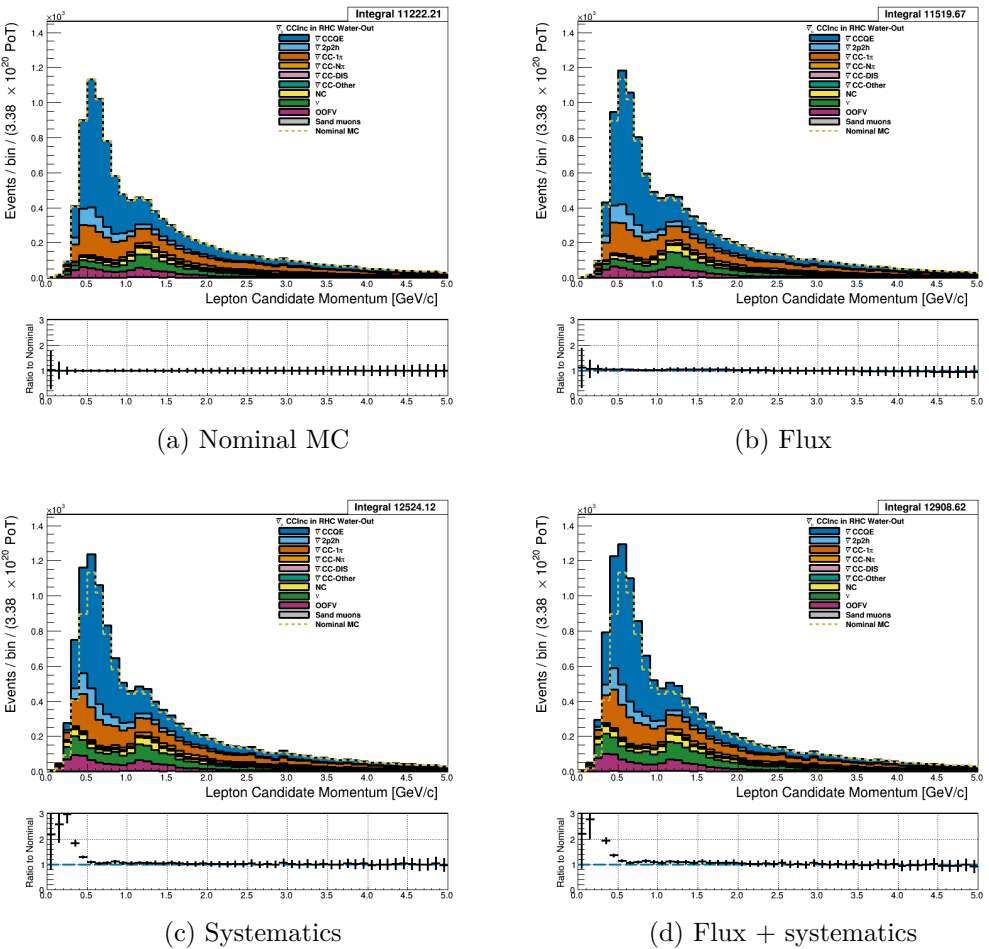


Figure 3.10: Reconstructed lepton candidate momentum separated by NEUT model interaction mode for RHC  $\bar{\nu}_\mu$  CC Inc. events occurring in the PØD in water-out mode. (a) The nominal MC prediction without any weights applied. (b) The flux tuning are applied. (c) The systematic weighting are applied. (d) Both flux and systematic weighting are applied.

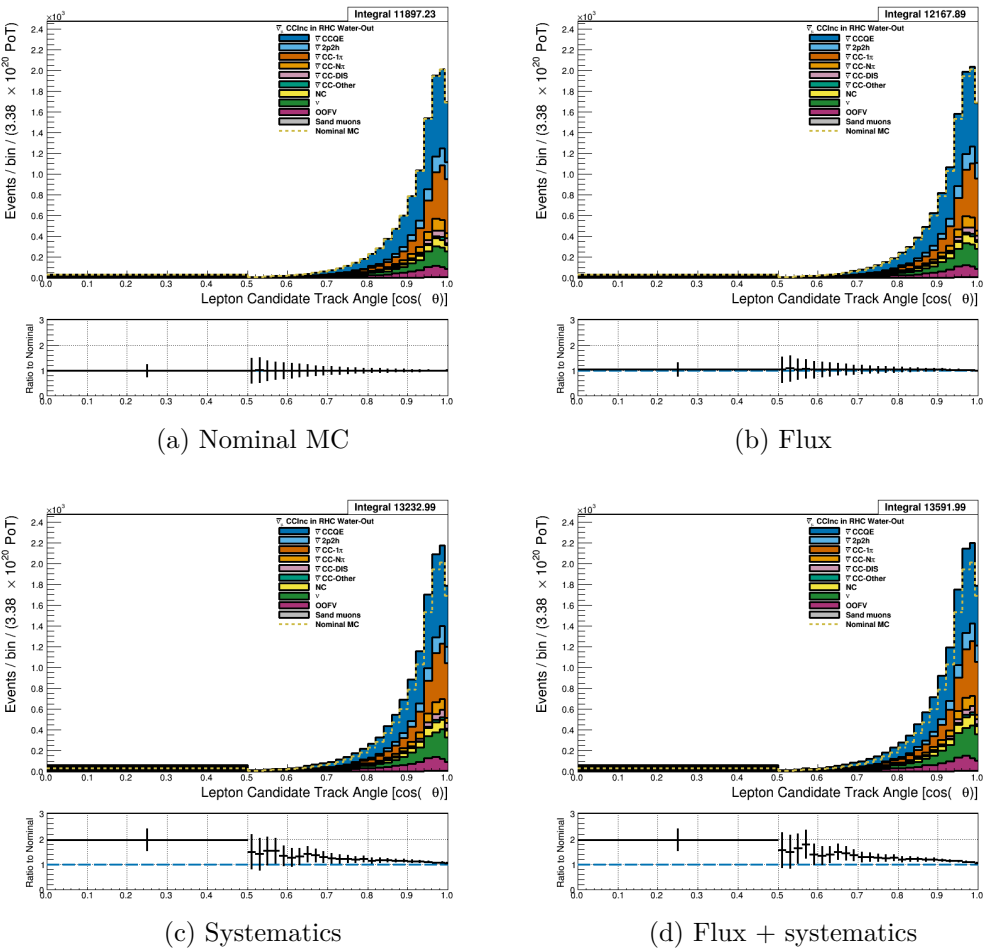


Figure 3.11: Reconstructed lepton candidate  $\cos \theta$  separated by NEUT model interaction mode for RHC  $\bar{\nu}_\mu$  CC Inc. events occurring in the PØD in water-out mode. (a) The nominal MC prediction without any weights applied. (b) The flux tuning are applied. (c) The systematic weighting are applied. (d) Both flux and systematic weighting are applied.

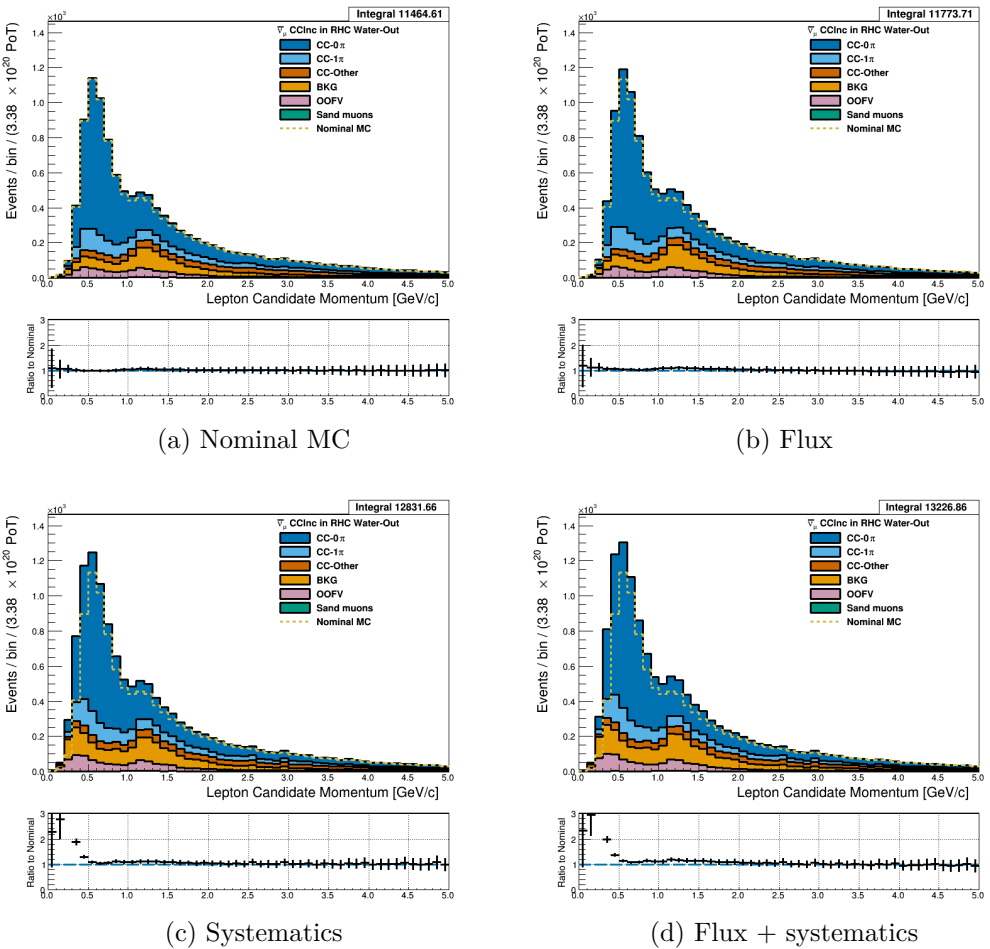


Figure 3.12: Reconstructed lepton candidate momentum separated by topology for RHC  $\bar{\nu}_\mu$  CC Inc. events occurring in the PØD in water-out mode. (a) The nominal MC prediction without any weights applied. (b) The flux tuning are applied. (c) The systematic weighting are applied. (d) Both flux and systematic weighting are applied.

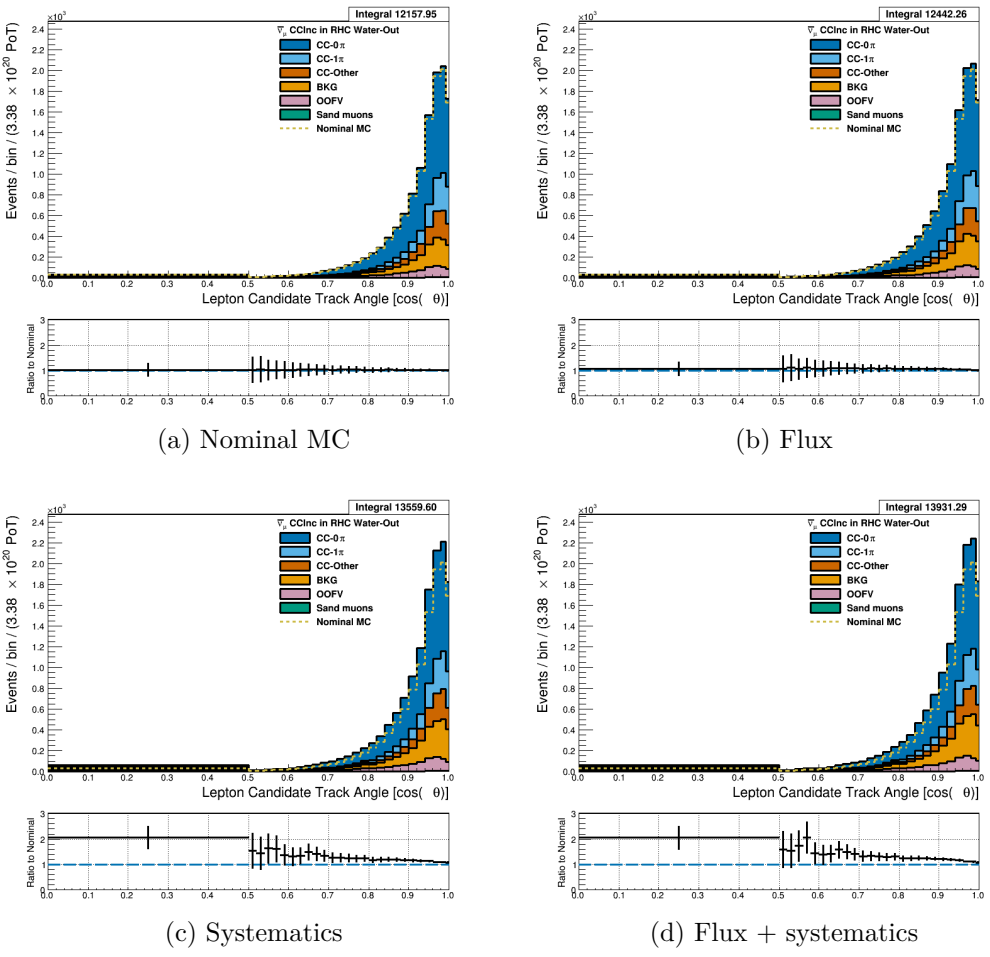


Figure 3.13: Reconstructed lepton candidate  $\cos \theta$  separated by topology for RHC  $\bar{\nu}_\mu$  CC Inc. events occurring in the PØD in water-out mode. (a) The nominal MC prediction without any weights applied. (b) The flux tuning are applied. (c) The systematic weighting are applied. (d) Both flux and systematic weighting are applied.

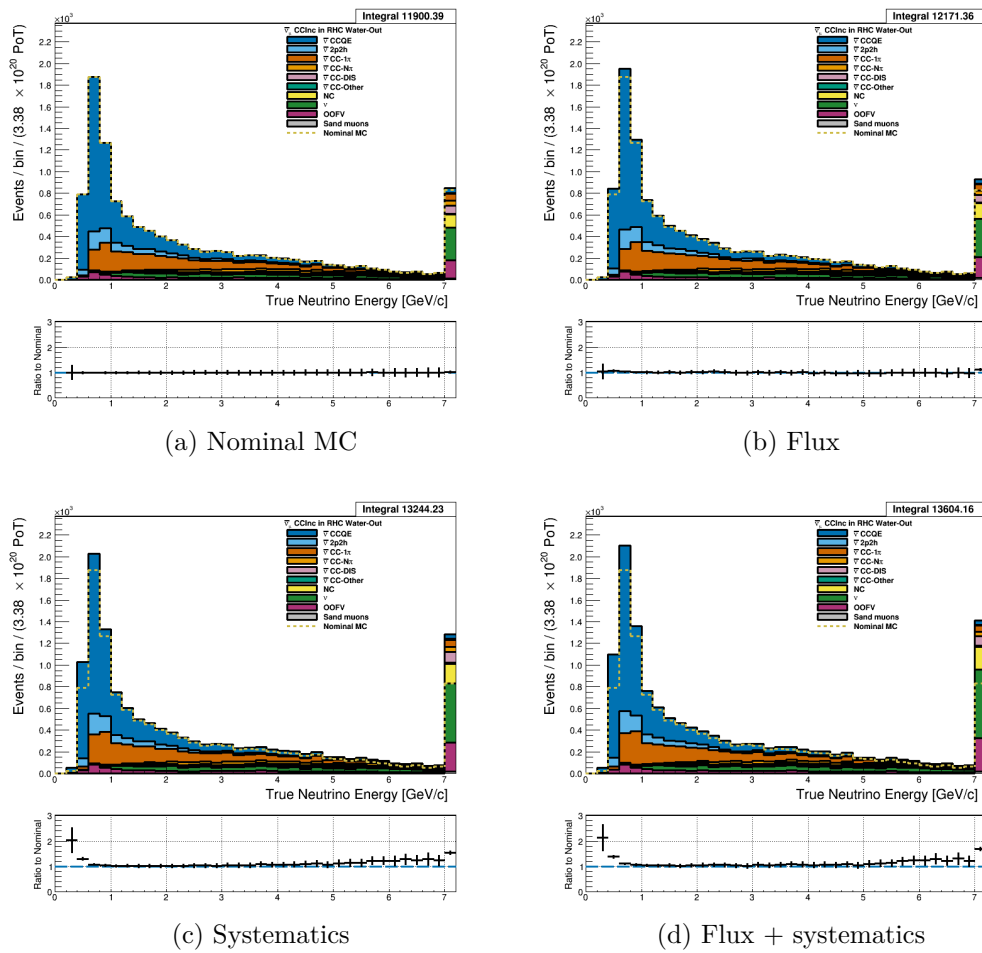


Figure 3.14: True neutrino energy associated with the lepton candidate separated by NEUT model interaction mode for RHC  $\bar{\nu}_\mu$  CC Inc. events occurring in the PØD in water-out mode. (a) The nominal MC prediction without any weights applied. (b) The flux tuning are applied. (c) The systematic weighting are applied. (d) Both flux and systematic weighting are applied.

547 **3.4.1.3  $\nu_\mu$  Background Selection in RHC Mode:** Shown in Figures 3.15, 3.16 and 3.19

548 to 3.21 and ????

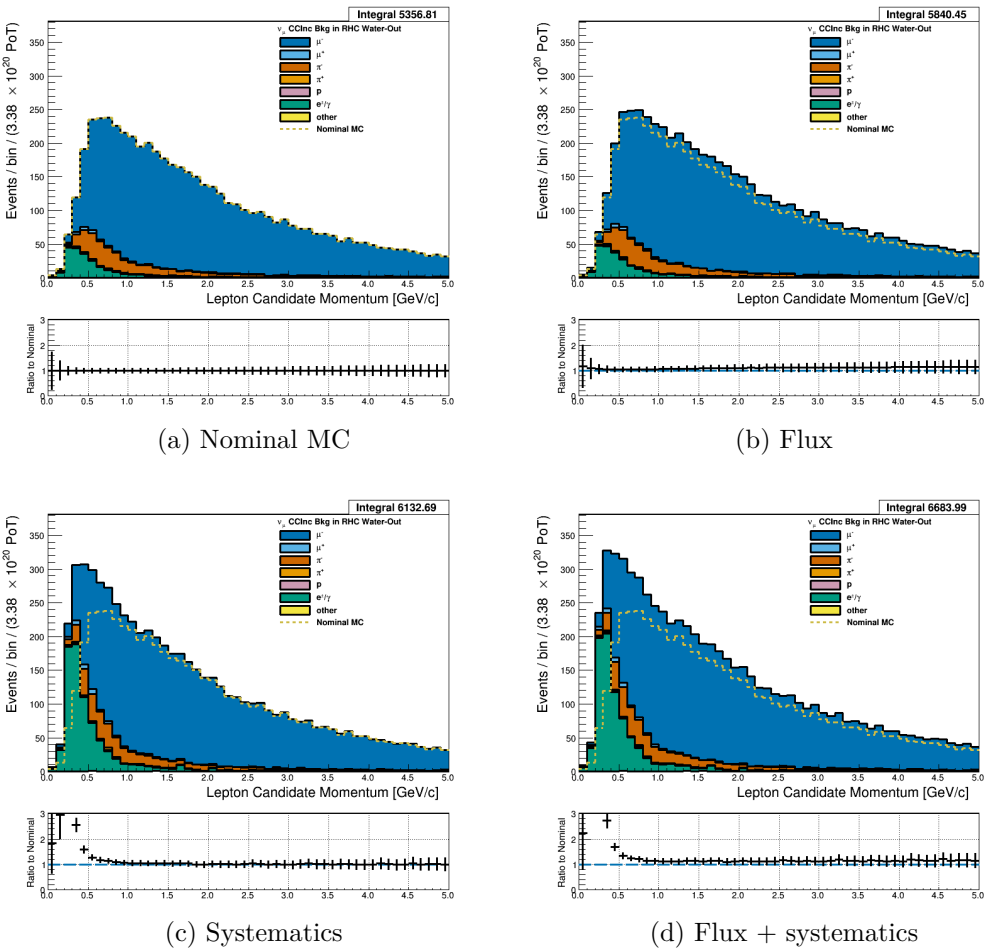


Figure 3.15: Reconstructed lepton candidate momentum separated by true particle species for RHC  $\nu_\mu$  CC Inc. events occurring in the PØD in water-out mode. (a) The nominal MC prediction without any weights applied. (b) The flux tuning are applied. (c) The systematic weighting are applied. (d) Both flux and systematic weighting are applied.

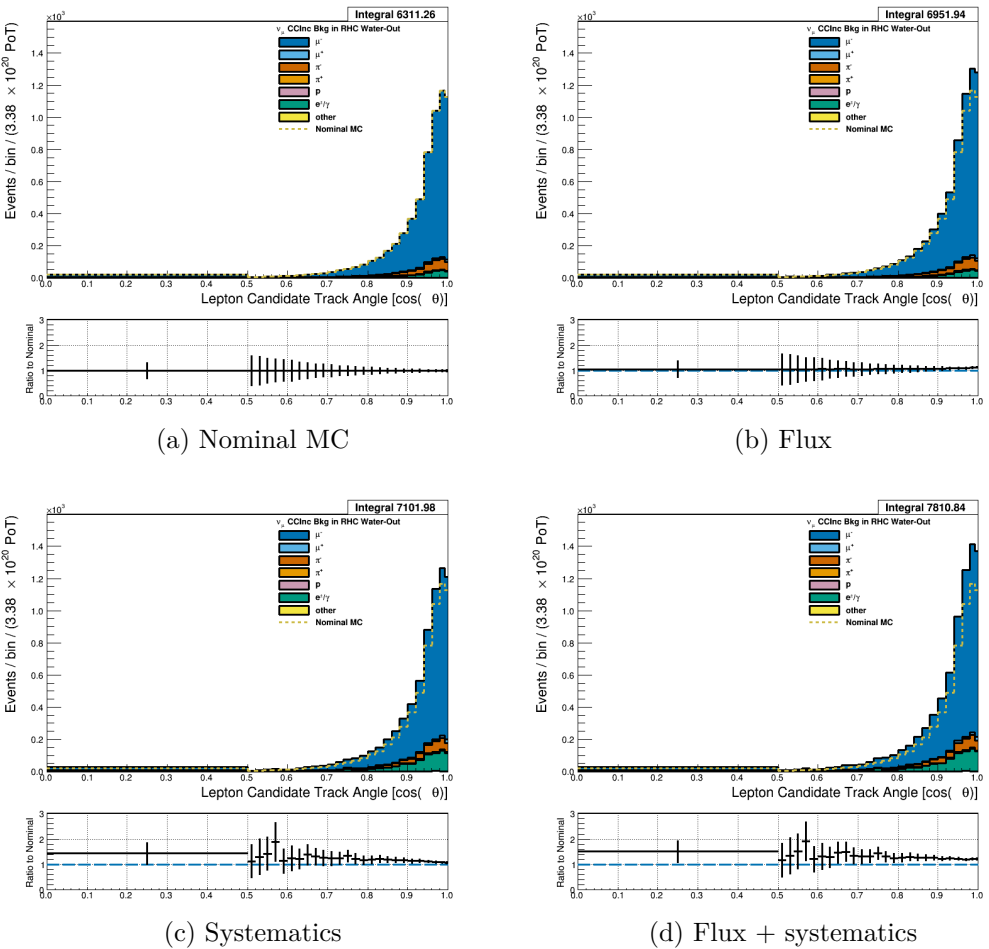


Figure 3.16: Reconstructed lepton candidate angle separated by true particle species for RHC  $\nu_\mu$  CC Inc. events occurring in the PØD in water-out mode. (a) The nominal MC prediction without any weights applied. (b) The flux tuning are applied. (c) The systematic weighting are applied. (d) Both flux and systematic weighting are applied.

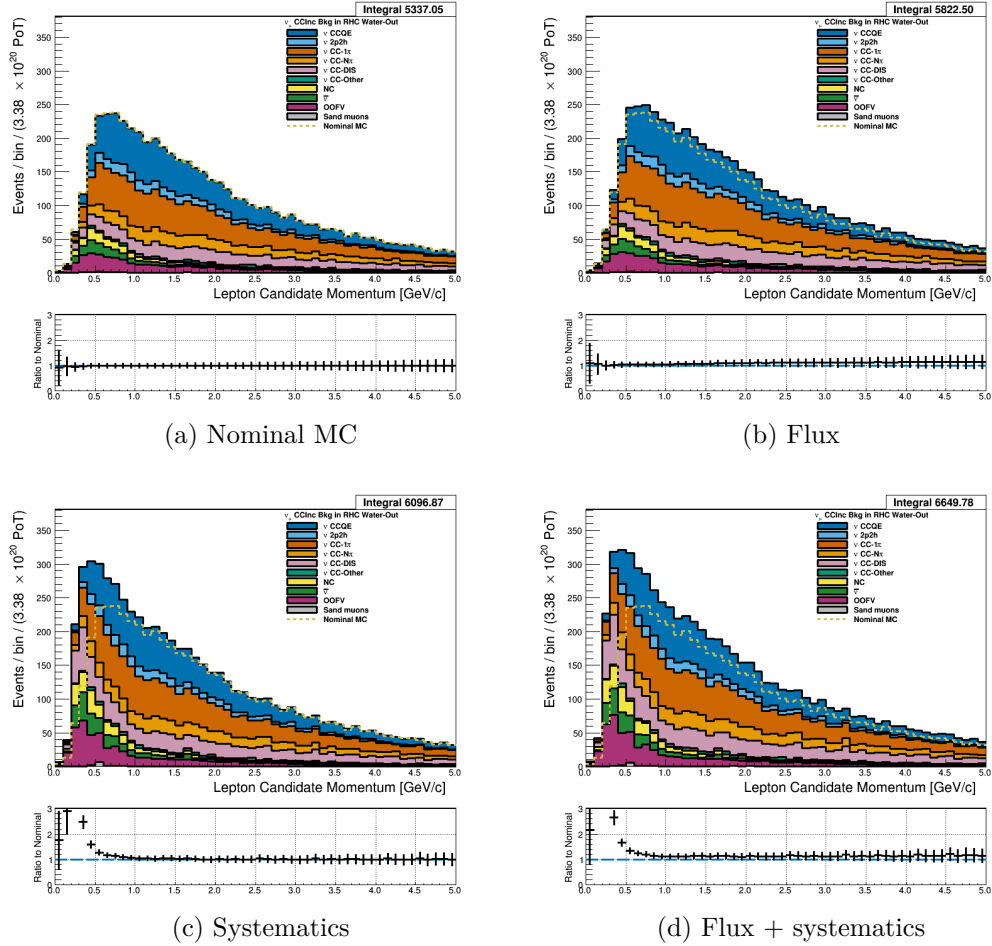


Figure 3.17: Reconstructed lepton candidate momentum separated by NEUT model interaction mode for RHC  $\nu_\mu$  CC Inc. events occurring in the PØD in water-out mode. (a) The nominal MC prediction without any weights applied. (b) The flux tuning are applied. (c) The systematic weighting are applied. (d) Both flux and systematic weighting are applied.

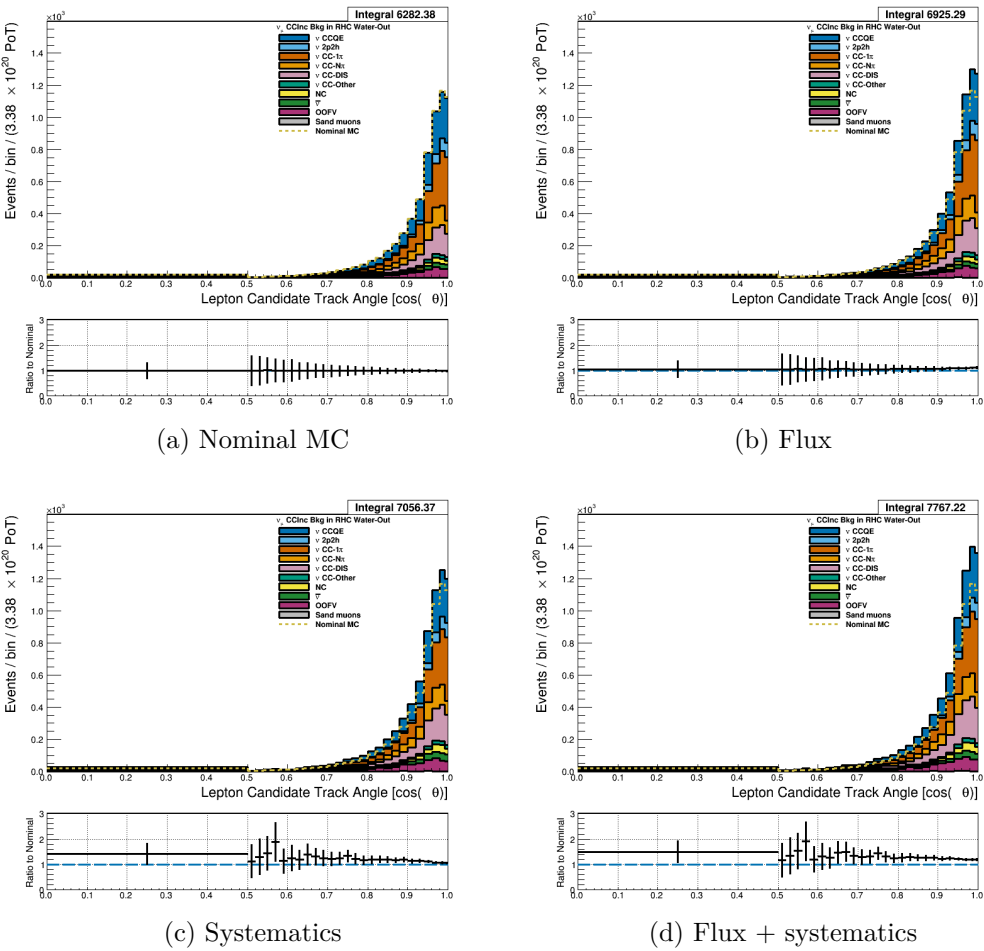


Figure 3.18: Reconstructed lepton candidate  $\cos \theta$  separated by NEUT model interaction mode for FHC  $\nu_\mu$  CC Inc. events occurring in the PØD in water-out mode. (a) The nominal MC prediction without any weights applied. (b) The flux tuning are applied. (c) The systematic weighting are applied. (d) Both flux and systematic weighting are applied.

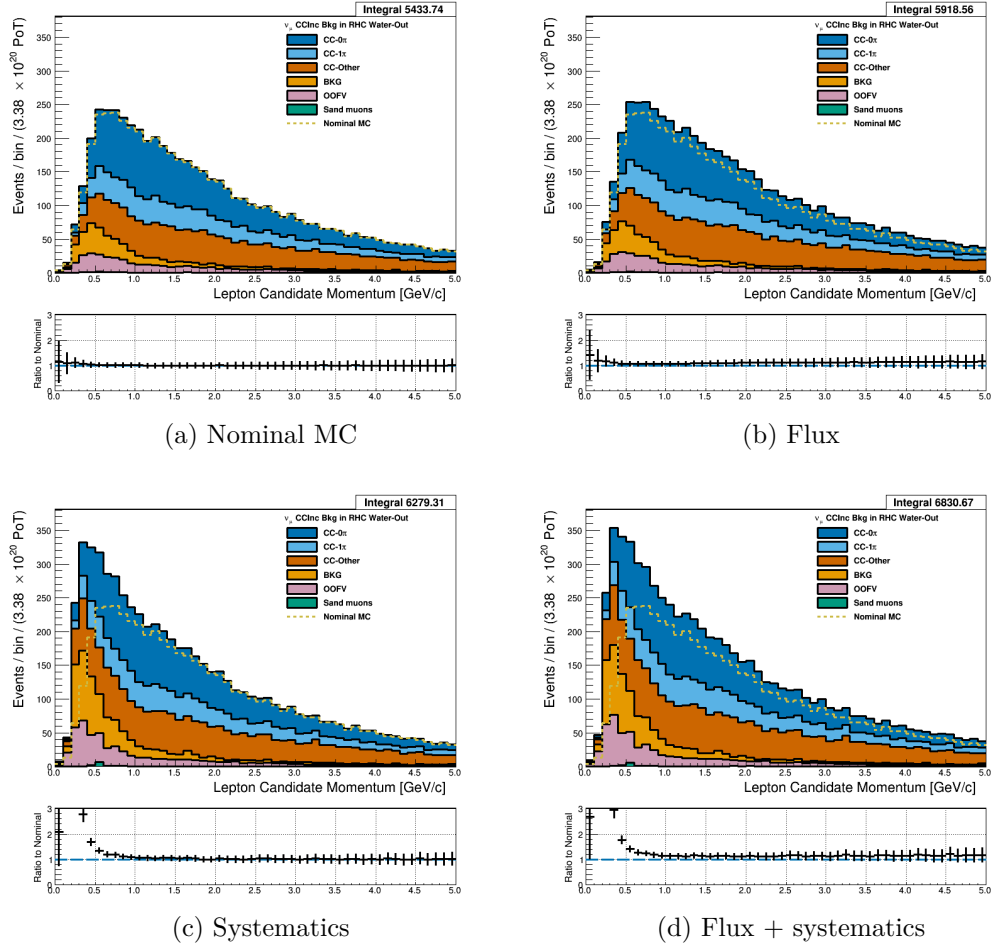


Figure 3.19: Reconstructed lepton candidate momentum separated by topology for FHC  $\nu_\mu$  CC Inc. events occurring in the PØD in water-out mode. (a) The nominal MC prediction without any weights applied. (b) The flux tuning are applied. (c) The systematic weighting are applied. (d) Both flux and systematic weighting are applied.

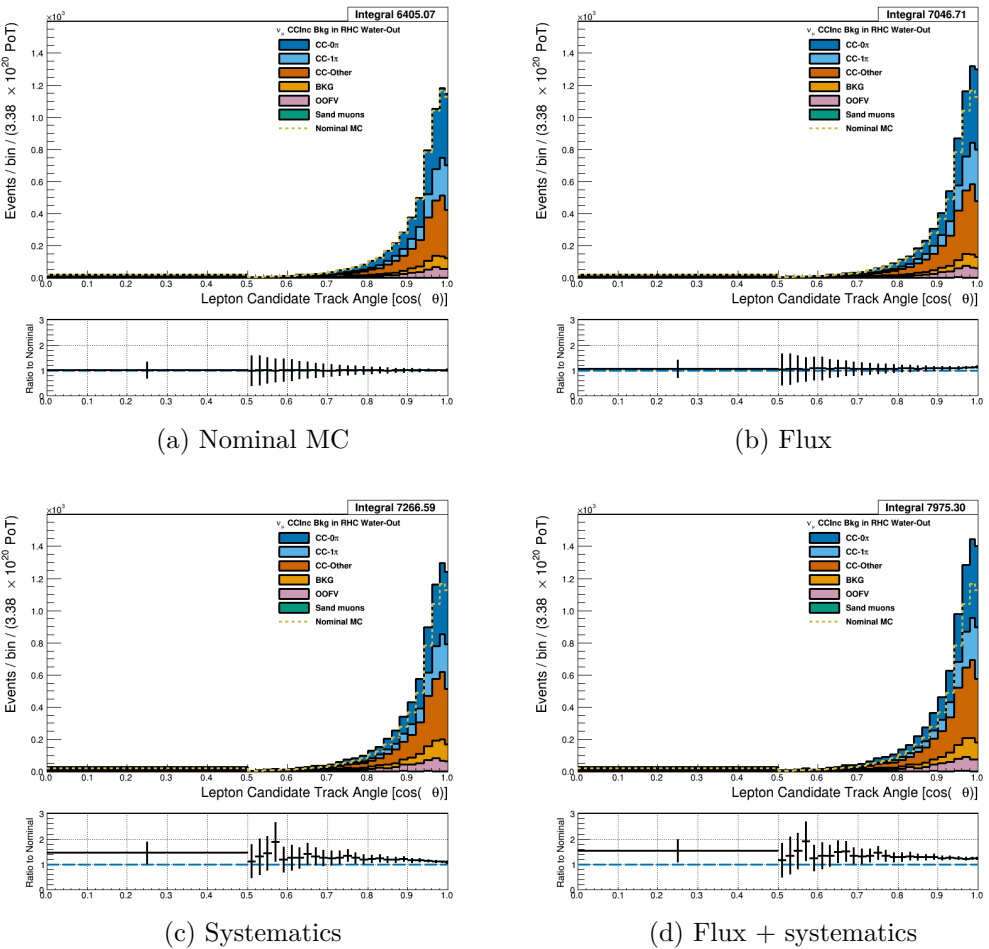


Figure 3.20: Reconstructed lepton candidate  $\cos \theta$  separated by topology for FHC  $\nu_\mu$  CC Inc. events occurring in the PØD in water-out mode. (a) The nominal MC prediction without any weights applied. (b) The flux tuning are applied. (c) The systematic weighting are applied. (d) Both flux and systematic weighting are applied.

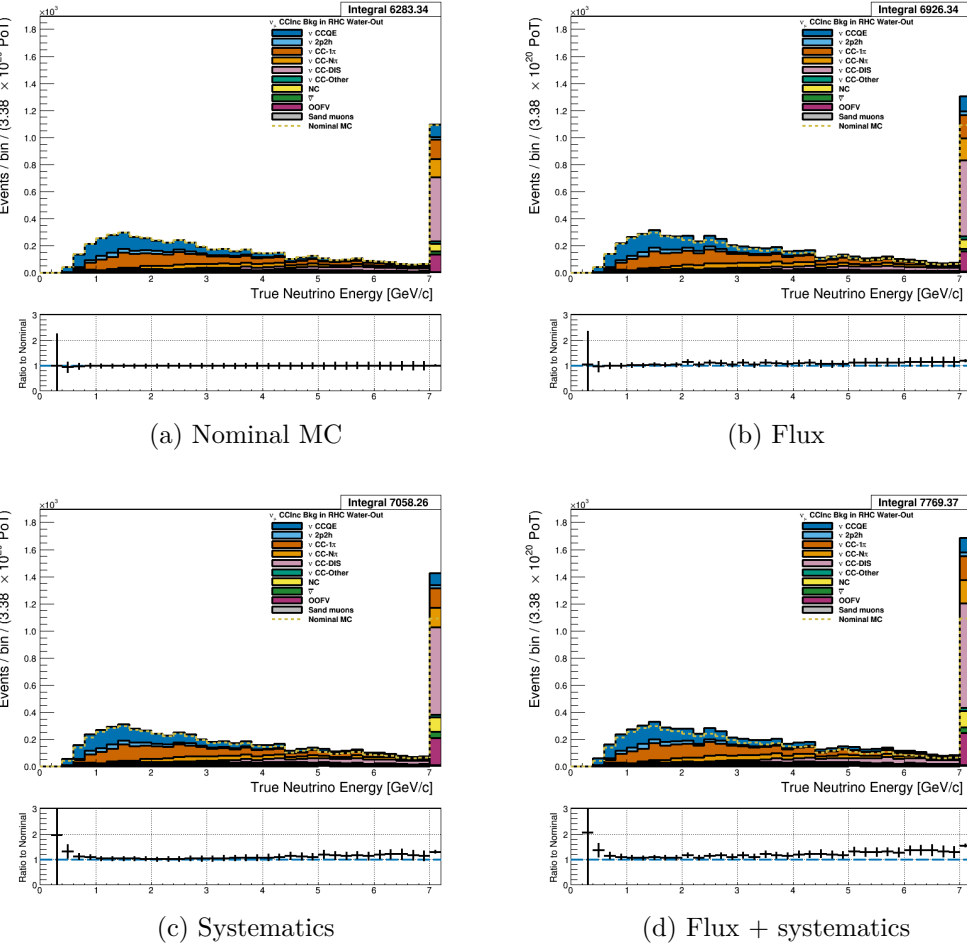


Figure 3.21: True neutrino energy associated with the lepton candidate separated by NEUT model interaction mode for FHC  $\nu_\mu$  CC Inc. events occurring in the PØD in water-out mode. (a) The nominal MC prediction without any weights applied. (b) The flux tuning are applied. (c) The systematic weighting are applied. (d) Both flux and systematic weighting are applied.

### 549 3.4.2 CC 1-Track (CCQE Enhanced)

550 3.4.2.1  $\nu_\mu$  Selection in FHC Mode: Shown in

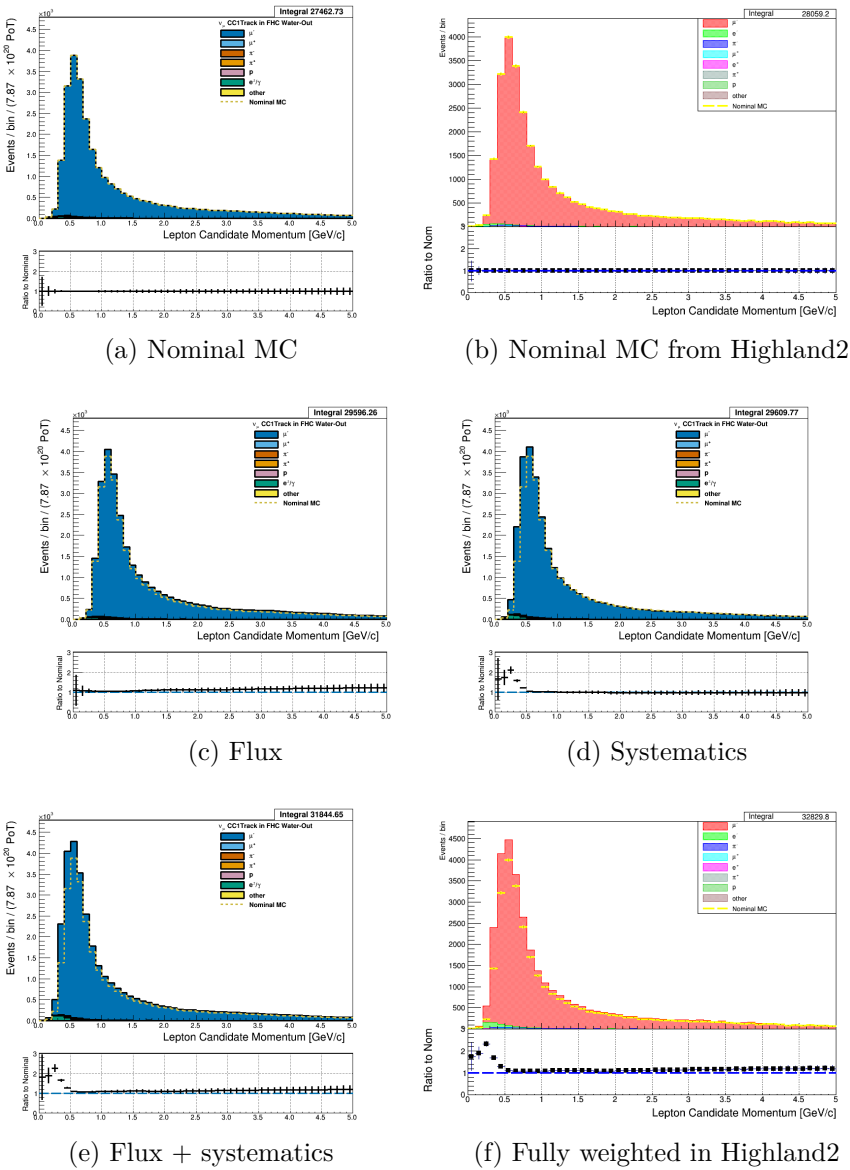


Figure 3.22: Reconstructed lepton candidate momentum separated by true particle species for FHC  $\nu_\mu$  CC 1-Track events occurring in the PØD in water-out mode. (a) The nominal MC prediction without any weights applied. (b) The same POT-normalized plot as (a) using a subset of the water-out MC in Highland. (c) The flux tuning are applied. (d) The systematic weighting are applied. (e) Both flux and systematic weighting are applied. (f) The same POT-normalized plot as (e) using a subset of the water-out MC in Highland. There is a  $\sim 1\%$  difference between Highland2 and BANFF since a subset of the MC was used to generate Highland plots.

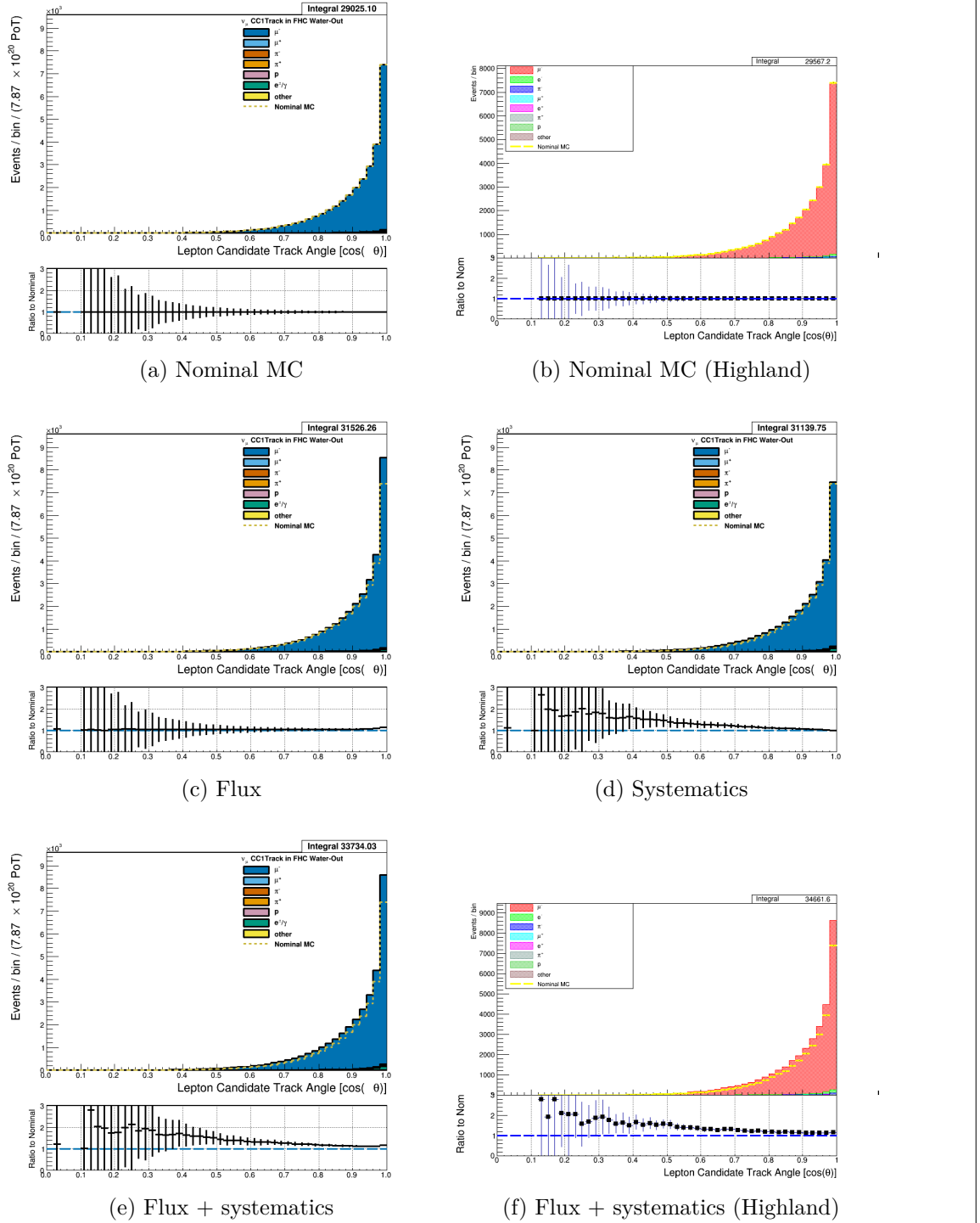


Figure 3.23: Reconstructed lepton candidate angle separated by true particle species for FHC  $\nu_\mu$  CC 1-Track events occurring in the PØD in water-out mode. (a) The nominal MC prediction without any weights applied. (b) The same POT-normalized plot as (a) using a subset of the water-out MC in Highland. (c) The flux tuning are applied. (d) The systematic weighting are applied. (e) Both flux and systematic weighting are applied. (f) The same POT-normalized plot as (e) using a subset of the water-out MC in Highland. There is a ~1% difference between Highland2 and BANFF since a subset of the MC was used to generate Highland plots.

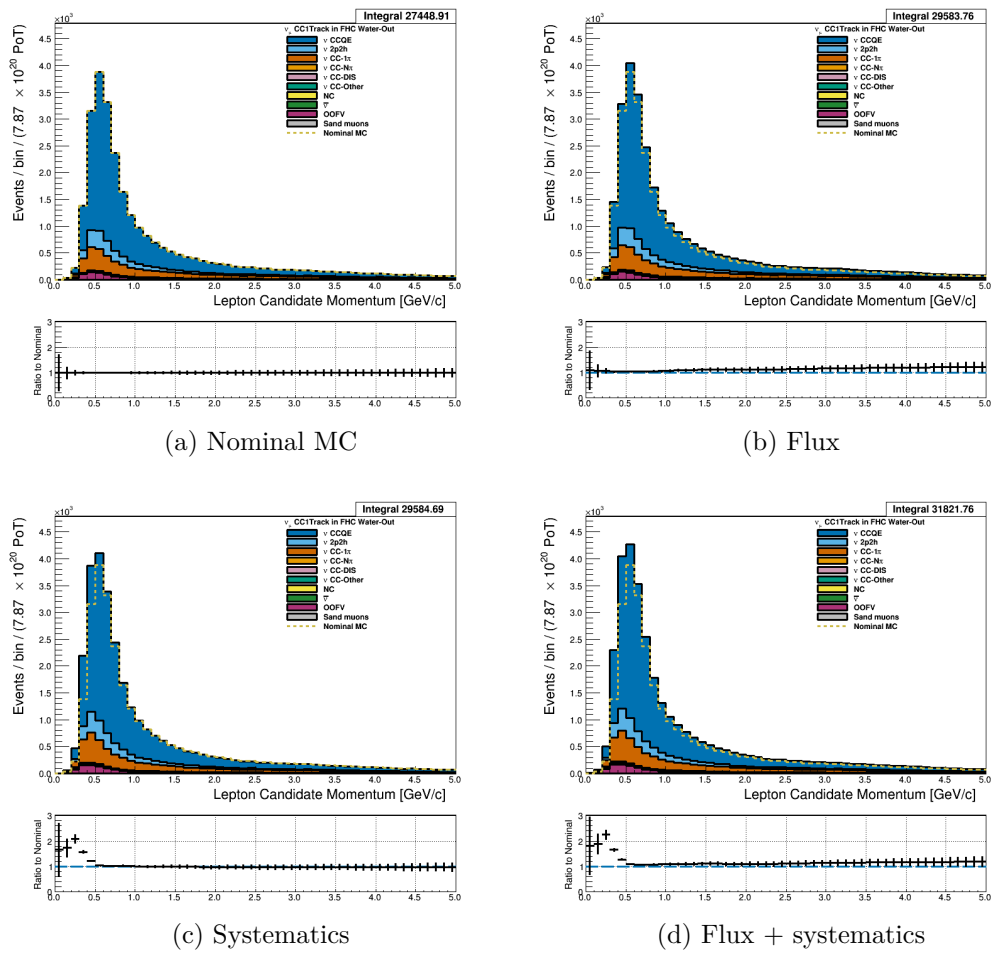


Figure 3.24: Reconstructed lepton candidate momentum separated by NEUT model interaction mode for FHC  $\nu_\mu$  CC 1-Track events occurring in the PØD in water-out mode. (a) The nominal MC prediction without any weights applied. (b) The flux tuning are applied. (c) The systematic weighting are applied. (d) Both flux and systematic weighting are applied.

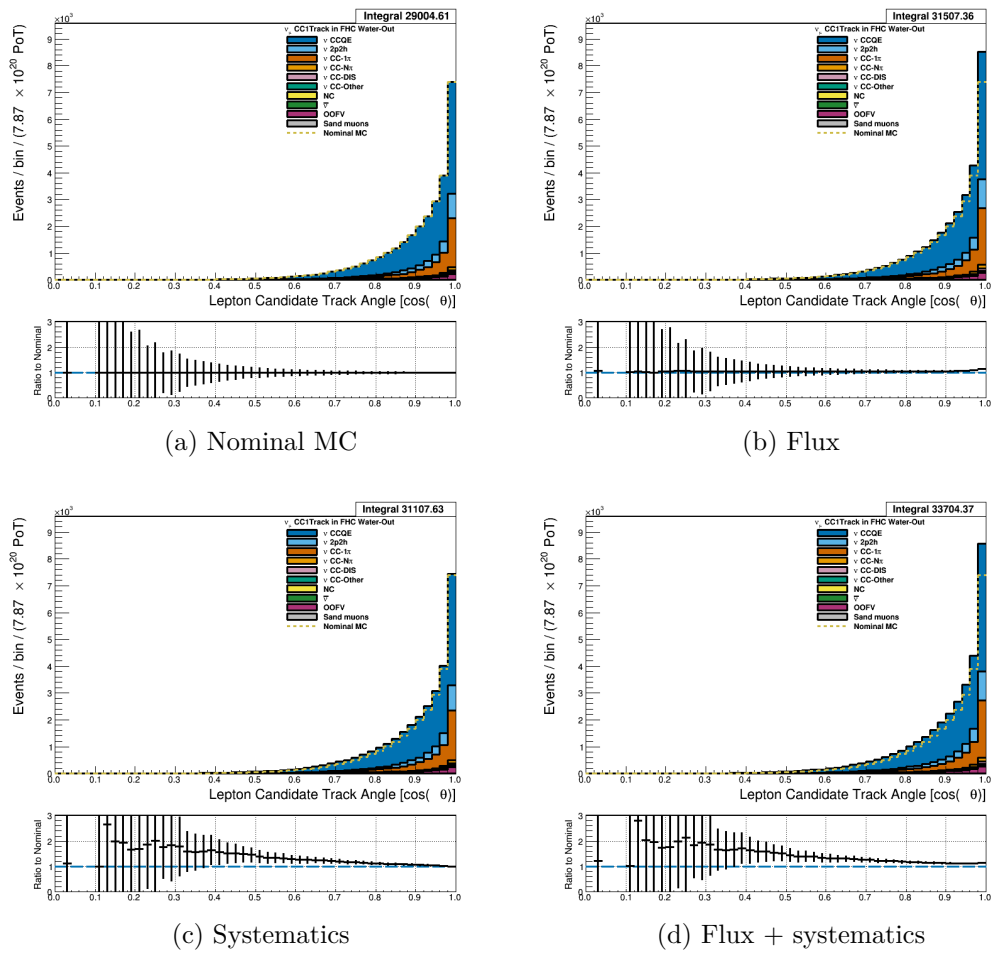


Figure 3.25: Reconstructed lepton candidate  $\cos \theta$  separated by NEUT model interaction mode for FHC  $\nu_\mu$  CC 1-Track events occurring in the PØD in water-out mode. (a) The nominal MC prediction without any weights applied. (b) The flux tuning are applied. (c) The systematic weighting are applied. (d) Both flux and systematic weighting are applied.

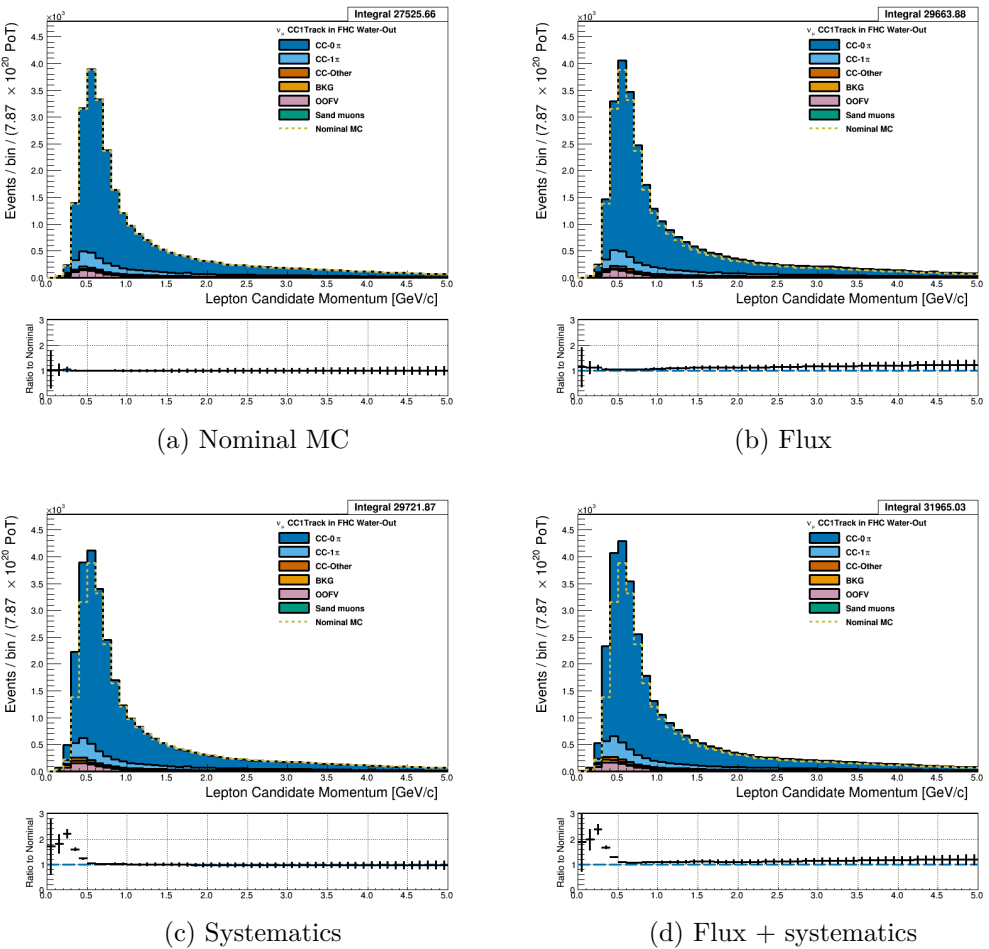


Figure 3.26: Reconstructed lepton candidate momentum separated by topology for FHC  $\nu_\mu$  CC 1-Track events occurring in the PØD in water-out mode. (a) The nominal MC prediction without any weights applied. (b) The flux tuning are applied. (c) The systematic weighting are applied. (d) Both flux and systematic weighting are applied.

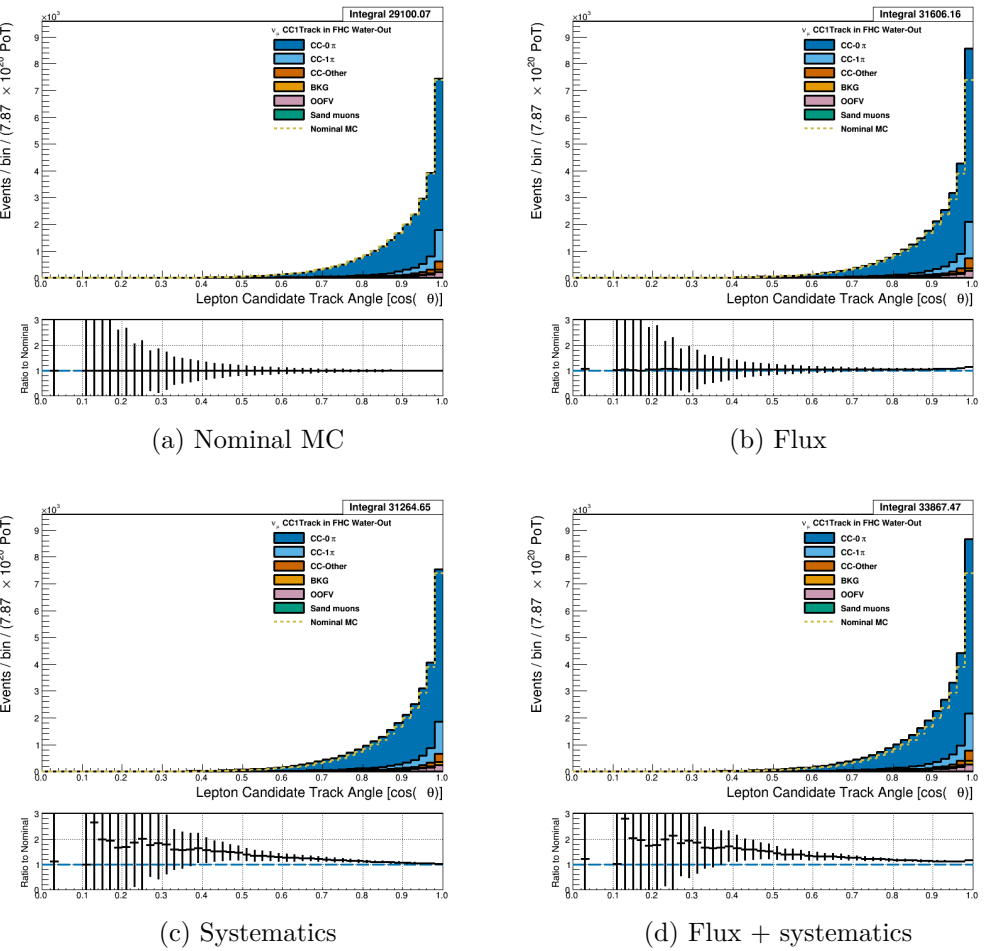


Figure 3.27: Reconstructed lepton candidate  $\cos \theta$  separated by topology for FHC  $\nu_\mu$  CC-1-Track events occurring in the PØD in water-out mode. (a) The nominal MC prediction without any weights applied. (b) The flux tuning are applied. (c) The systematic weighting are applied. (d) Both flux and systematic weighting are applied.

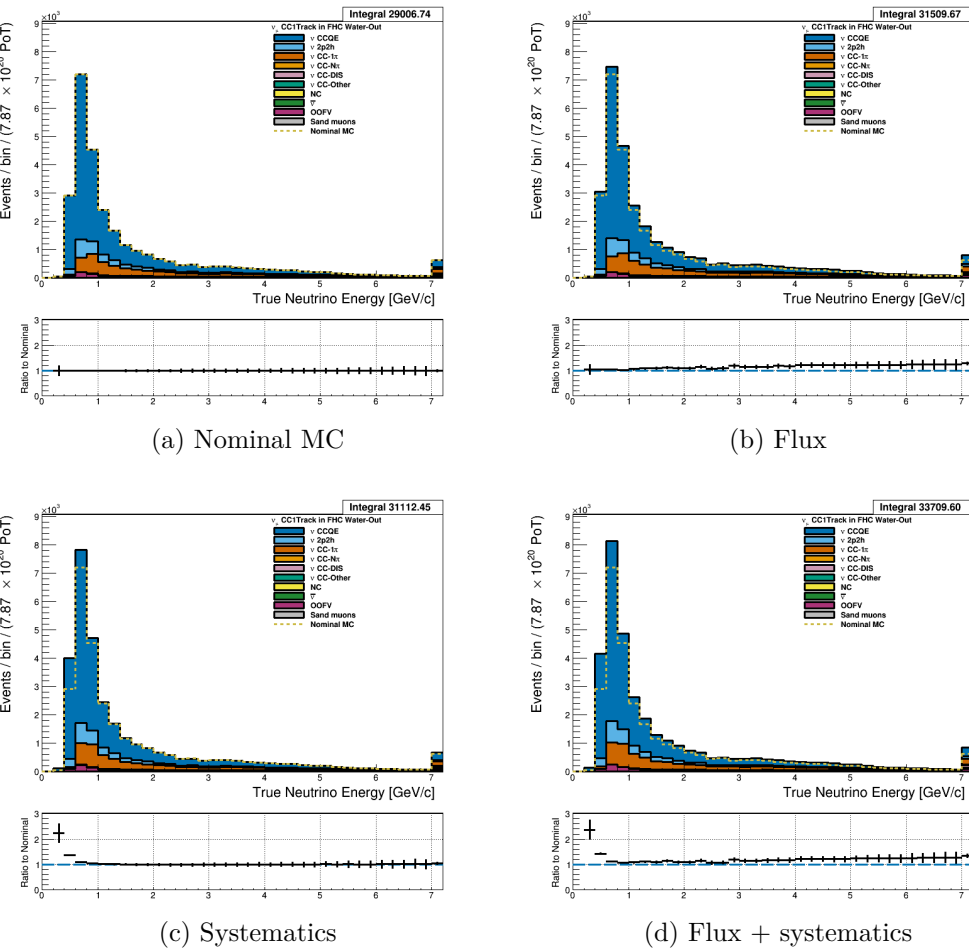


Figure 3.28: True neutrino energy associated with the lepton candidate separated by NEUT model interaction mode for FHC  $\nu_\mu$  CC 1-Track events occurring in the PØD in water-out mode. (a) The nominal MC prediction without any weights applied. (b) The flux tuning are applied. (c) The systematic weighting are applied. (d) Both flux and systematic weighting are applied.

#### 551 3.4.2.2 $\bar{\nu}_\mu$ Selection in RHC Mode: Figures

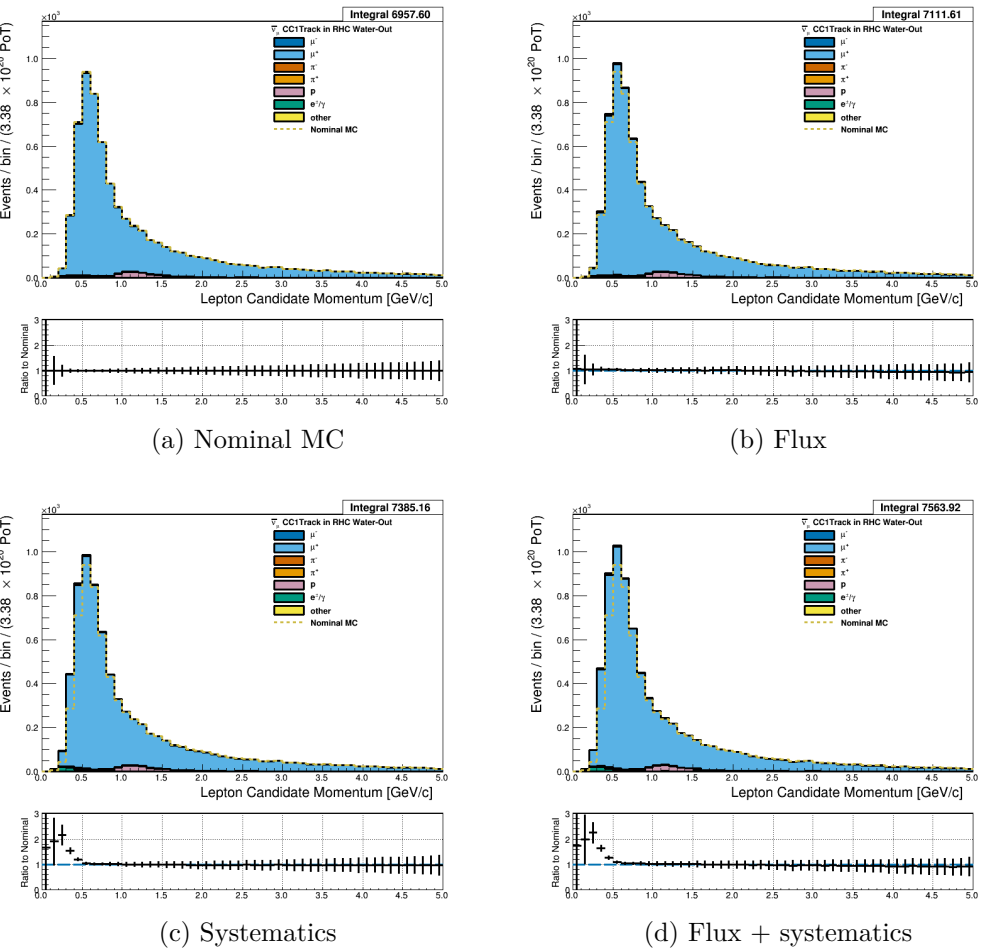


Figure 3.29: Reconstructed lepton candidate momentum separated by true particle species for RHC  $\bar{\nu}_\mu$  CC 1-Track events occurring in the PØD in water-out mode. Reconstructed lepton candidate angle separated by true particle species for RHC  $\bar{\nu}_\mu$  CC Inc. events occurring in the PØD in water-in mode. (a) The nominal MC prediction without any weights applied. (b) The flux tuning are applied. (c) The systematic weighting are applied. (c) Both flux and systematic weighting are applied.

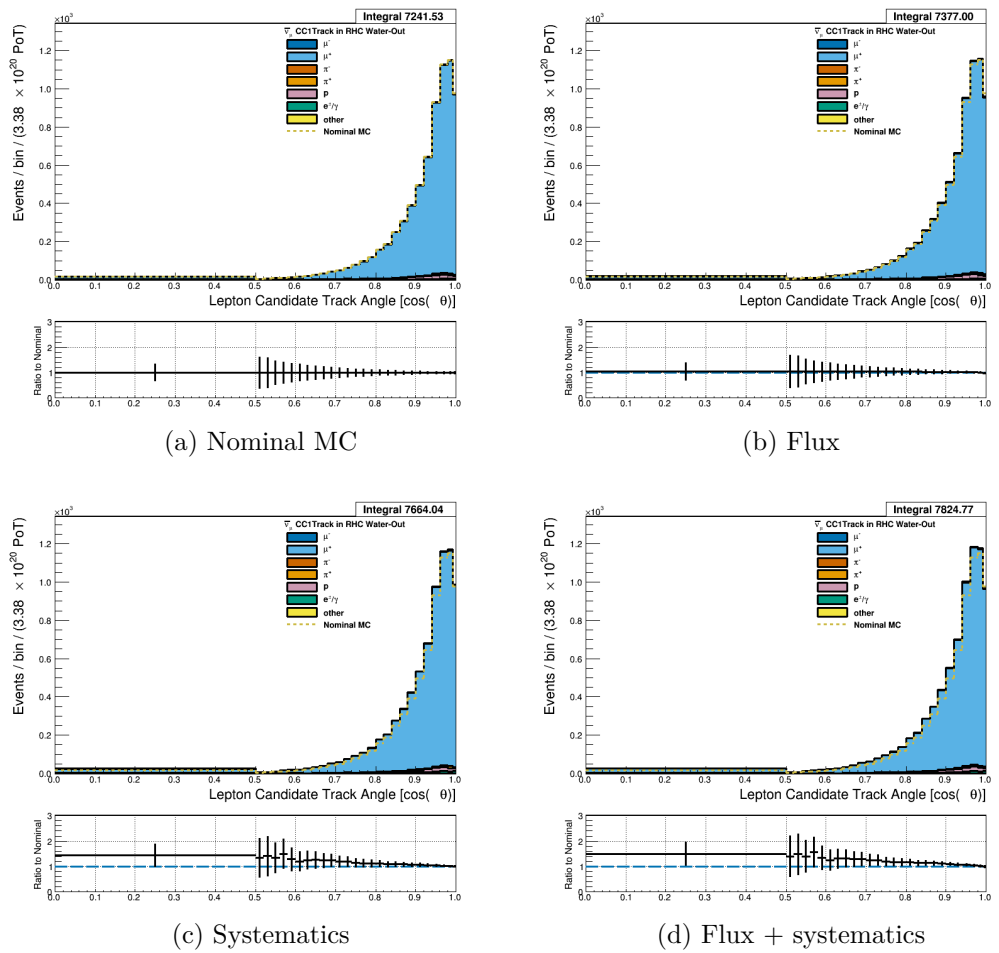


Figure 3.30: Reconstructed lepton candidate angle separated by true particle species for RHC  $\bar{\nu}_\mu$  CC 1-Track events occurring in the PØD in water-out mode. (a) The nominal MC prediction without any weights applied. (b) The flux tuning are applied. (c) The systematic weighting are applied. (d) Both flux and systematic weighting are applied.

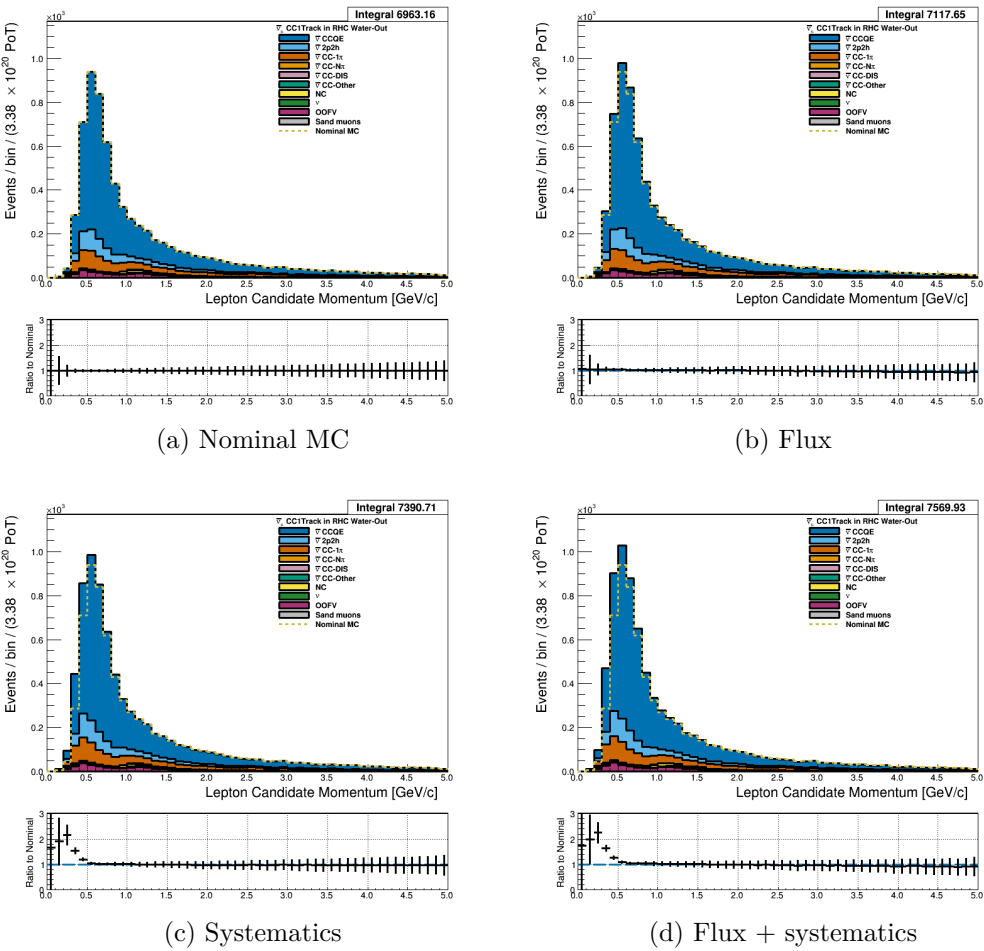


Figure 3.31: Reconstructed lepton candidate momentum separated by NEUT model interaction mode for RHC  $\bar{\nu}_\mu$  CC 1-Track events occurring in the PØD in water-out mode. (a) The nominal MC prediction without any weights applied. (b) The flux tuning are applied. (c) The systematic weighting are applied. (d) Both flux and systematic weighting are applied.

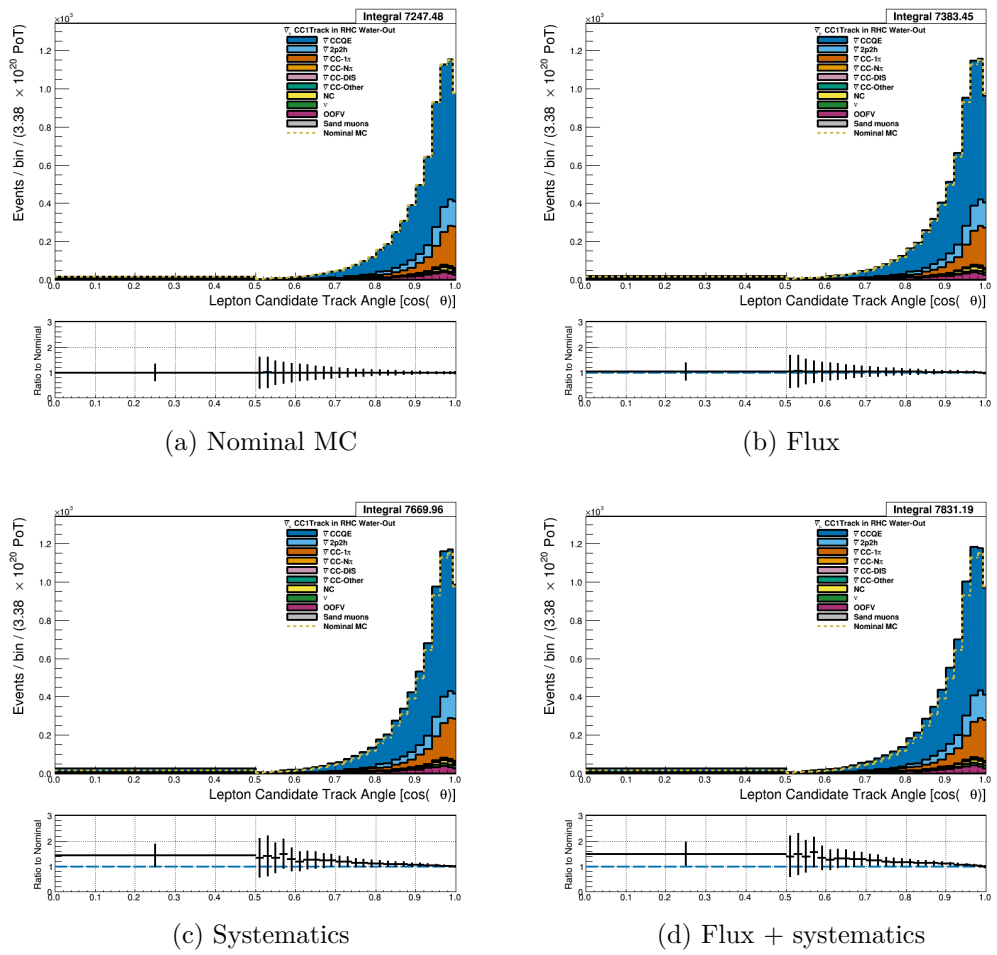


Figure 3.32: Reconstructed lepton candidate  $\cos \theta$  separated by NEUT model interaction mode for RHC  $\bar{\nu}_\mu$  CC 1-TracI events occurring in the P0D in water-out mode. (a) The nominal MC prediction without any weights applied. (b) The flux tuning are applied. (c) The systematic weighting are applied. (d) Both flux and systematic weighting are applied.

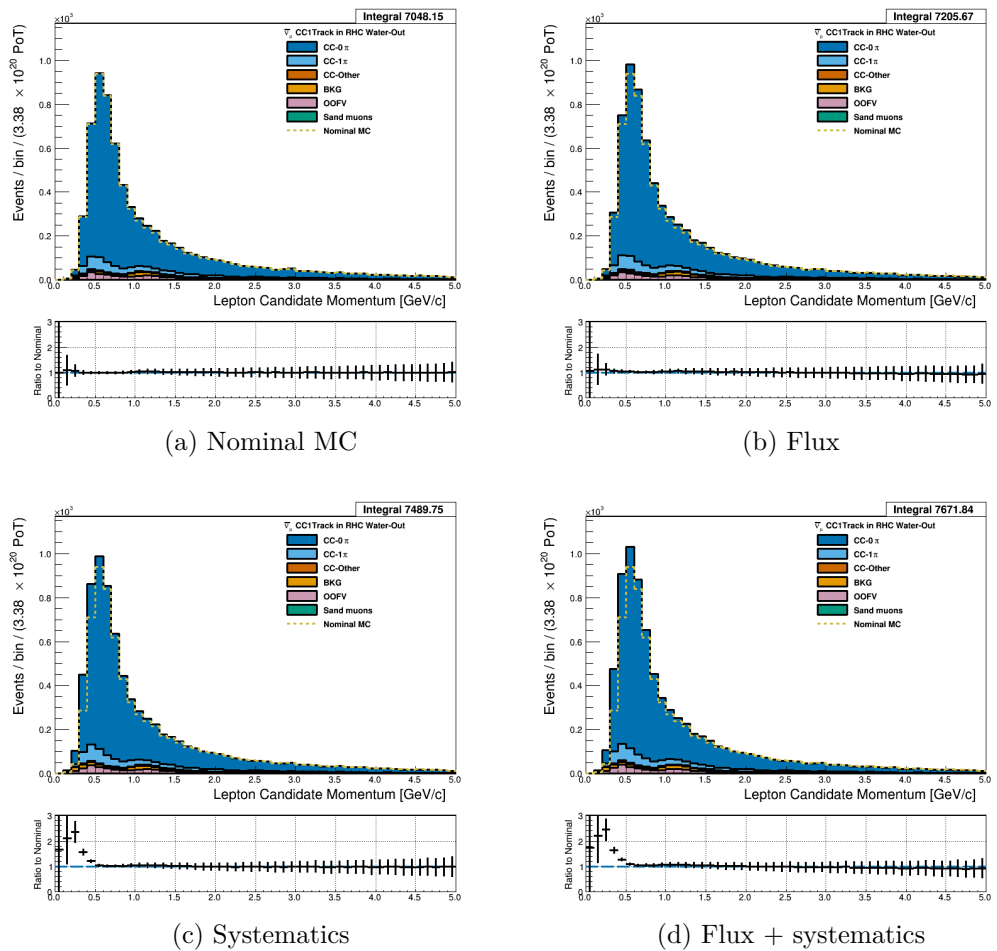


Figure 3.33: Reconstructed lepton candidate momentum separated by topology for RHC  $\bar{\nu}_\mu$  CC 1-Track events occurring in the PØD in water-out mode. (a) The nominal MC prediction without any weights applied. (b) The flux tuning are applied. (c) The systematic weighting are applied. (d) Both flux and systematic weighting are applied.

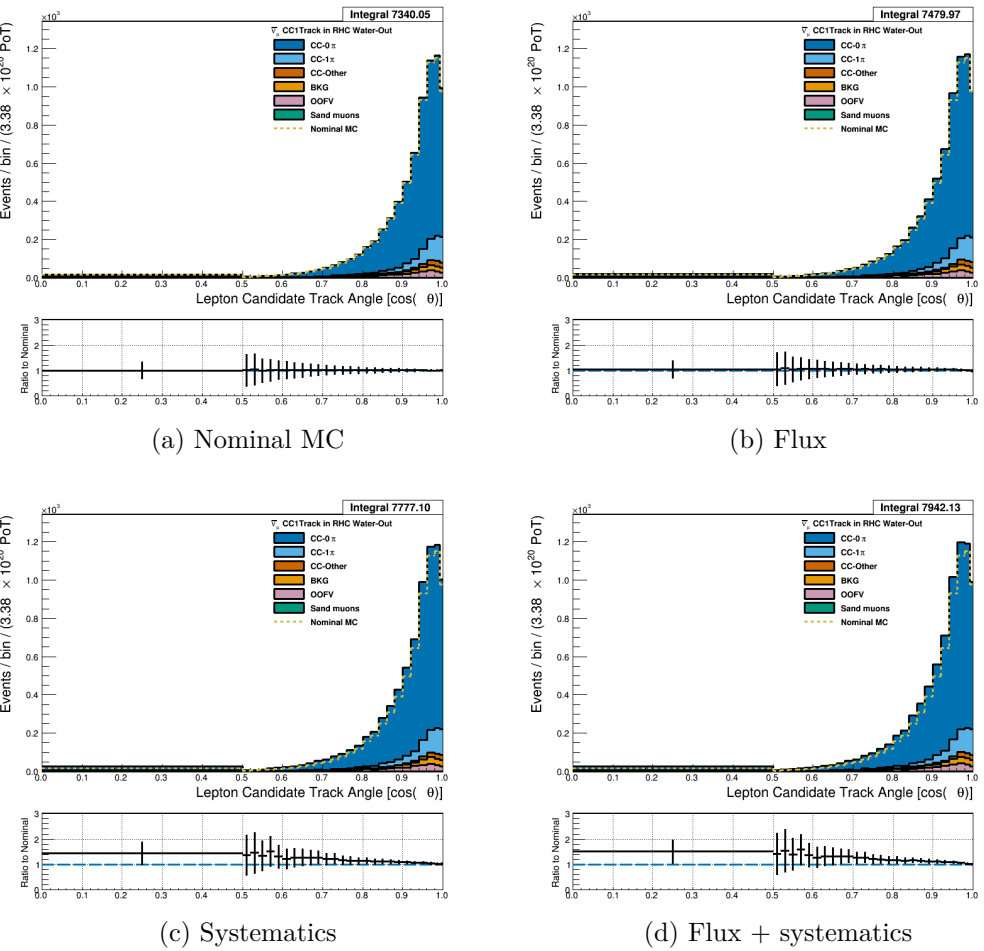


Figure 3.34: Reconstructed lepton candidate  $\cos \theta$  separated by topology for RHC  $\bar{\nu}_\mu$  CC 1-Track events occurring in the PØD in water-out mode. (a) The nominal MC prediction without any weights applied. (b) The flux tuning are applied. (c) The systematic weighting are applied. (d) Both flux and systematic weighting are applied.

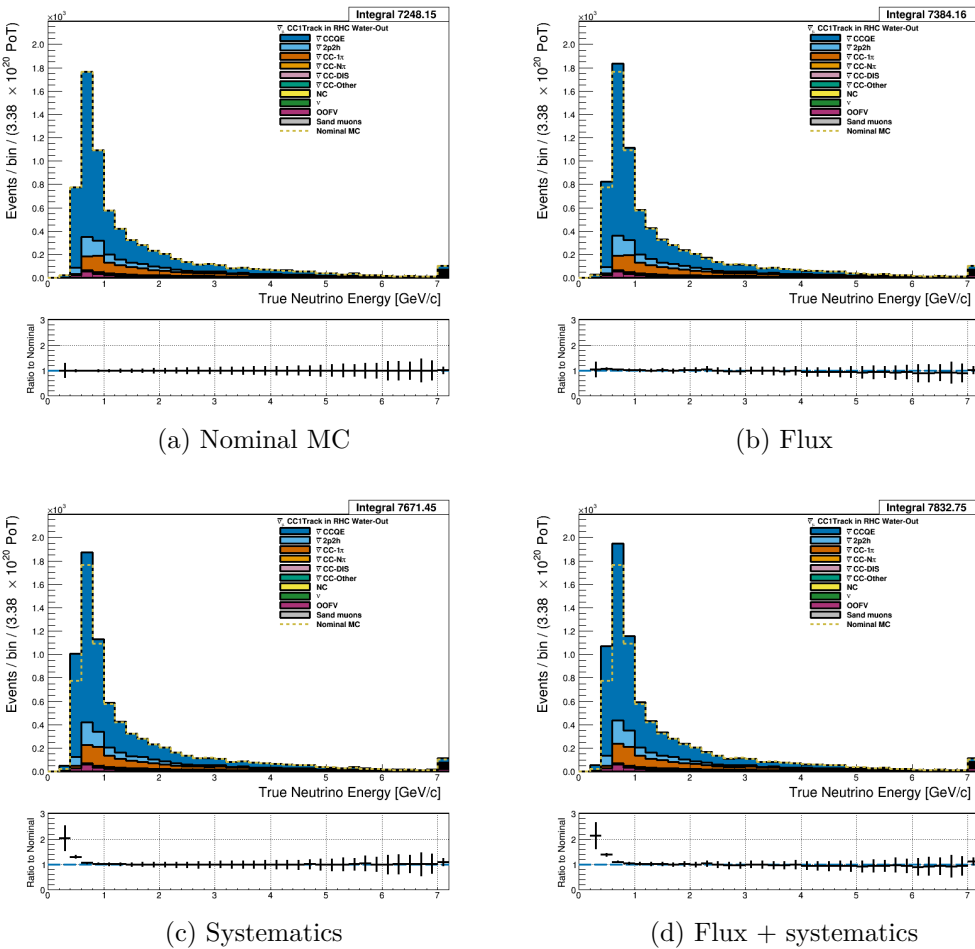


Figure 3.35: True neutrino energy associated with the lepton candidate separated by NEUT model interaction mode for RHC  $\bar{\nu}_\mu$  CC 1-Track events occurring in the PØD in water-out mode. (a) The nominal MC prediction without any weights applied. (b) The flux tuning are applied. (c) The systematic weighting are applied. (d) Both flux and systematic weighting are applied.

552     **3.4.2.3  $\nu_\mu$  Background Selection in RHC Mode:** Text [Add figures here](#)

553     **3.4.3 CC N-Tracks (CCnQE Enhanced)**

554     Text [Add figures here](#)

555     **3.4.3.1  $\nu_\mu$  Selection in FHC Mode:** Text

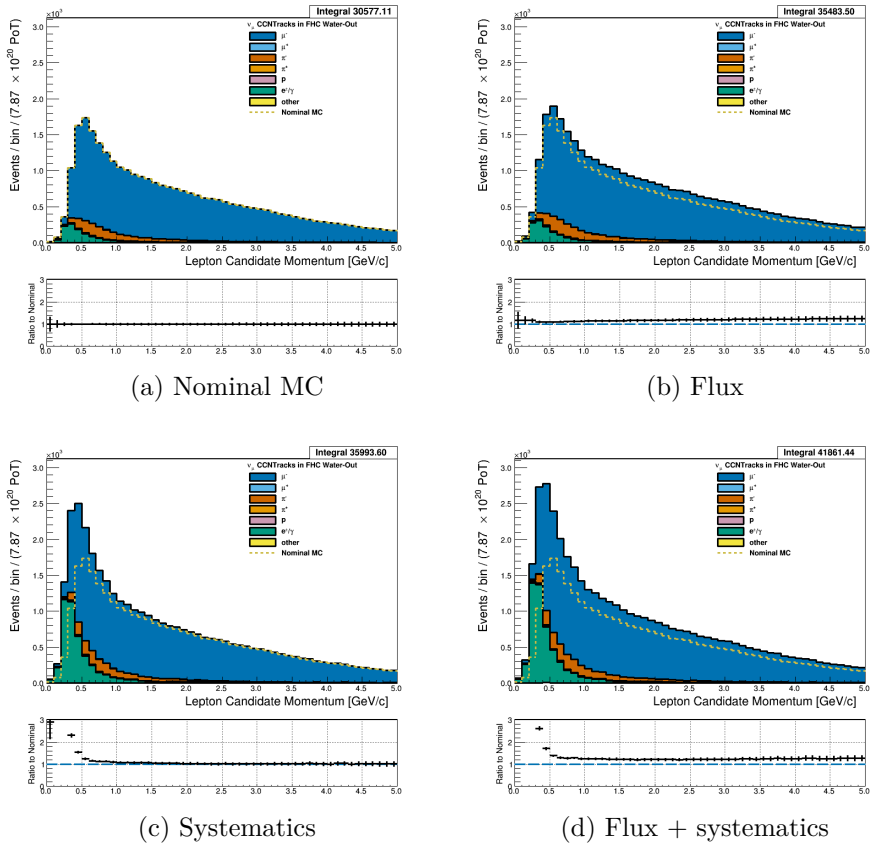


Figure 3.36: Reconstructed lepton candidate momentum separated by true particle species for FHC  $\nu_\mu$  CC N-Tracks events occurring in the PØD in water-out mode. (a) The nominal MC prediction without any weights applied. (b) The flux tuning are applied. (c) The systematic weighting are applied. (e) Both flux and systematic weighting are applied.

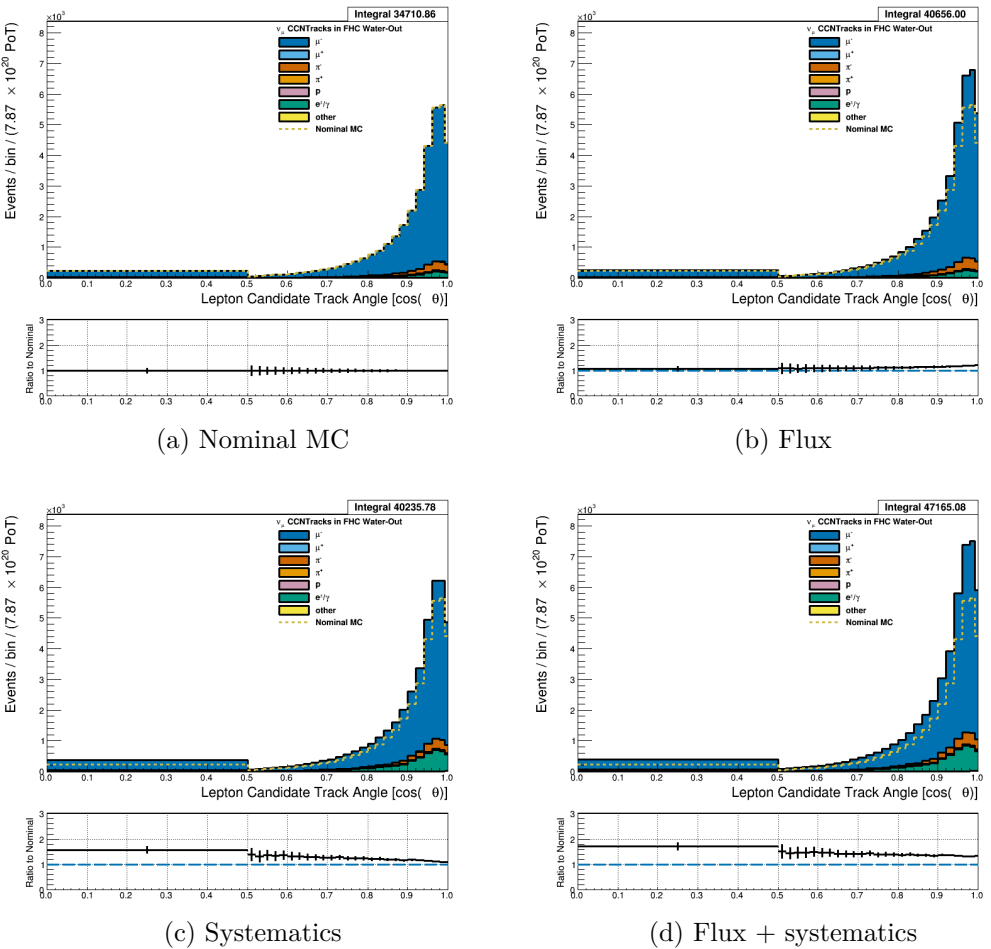


Figure 3.37: Reconstructed lepton candidate angle separated by true particle species for FHC  $\nu_\mu$  CC N-Tracks events occurring in the PØD in water-out mode. (a) The nominal MC prediction without any weights applied. (b) The flux tuning are applied. (c) The systematic weighting are applied. (d) Both flux and systematic weighting are applied.

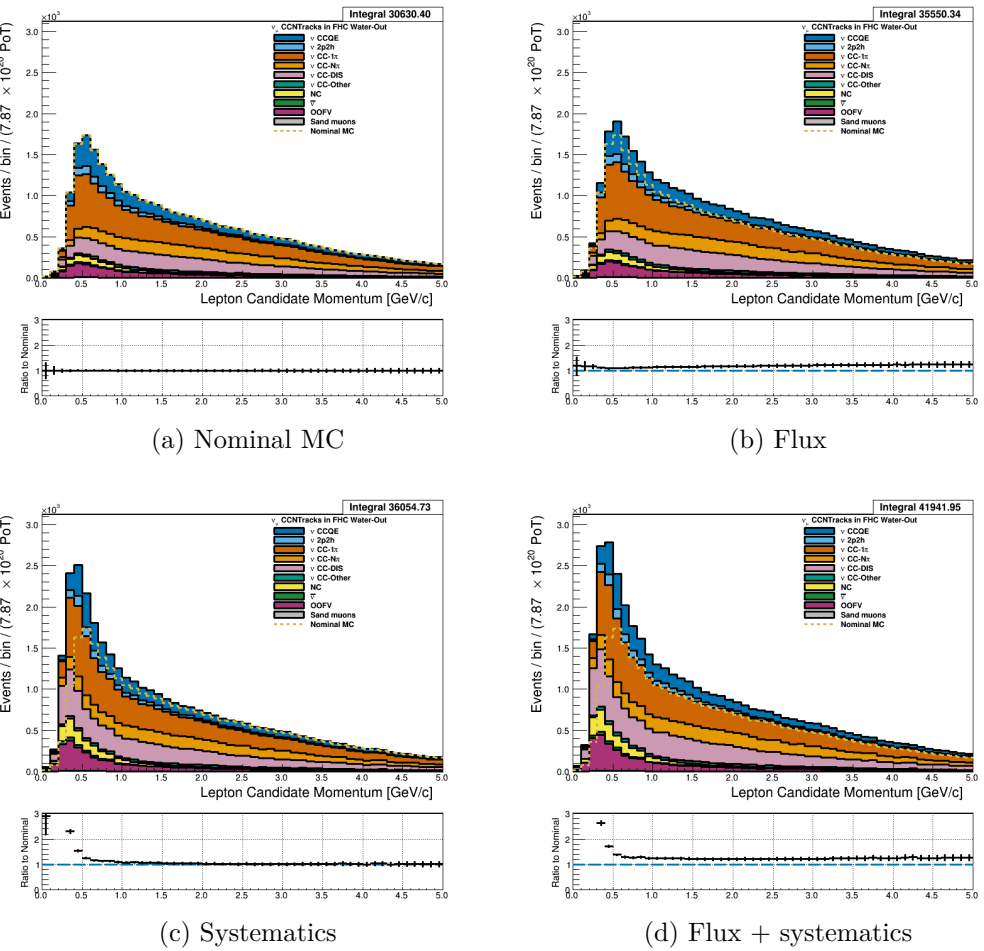


Figure 3.38: Reconstructed lepton candidate momentum separated by NEUT model interaction mode for FHC  $\nu_\mu$  CC N-Tracks events occurring in the PØD in water-out mode. (a) The nominal MC prediction without any weights applied. (b) The flux tuning are applied. (c) The systematic weighting are applied. (d) Both flux and systematic weighting are applied.

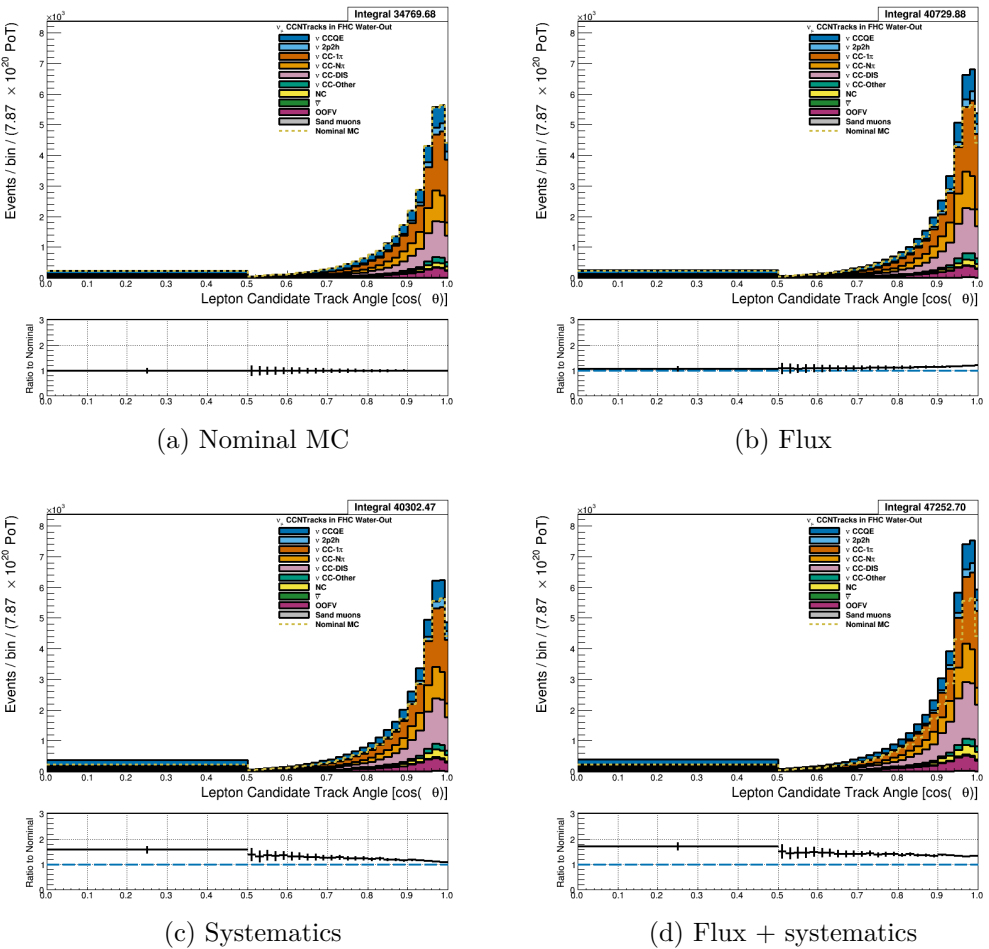


Figure 3.39: Reconstructed lepton candidate  $\cos \theta$  separated by NEUT model interaction mode for FHC  $\nu_\mu$  CC N-Tracks events occurring in the PØD in water-out mode. (a) The nominal MC prediction without any weights applied. (b) The flux tuning are applied. (c) The systematic weighting are applied. (d) Both flux and systematic weighting are applied.

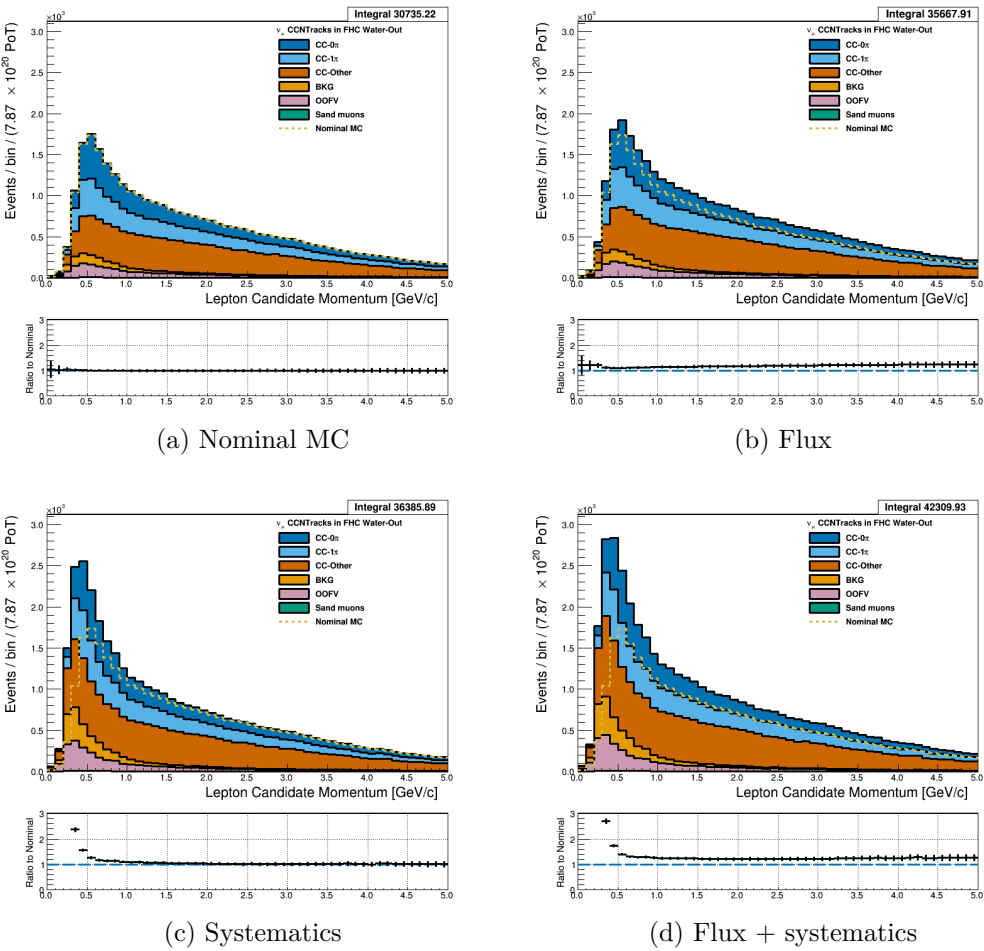


Figure 3.40: Reconstructed lepton candidate momentum separated by topology for FHC  $\nu_\mu$  CC N-Tracks events occurring in the PØD in water-out mode. (a) The nominal MC prediction without any weights applied. (b) The flux tuning are applied. (c) The systematic weighting are applied. (d) Both flux and systematic weighting are applied.

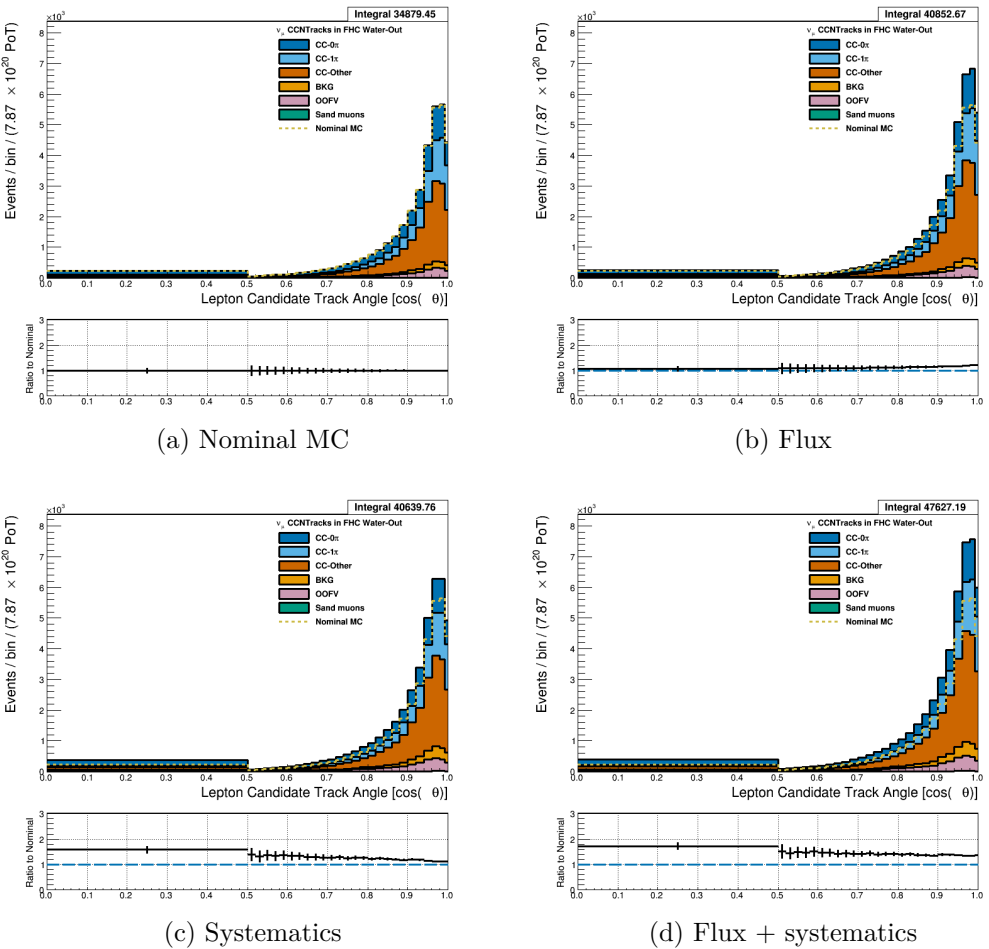


Figure 3.41: Reconstructed lepton candidate  $\cos \theta$  separated by topology for FHC  $\nu_\mu$  CC N-Tracks events occurring in the PØD in water-out mode. (a) The nominal MC prediction without any weights applied. (b) The flux tuning are applied. (c) The systematic weighting are applied. (d) Both flux and systematic weighting are applied.

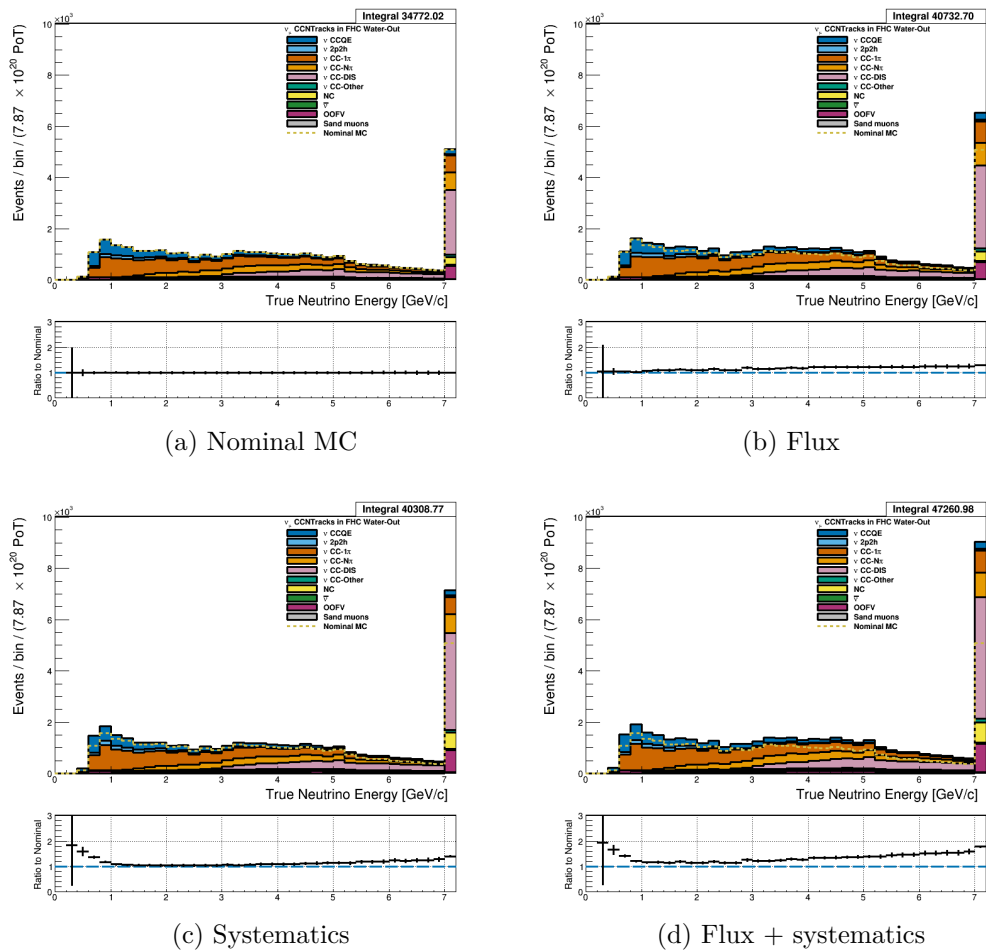


Figure 3.42: True neutrino energy associated with the lepton candidate separated by NEUT model interaction mode for FHC  $\nu_\mu$  CC N-Tracks events occurring in the PØD in water-out mode. (a) The nominal MC prediction without any weights applied. (b) The flux tuning are applied. (c) The systematic weighting are applied. (d) Both flux and systematic weighting are applied.

### 3.4.3.2 $\bar{\nu}_\mu$ Selection in RHC Mode: Text goes here

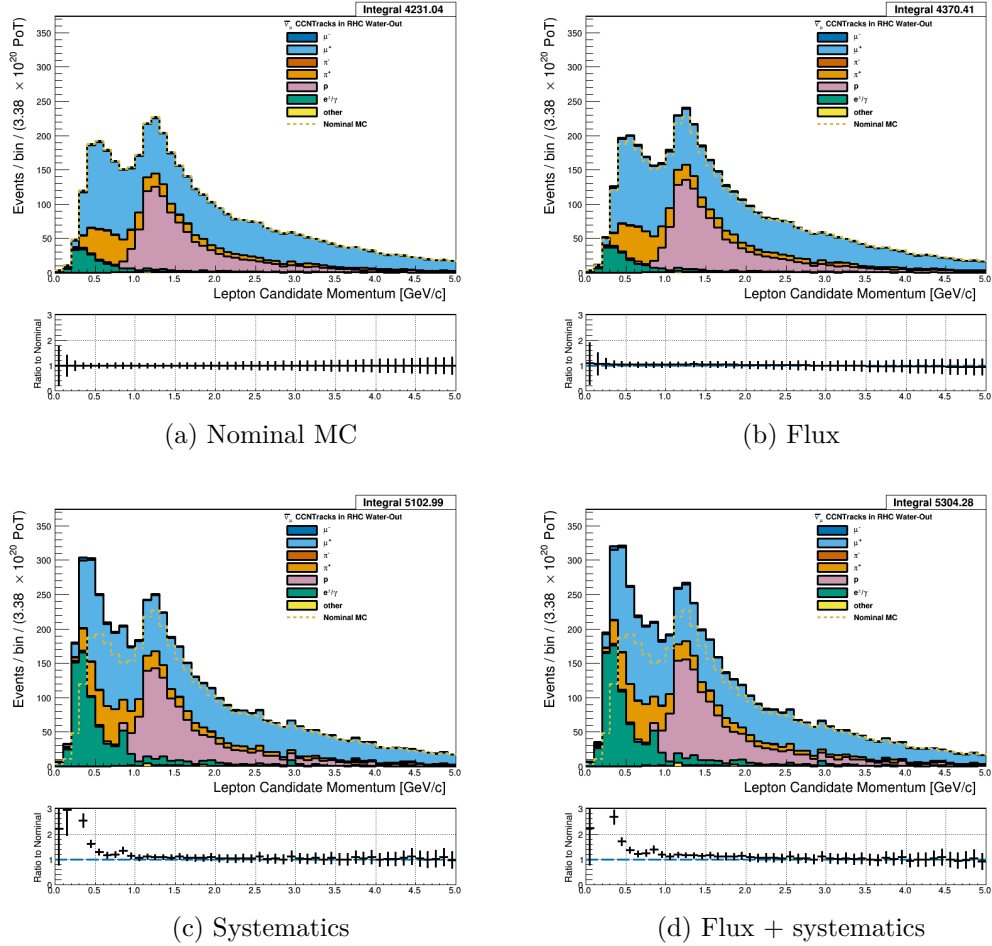


Figure 3.43: Reconstructed lepton candidate momentum separated by true particle species for RHC  $\bar{\nu}_\mu$  CC N-Tracks events occurring in the PØD in water-out mode. Reconstructed lepton candidate angle separated by true particle species for RHC  $\bar{\nu}_\mu$  CC N-Tracks events occurring in the PØD in water-in mode. (a) The nominal MC prediction without any weights applied. (b) The flux tuning are applied. (c) The systematic weighting are applied. (d) Both flux and systematic weighting are applied.

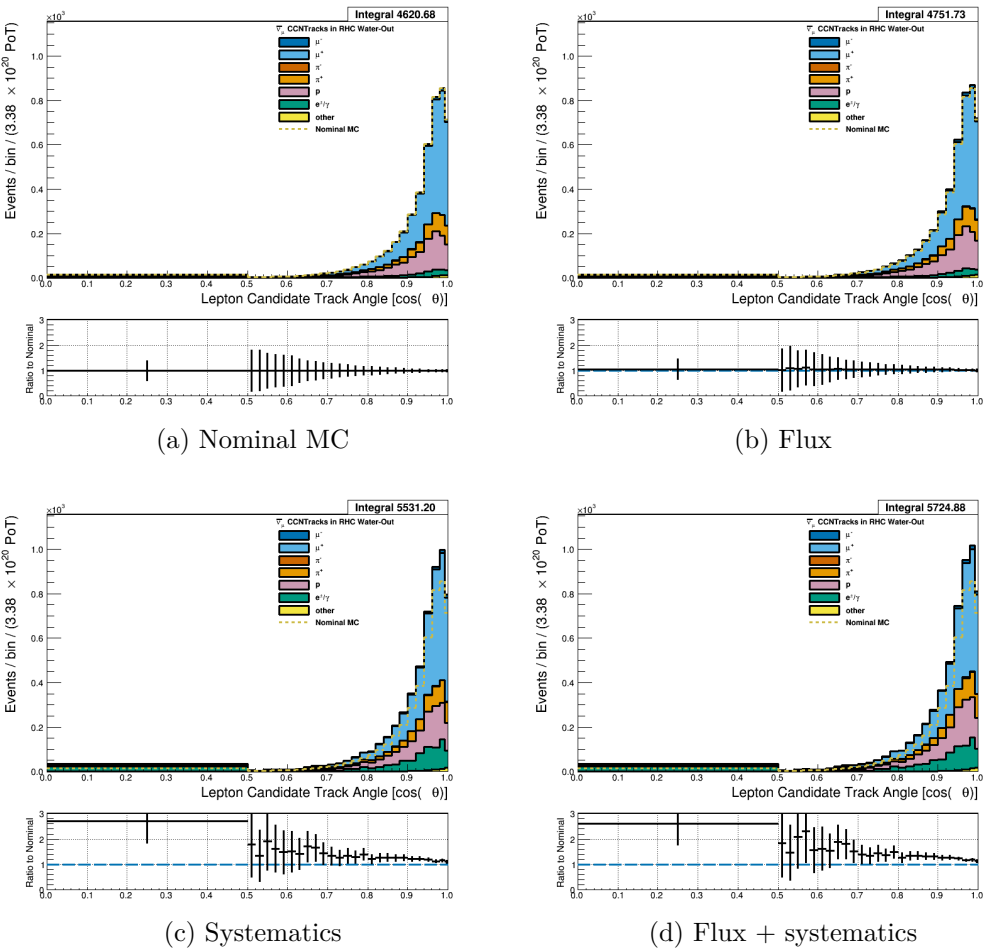


Figure 3.44: Reconstructed lepton candidate angle separated by true particle species for RHC  $\bar{\nu}_\mu$  CC N-Tracks events occurring in the PØD in water-out mode. (a) The nominal MC prediction without any weights applied. (b) The flux tuning are applied. (c) The systematic weighting are applied. (d) Both flux and systematic weighting are applied.

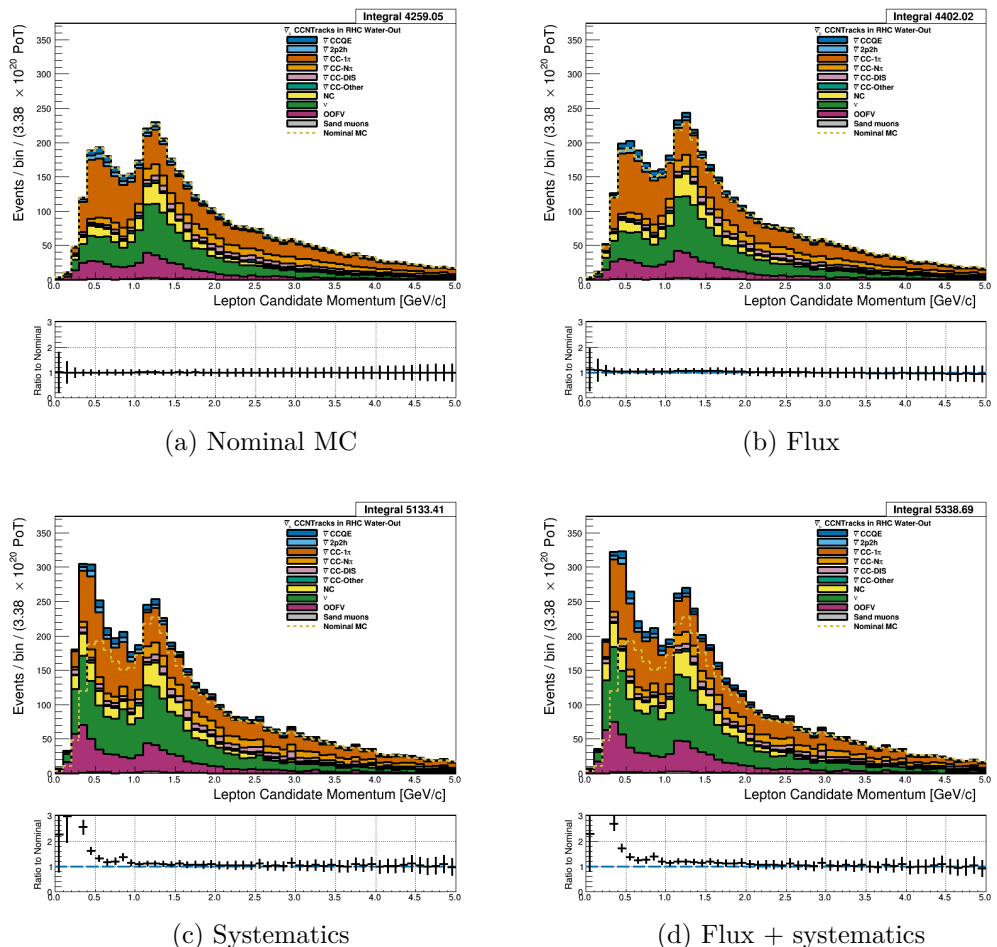


Figure 3.45: Reconstructed lepton candidate momentum separated by NEUT model interaction mode for RHC  $\bar{\nu}_\mu$  CC N-Tracks events occurring in the PØD in water-out mode. (a) The nominal MC prediction without any weights applied. (b) The flux tuning are applied. (c) The systematic weighting are applied. (d) Both flux and systematic weighting are applied.

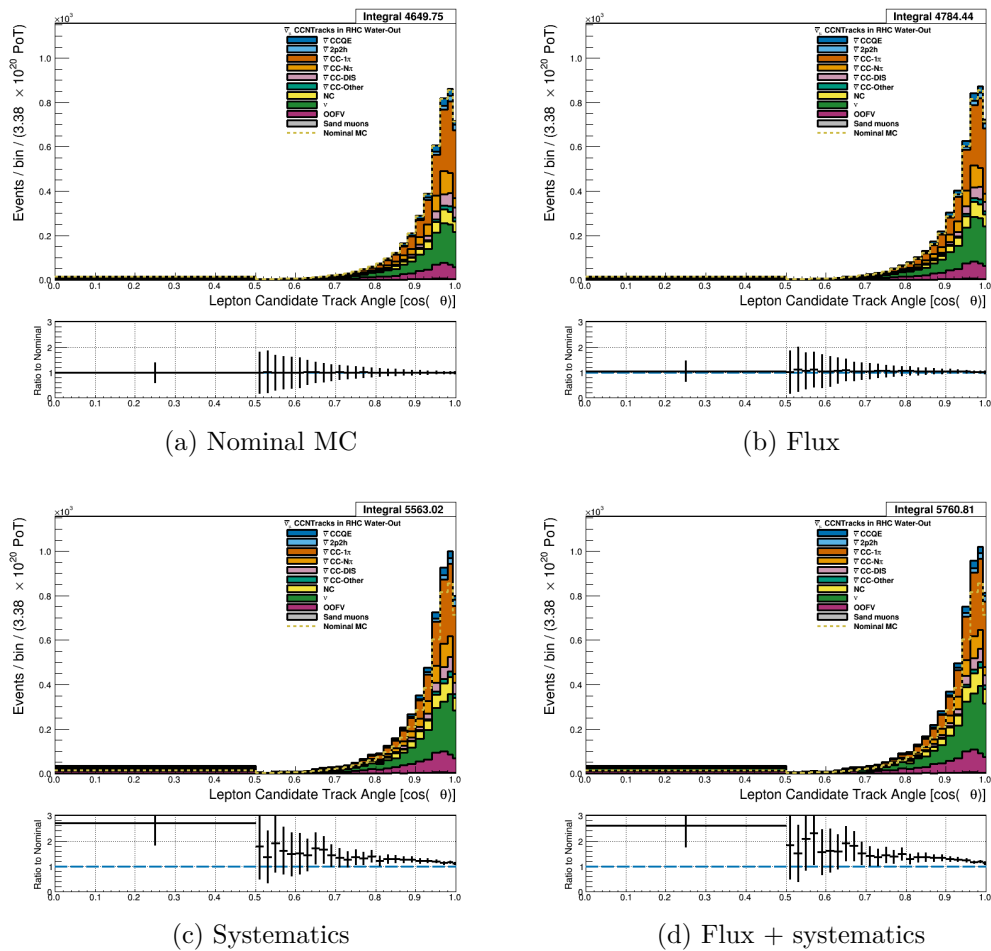


Figure 3.46: Reconstructed lepton candidate  $\cos \theta$  separated by NEUT model interaction mode for RHC  $\bar{\nu}_\mu$  CC N-Tracks events occurring in the PØD in water-out mode. (a) The nominal MC prediction without any weights applied. (b) The flux tuning are applied. (c) The systematic weighting are applied. (d) Both flux and systematic weighting are applied.

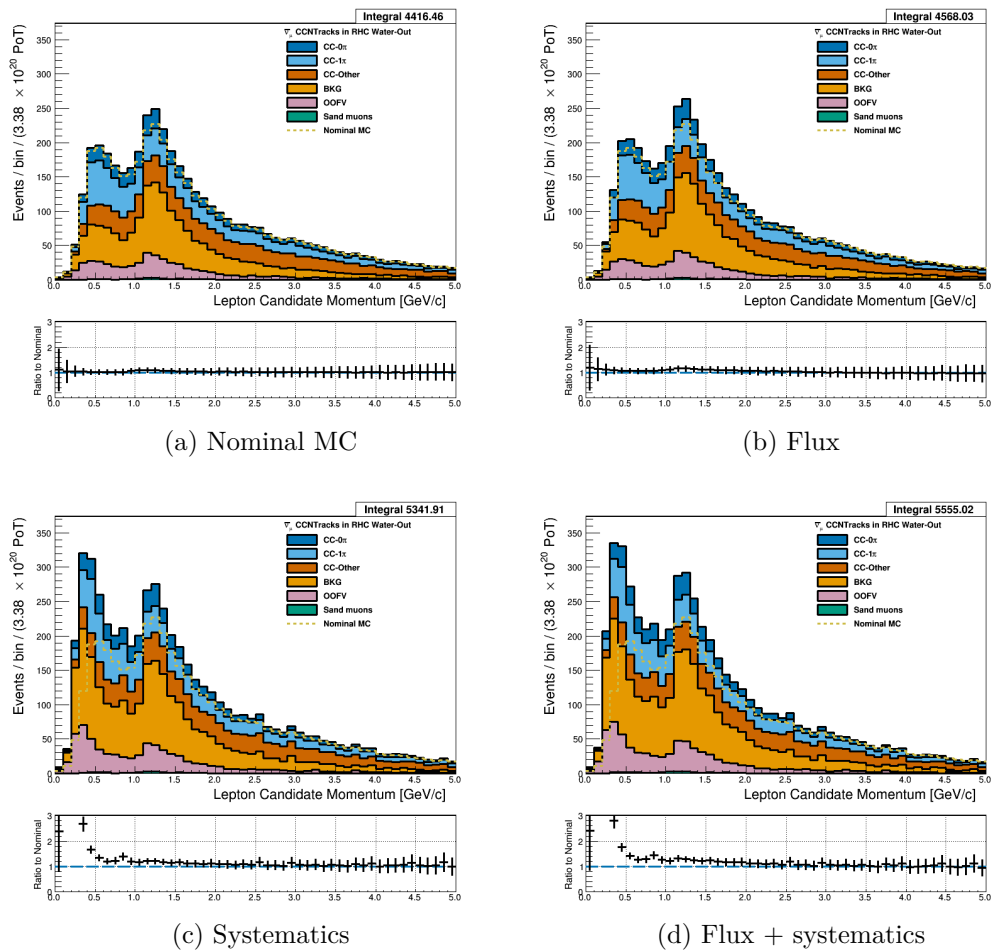


Figure 3.47: Reconstructed lepton candidate momentum separated by topology for RHC  $\bar{\nu}_\mu$  CC N-Tracks events occurring in the PØD in water-out mode. (a) The nominal MC prediction without any weights applied. (b) The flux tuning are applied. (c) The systematic weighting are applied. (d) Both flux and systematic weighting are applied.

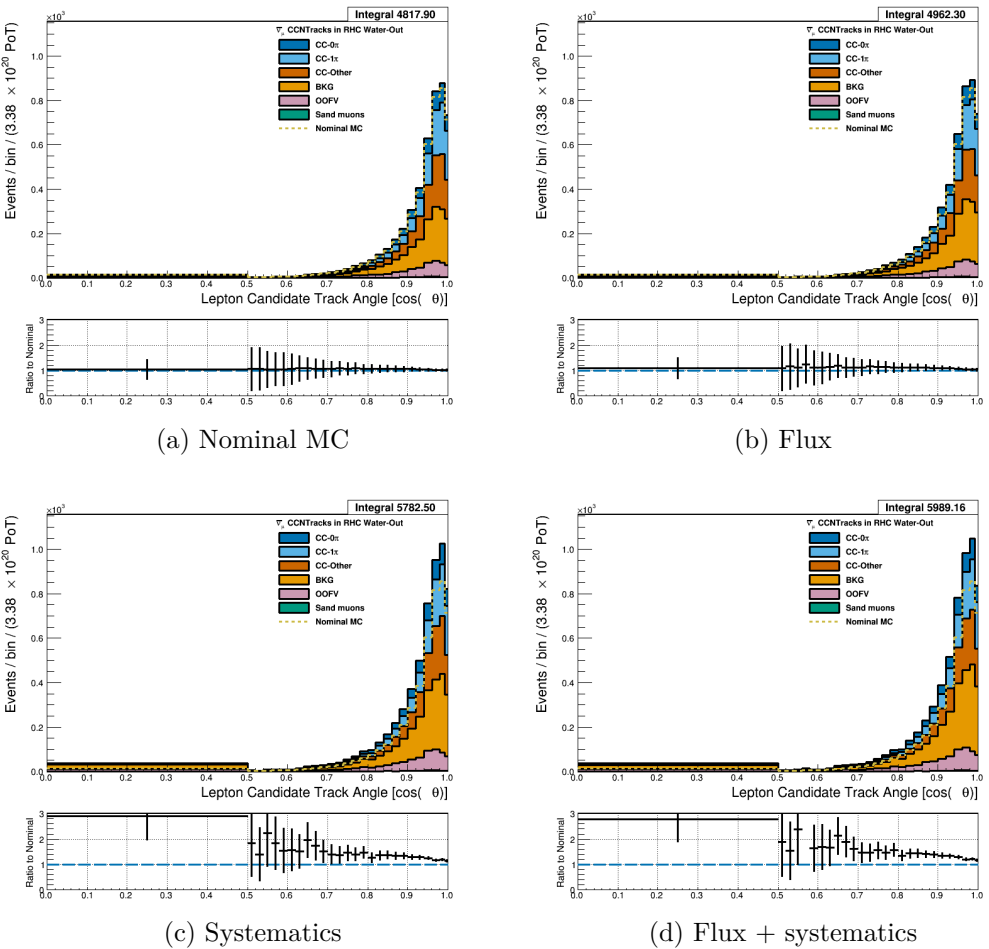


Figure 3.48: Reconstructed lepton candidate  $\cos \theta$  separated by topology for RHC  $\bar{\nu}_\mu$  CC N-Tracks events occurring in the PØD in water-out mode. (a) The nominal MC prediction without any weights applied. (b) The flux tuning are applied. (c) The systematic weighting are applied. (d) Both flux and systematic weighting are applied.

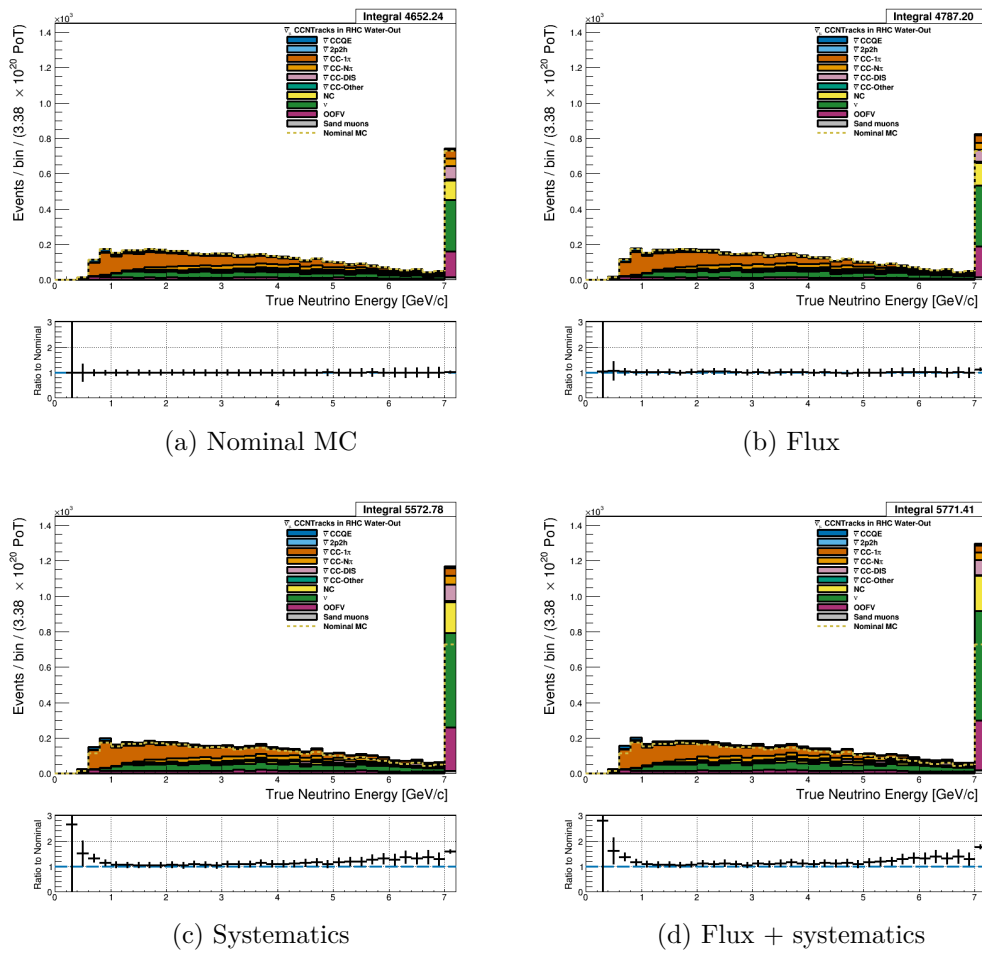


Figure 3.49: True neutrino energy associated with the lepton candidate separated by NEUT model interaction mode for RHC  $\bar{\nu}_\mu$  CC N-Tracks events occurring in the PØD in water-out mode. (a) The nominal MC prediction without any weights applied. (b) The flux tuning are applied. (c) The systematic weighting are applied. (d) Both flux and systematic weighting are applied.

557 **3.4.3.3  $\nu_\mu$  Background Selection in RHC Mode:** Text

558 **3.5 PØD Water-In Samples**

559 This section shows the kinematic distributions for the PØD water-in samples. These samples  
 560 will demonstrate the similarities between it and water-out modes. First an examination of  
 561 the CC Inclusive samples and the effects of the systematic weights will be explored. The

562 samples are then examined as CC 1-track and CC N-tracks.

563 **3.5.1 CC Inclusive**

564 The CC Inclusive sample cuts are discussed 3.2.1. Since both flux and detector systematic  
565 weights are applied to all MC events in BANFF, it is important to validate the event weights.  
566 Using neither set of weights is referred to as the nominal MC.

567 **3.5.1.1  $\nu_\mu$  Selection in FHC Mode:** Shown in Figures 3.50 to 3.56 are the momentum  
568 and  $\cos\theta$  distributions for  $\nu_\mu$ CC Inclusive events in FHC mode. There are three pairs of  
569  $P, \theta$  figures with the same truth information break down accompanied by one of neutrino  
570 energy. The truth information categories are lepton candidate particle, NEUT reaction, and  
571 topology. Each figure consists of a set of four sub-figures which illustrate the application of  
572 flux and detector systematic weights.

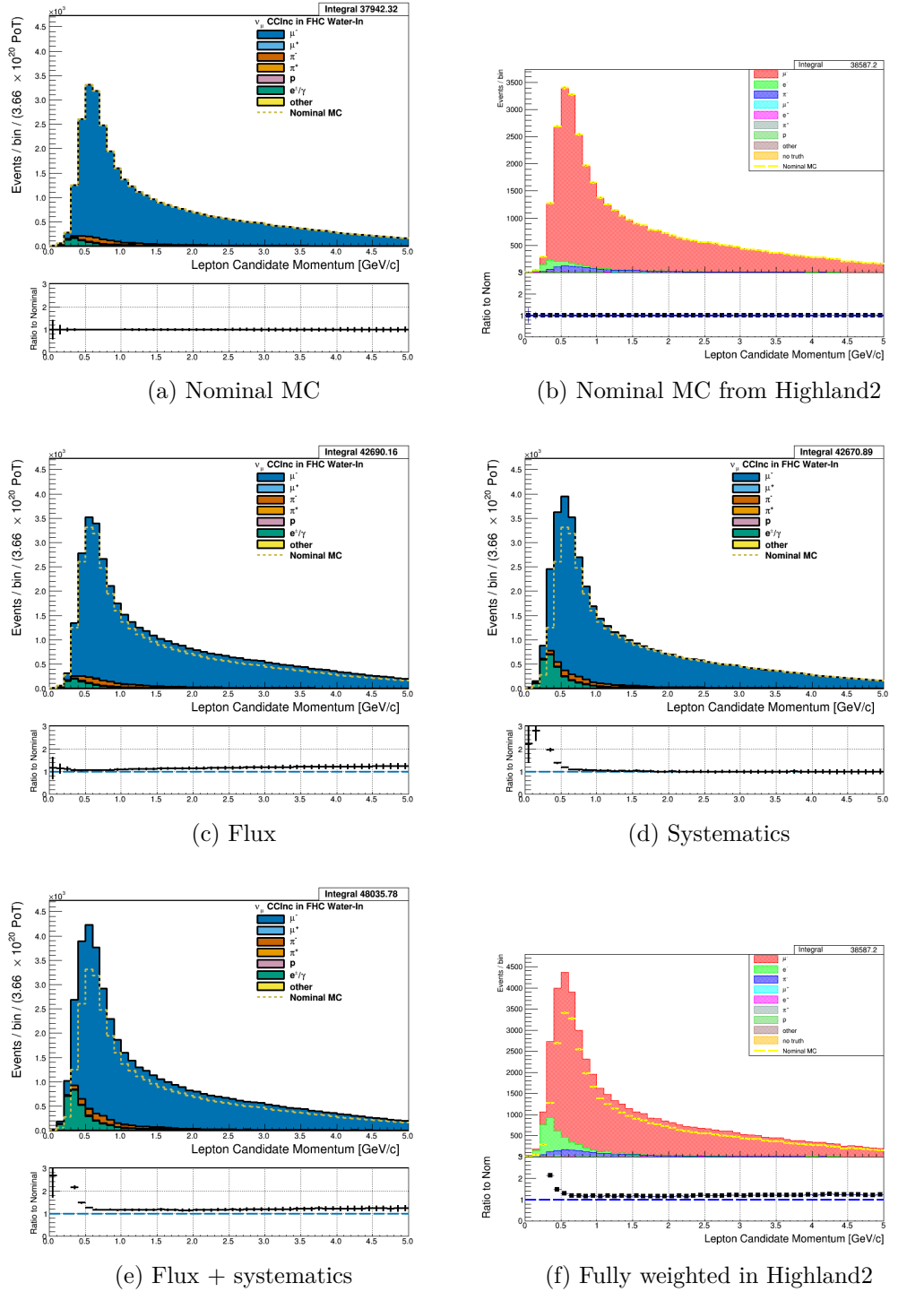


Figure 3.50: Reconstructed lepton candidate momentum separated by true particle species for FHC  $\nu_\mu$  CC Inc. events occurring in the PØD in water-in mode. (a) The nominal MC prediction without any weights applied. (b) Highland2 comparison for (a) without any weights applied using the “NOW” draw option. (c) The flux tuning are applied. (d) The systematic weighting are applied. (e) Both flux and systematic weighting are applied. (f) Highland2 comparison for (e).

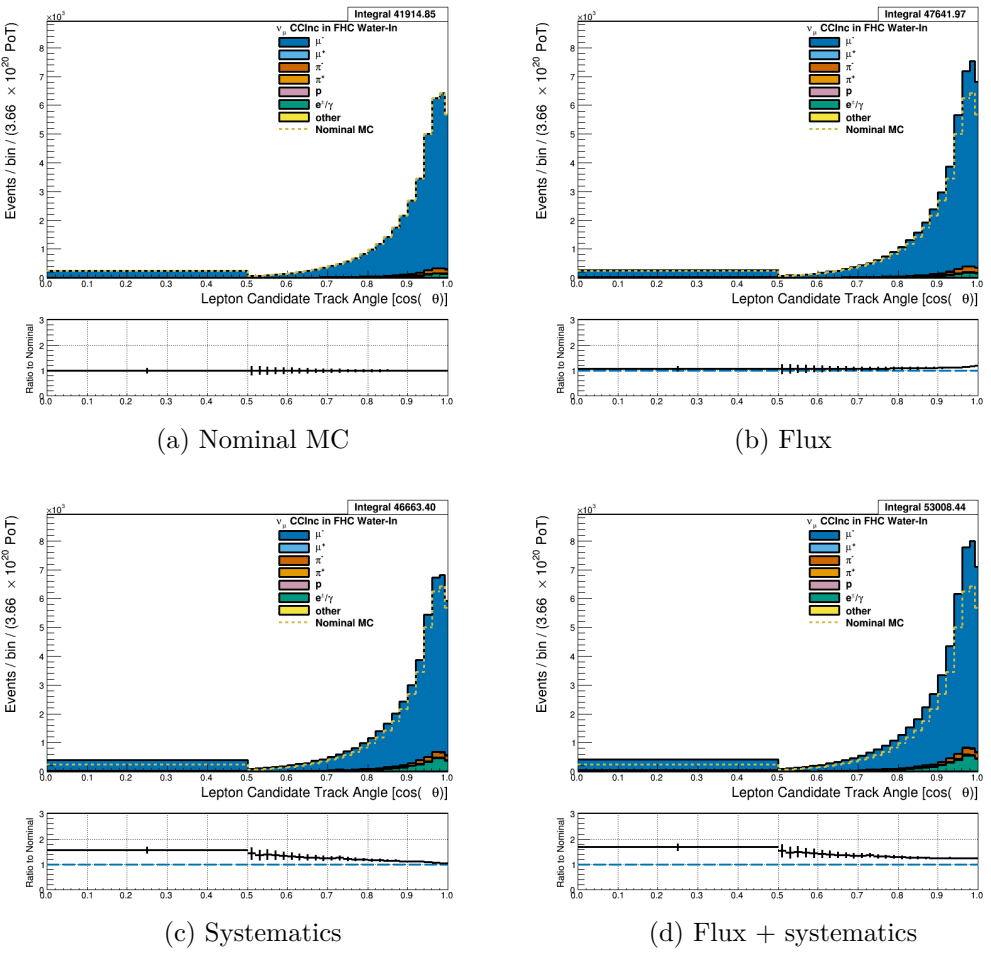


Figure 3.51: Reconstructed lepton candidate angle separated by true particle species for FHC  $\nu_\mu$  CC Inc. events occurring in the PØD in water-in mode. (a) The nominal MC prediction without any weights applied. (b) The flux tuning are applied. (c) The systematic weighting are applied. (d) Both flux and systematic weighting are applied.

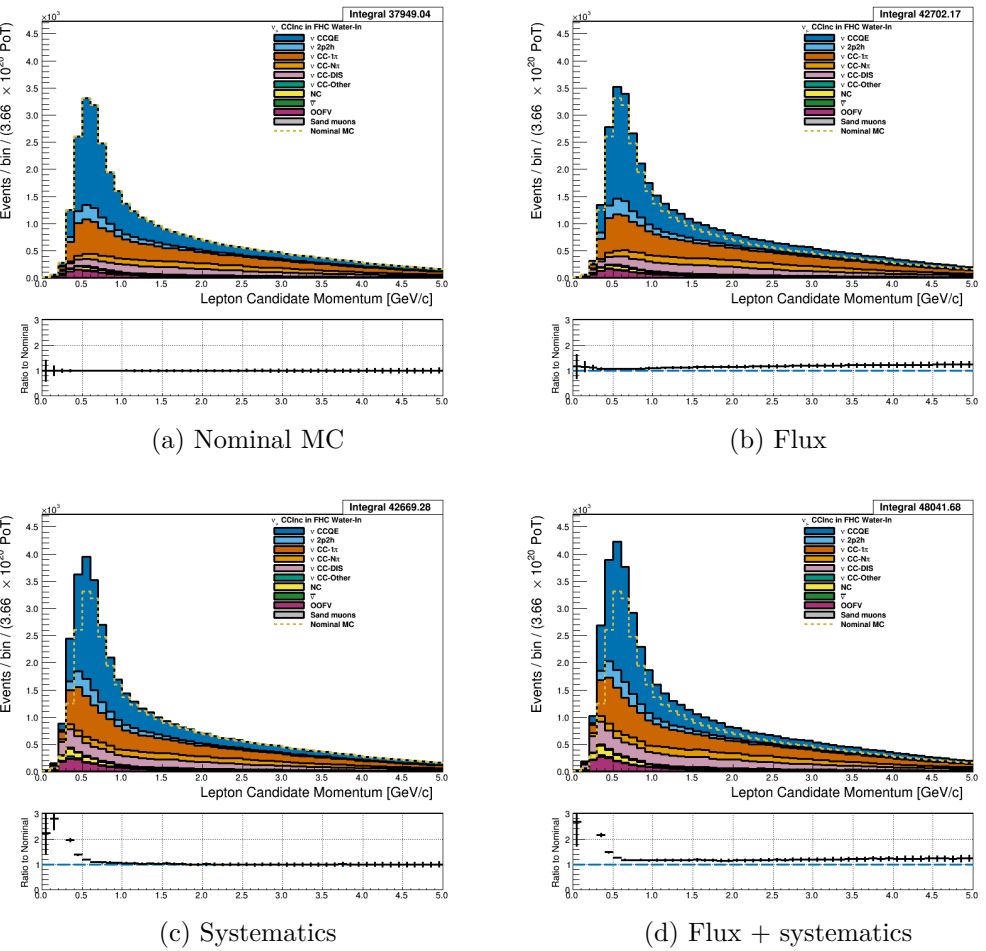


Figure 3.52: Reconstructed lepton candidate momentum separated by NEUT model interaction mode for FHC  $\nu_\mu$  CC Inc. events occurring in the PØD in water-in mode. (a) The nominal MC prediction without any weights applied. (b) The flux tuning are applied. (c) The systematic weighting are applied. (d) Both flux and systematic weighting are applied.

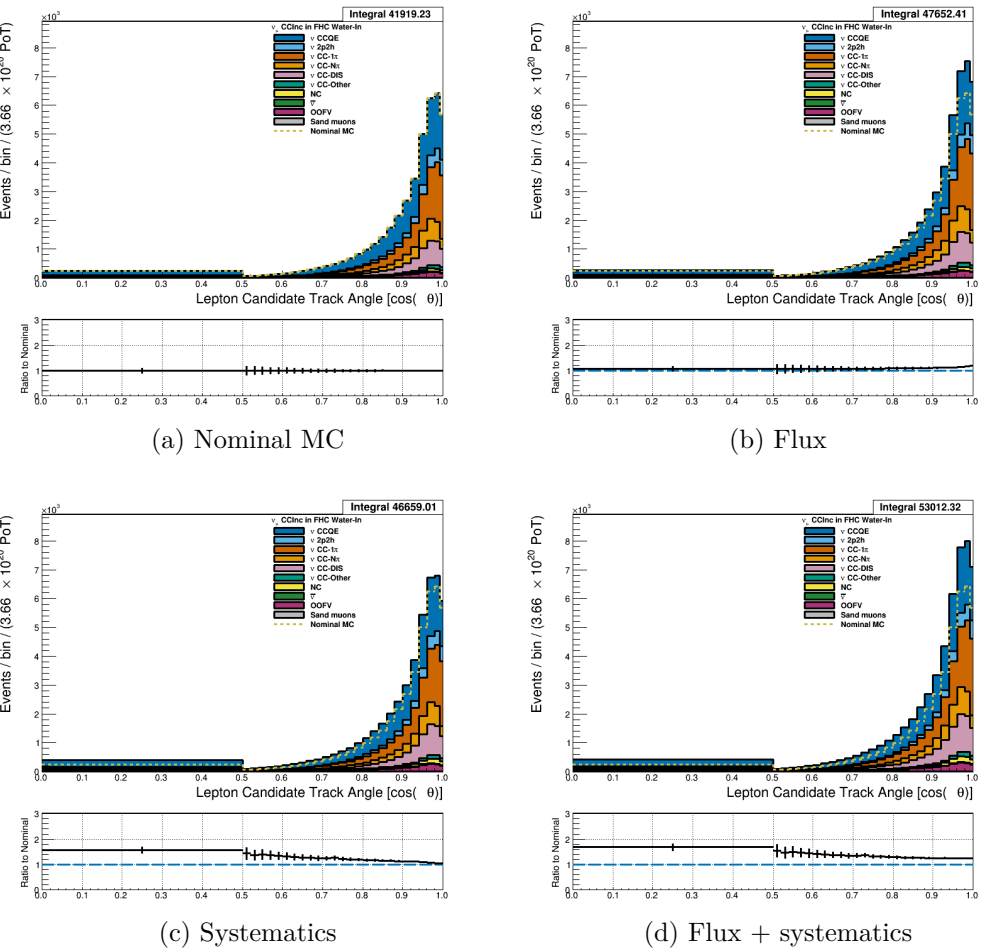


Figure 3.53: Reconstructed lepton candidate  $\cos \theta$  separated by NEUT model interaction mode for FHC  $\nu_\mu$  CC Inc. events occurring in the PØD in water-in mode. (a) The nominal MC prediction without any weights applied. (b) The flux tuning are applied. (c) The systematic weighting are applied. (d) Both flux and systematic weighting are applied.

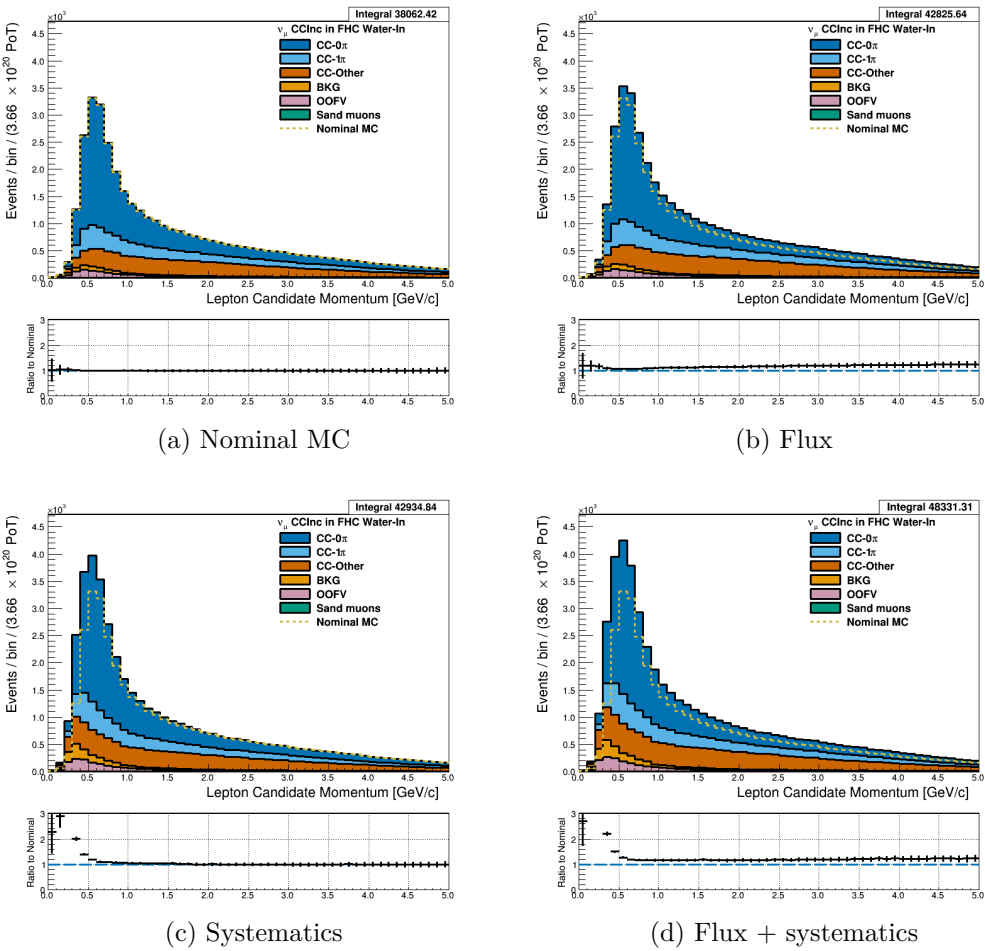


Figure 3.54: Reconstructed lepton candidate momentum separated by topology for FHC  $\nu_\mu$  CC Inc. events occurring in the PØD in water-in mode. (a) The nominal MC prediction without any weights applied. (b) The flux tuning are applied. (c) The systematic weighting are applied. (d) Both flux and systematic weighting are applied.

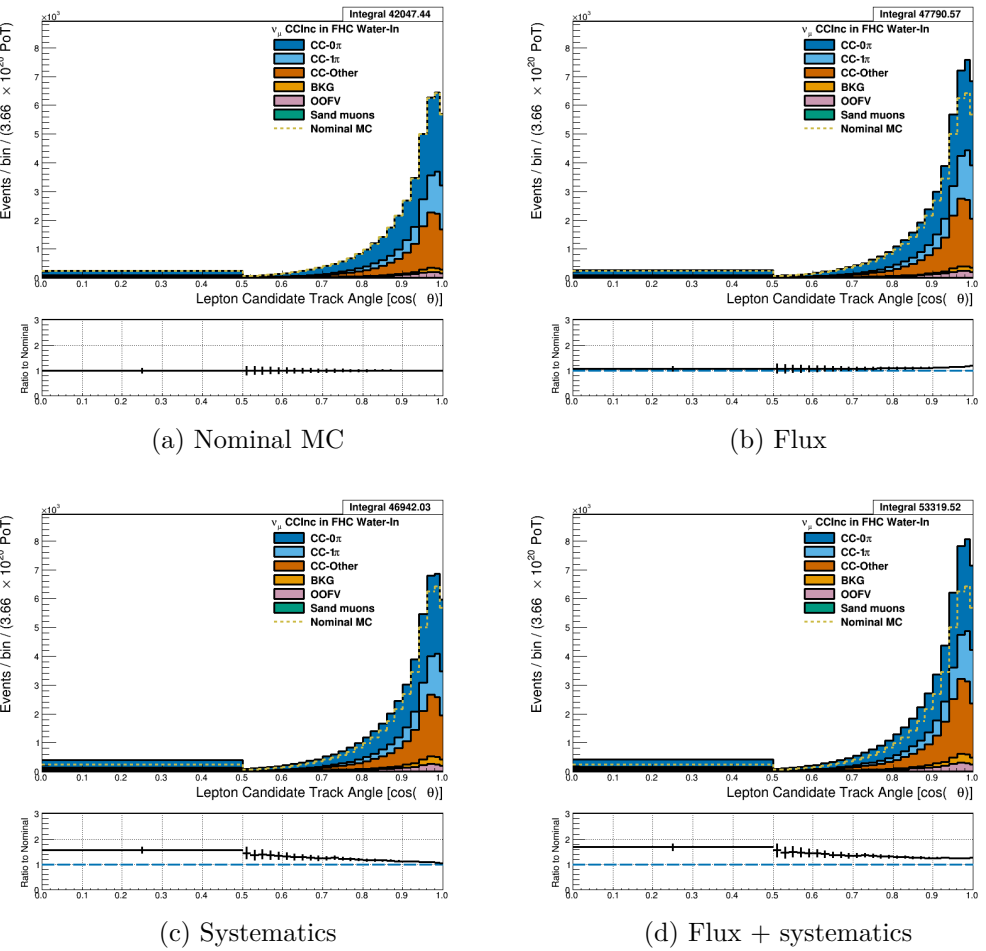


Figure 3.55: Reconstructed lepton candidate  $\cos \theta$  separated by topology for FHC  $\nu_\mu$  CC Inc. events occurring in the PØD in water-in mode. (a) The nominal MC prediction without any weights applied. (b) The flux tuning are applied. (c) The systematic weighting are applied. (d) Both flux and systematic weighting are applied.

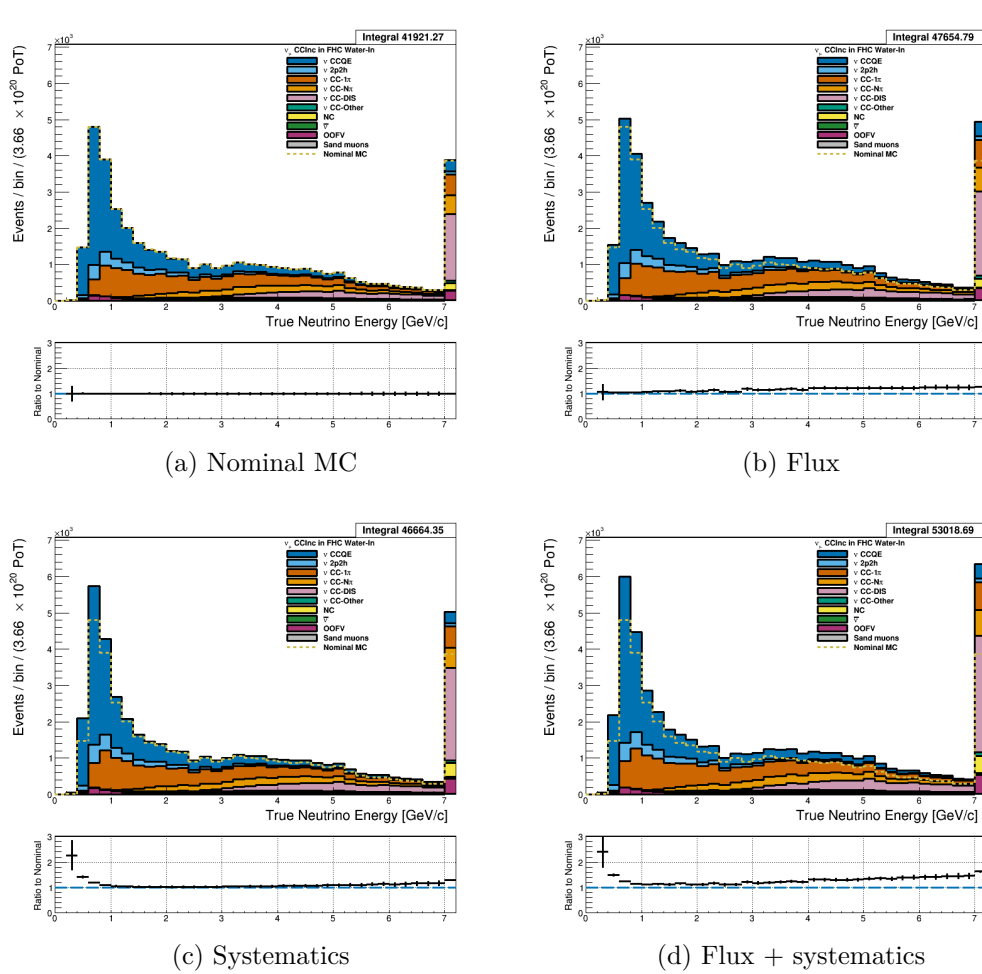


Figure 3.56: True neutrino energy associated with the lepton candidate separated by NEUT model interaction mode for FHC  $\nu_\mu$  CC Inc. events occurring in the PØD in water-out mode. (a) The nominal MC prediction without any weights applied. (b) The flux tuning are applied. (c) The systematic weighting are applied. (d) Both flux and systematic weighting are applied.

573 **3.5.1.2  $\bar{\nu}_\mu$  Selection in RHC Mode:** Shown in Figures 3.57 to 3.63 for  $\bar{\nu}_\mu$  CC Inclusive  
 574 events in RHC mode. There are three pairs of  $P, \theta$  figures with the same truth information  
 575 break down accompanied by one of neutrino energy. The truth information categories are  
 576 lepton candidate particle, NEUT reaction, and topology. Each figure consists of a set of four  
 577 sub-figures which illustrate the application of flux and detector systematic weights.

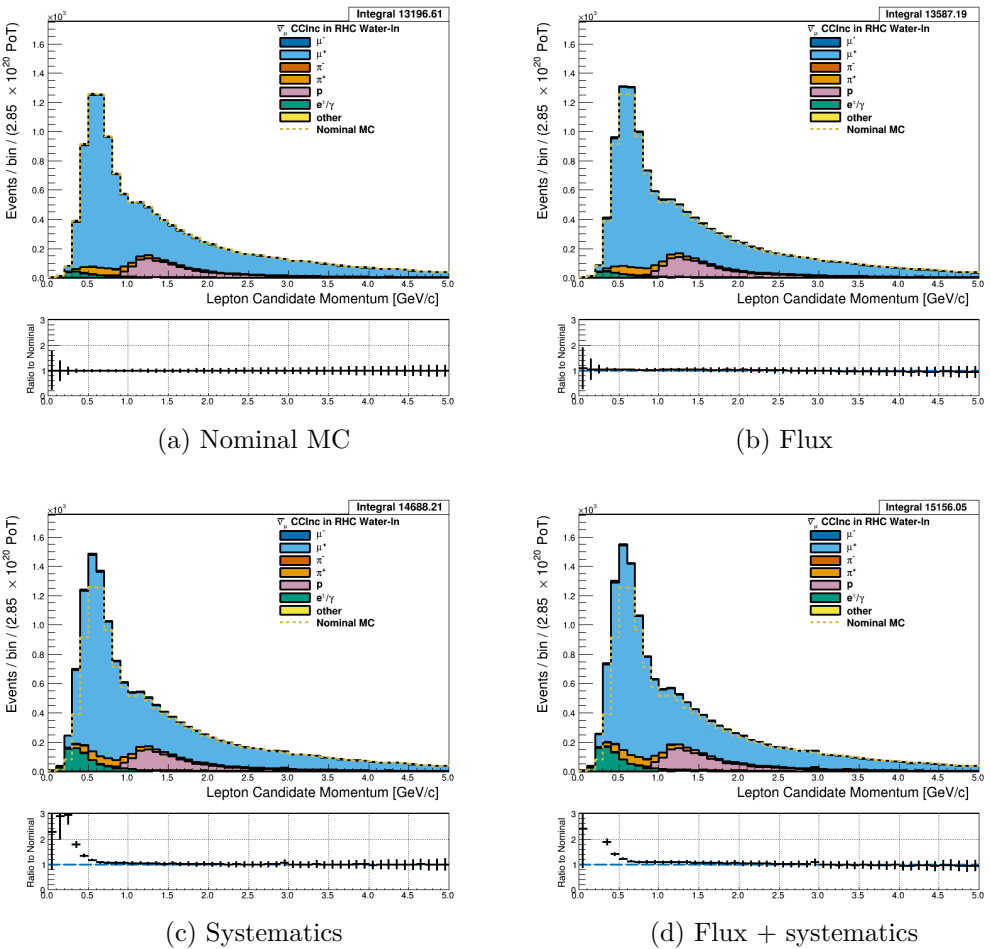


Figure 3.57: Reconstructed lepton candidate momentum separated by true particle species for RHC  $\bar{\nu}_\mu$  CC Inc. events occurring in the PØD in water-out mode. (a) The nominal MC prediction without any weights applied. (b) The flux tuning are applied. (c) The systematic weighting are applied. (d) Both flux and systematic weighting are applied.

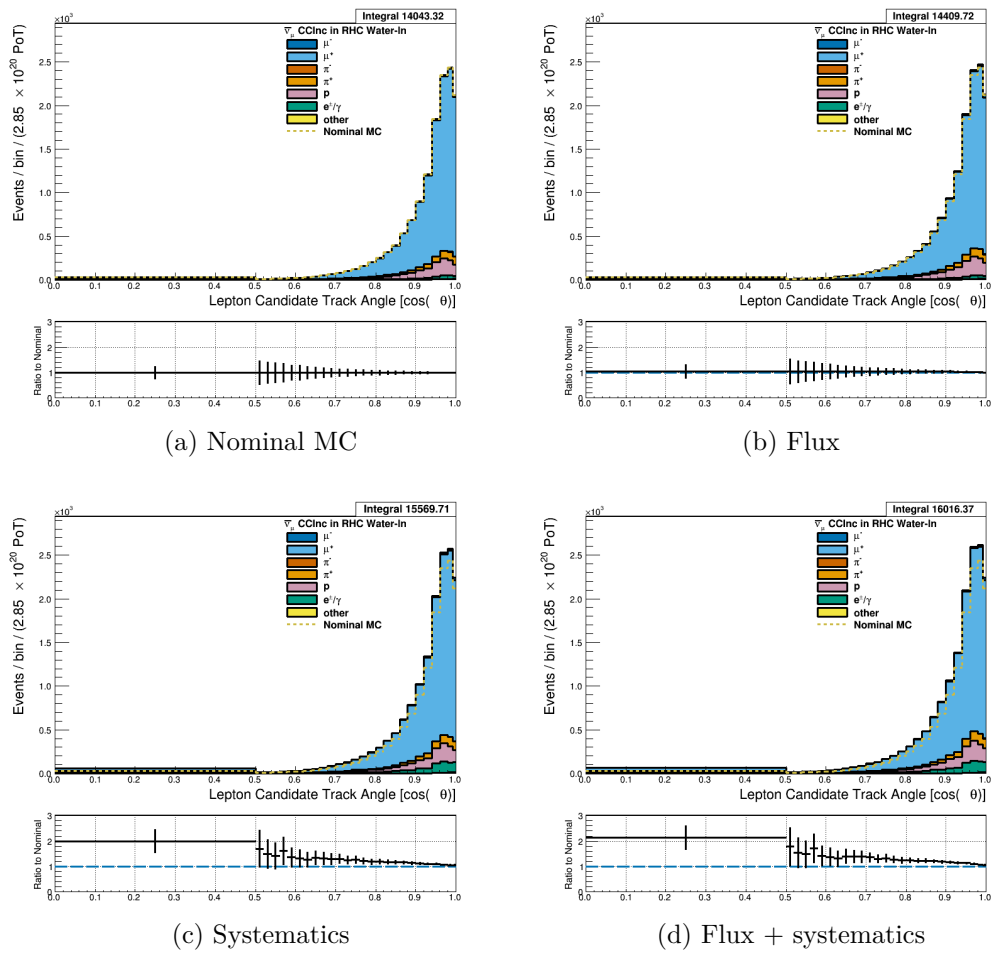


Figure 3.58: Reconstructed lepton candidate angle separated by true particle species for RHC  $\bar{\nu}_\mu$  CC Inc. events occurring in the PØD in water-in mode. (a) The nominal MC prediction without any weights applied. (b) The flux tuning are applied. (c) The systematic weighting are applied. (d) Both flux and systematic weighting are applied.

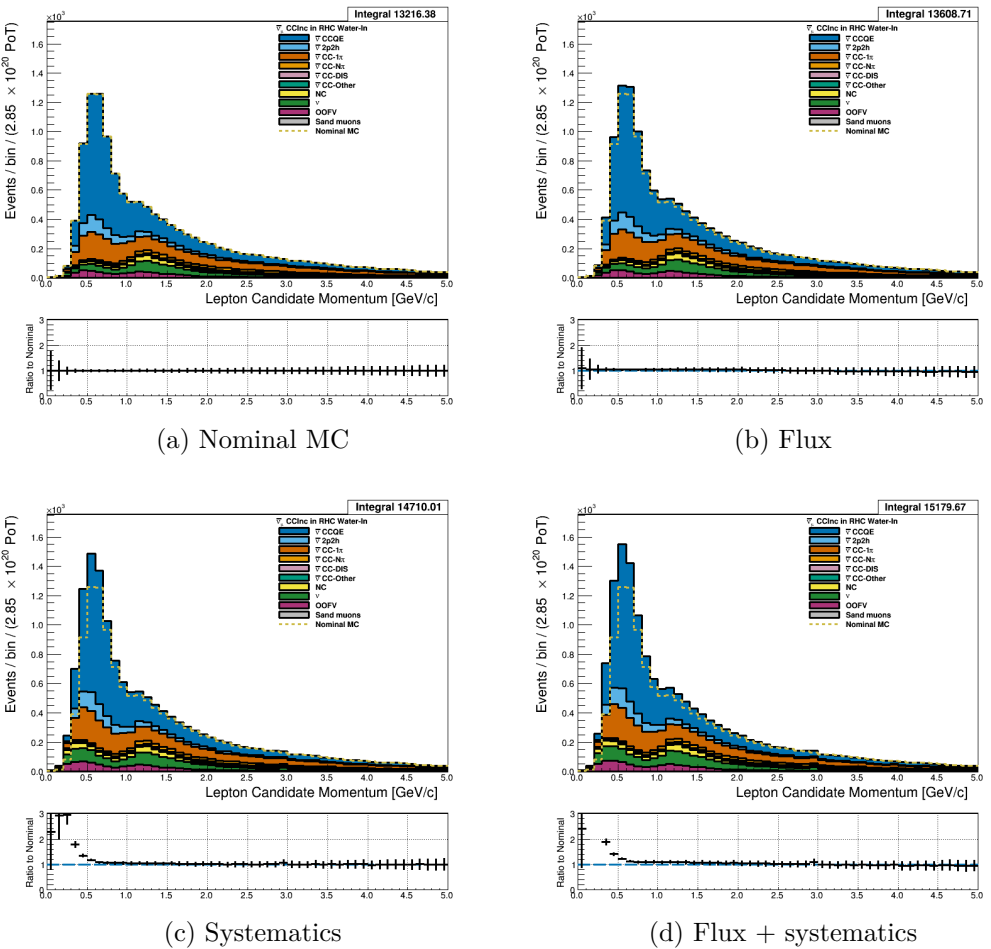


Figure 3.59: Reconstructed lepton candidate momentum separated by NEUT model interaction mode for RHC  $\bar{\nu}_\mu$  CC Inc. events occurring in the PØD in water-out mode. (a) The nominal MC prediction without any weights applied. (b) The flux tuning are applied. (c) The systematic weighting are applied. (d) Both flux and systematic weighting are applied.

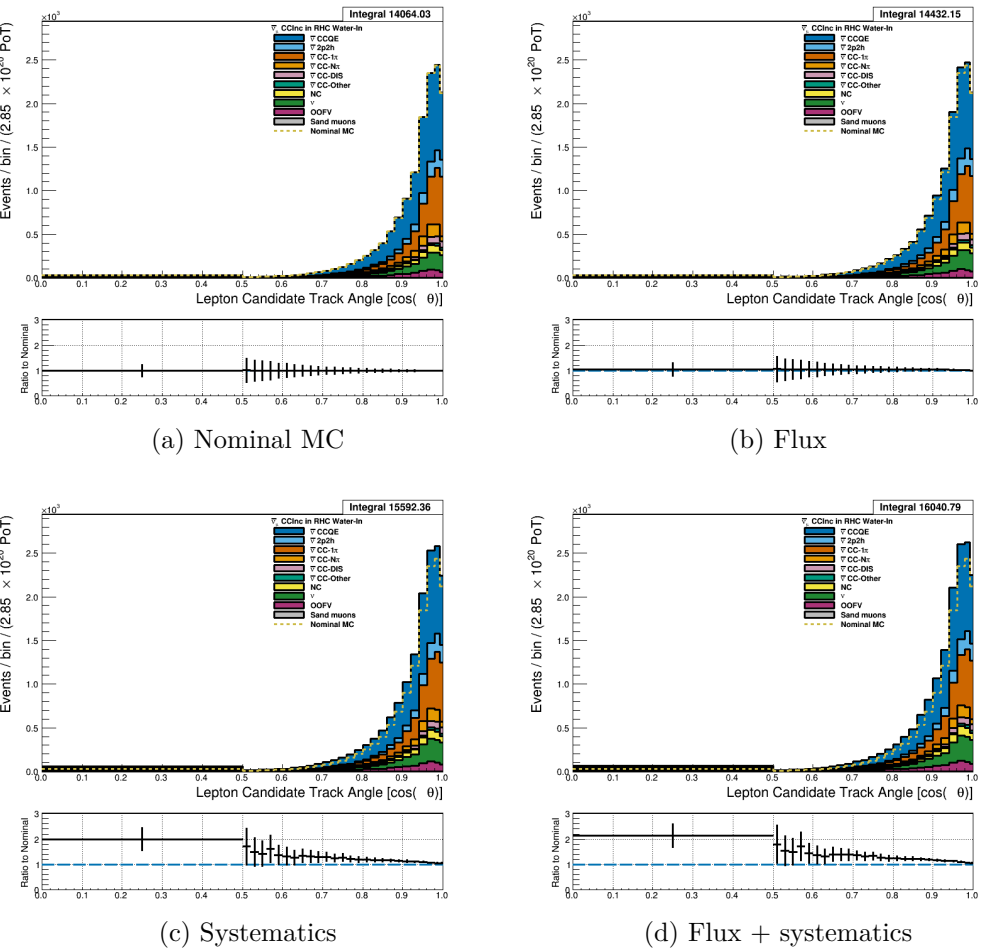


Figure 3.60: Reconstructed lepton candidate  $\cos \theta$  separated by NEUT model interaction mode for RHC  $\bar{\nu}_\mu$  CC Inc. events occurring in the PØD in water-out mode. (a) The nominal MC prediction without any weights applied. (b) The flux tuning are applied. (c) The systematic weighting are applied. (d) Both flux and systematic weighting are applied.

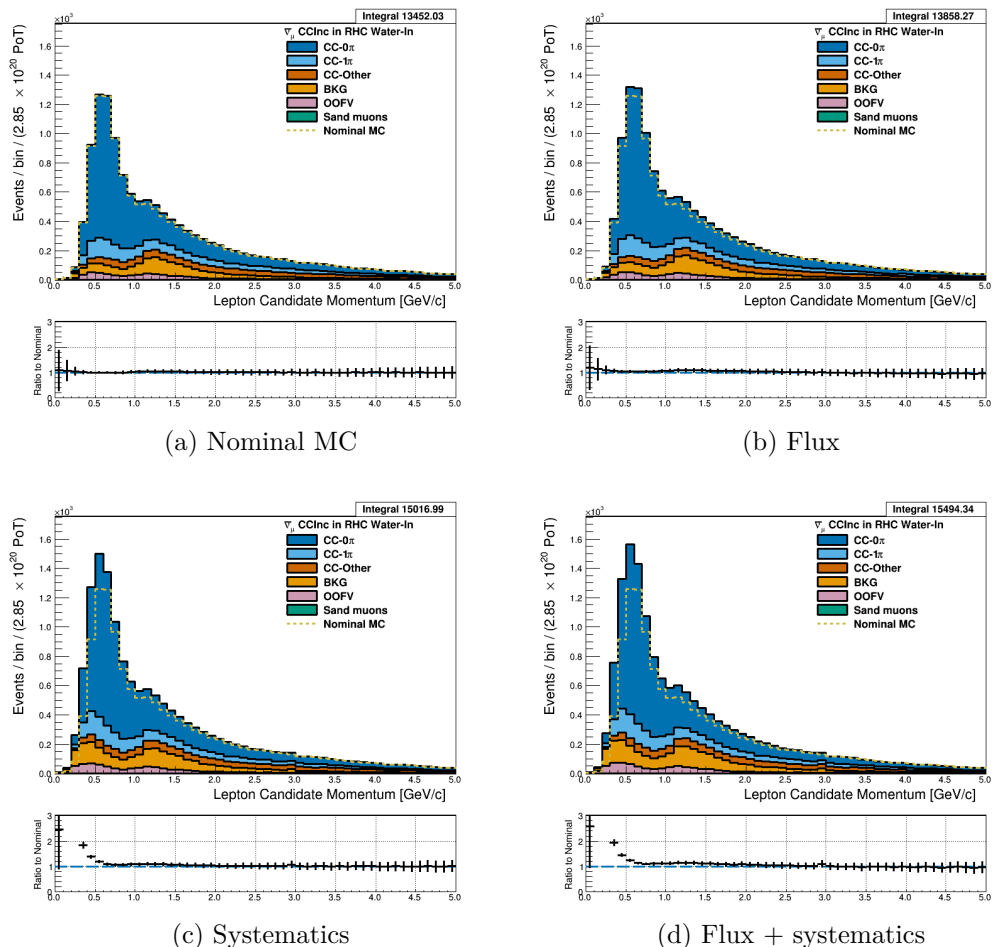


Figure 3.61: Reconstructed lepton candidate momentum separated by topology for RHC  $\bar{\nu}_\mu$  CC Inc. events occurring in the PØD in water-out mode. (a) The nominal MC prediction without any weights applied. (b) The flux tuning are applied. (c) The systematic weighting are applied. (d) Both flux and systematic weighting are applied.

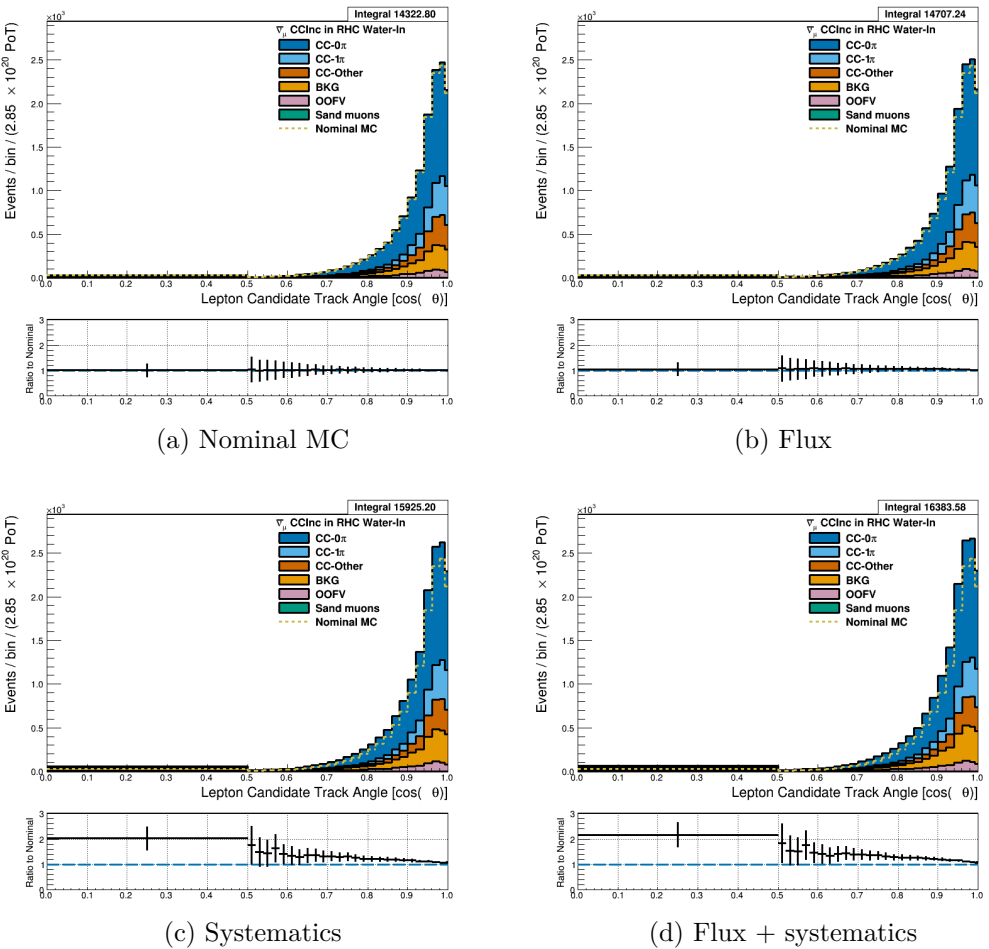


Figure 3.62: Reconstructed lepton candidate  $\cos \theta$  separated by topology for RHC  $\bar{\nu}_\mu$  CC Inc. events occurring in the PØD in water-out mode. (a) The nominal MC prediction without any weights applied. (b) The flux tuning are applied. (c) The systematic weighting are applied. (d) Both flux and systematic weighting are applied.

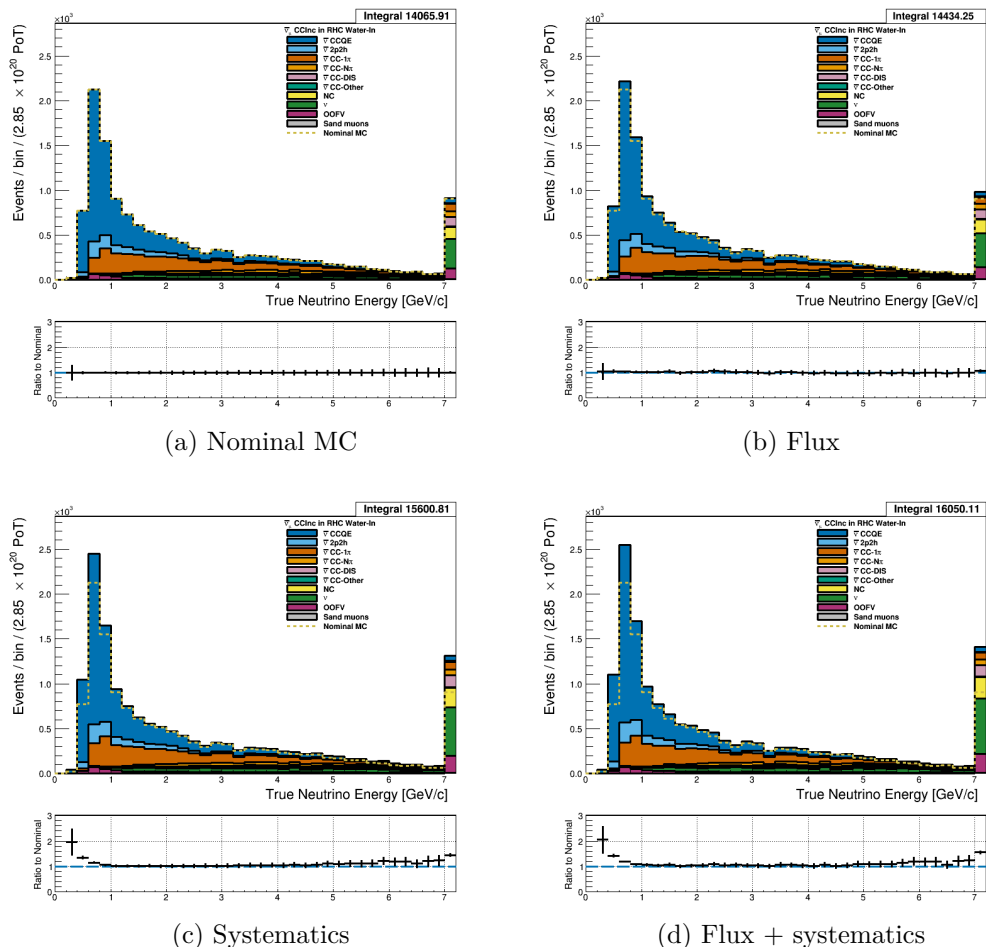


Figure 3.63: True neutrino energy associated with the lepton candidate separated by NEUT model interaction mode for RHC  $\bar{\nu}_\mu$  CC Inc. events occurring in the PØD in water-out mode. (a) The nominal MC prediction without any weights applied. (b) The flux tuning are applied. (c) The systematic weighting are applied. (d) Both flux and systematic weighting are applied.

### 3.5.1.3 $\nu_\mu$ Background Selection in RHC Mode: Add figures here

### 3.5.2 CC 1-Track (CCQE Enhanced)

Text

### 3.5.2.1 $\nu_\mu$ Selection in FHC Mode: Text

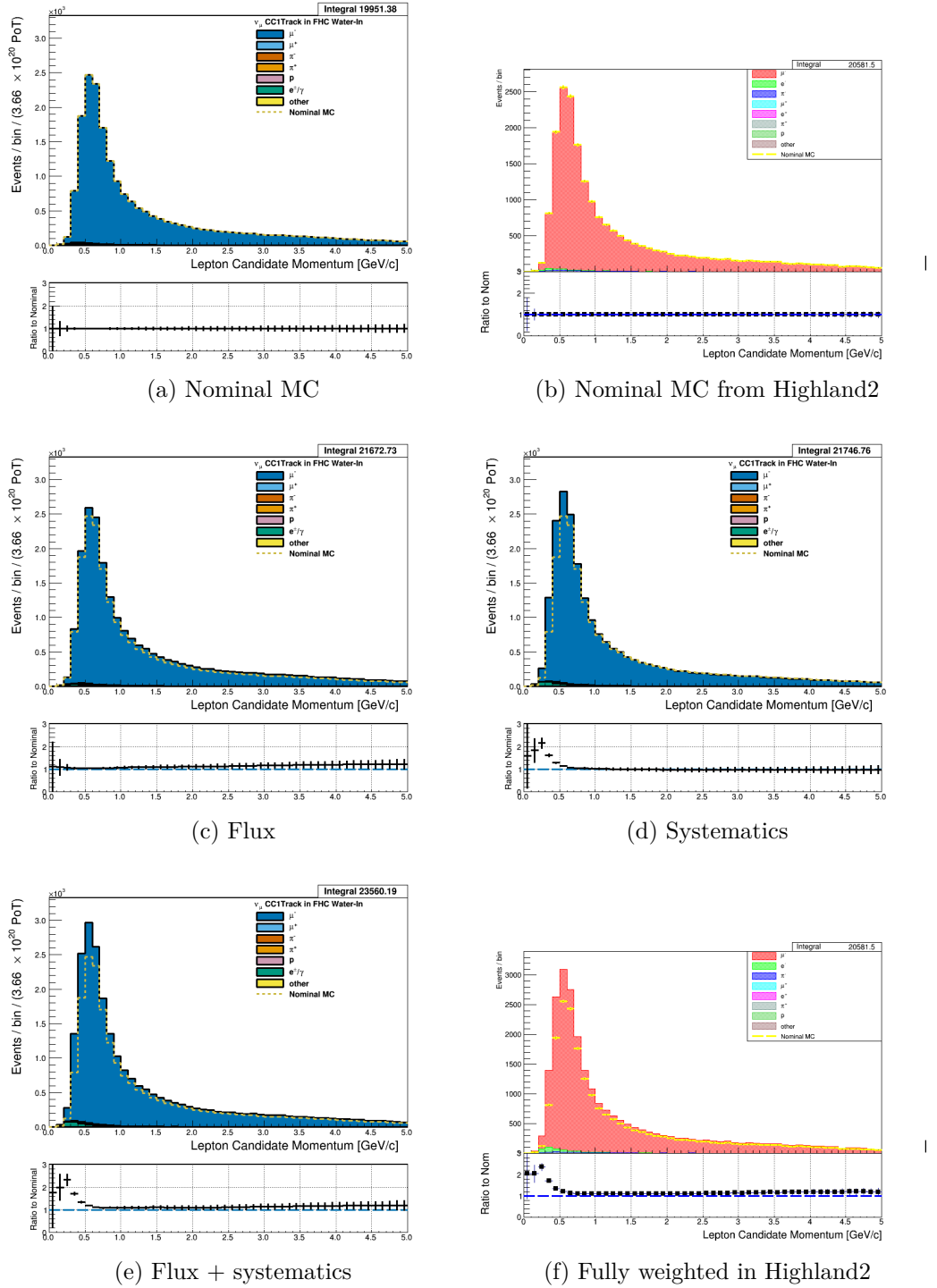


Figure 3.64: Reconstructed lepton candidate momentum separated by true particle species for FHC  $\nu_\mu$  CC 1-Track events occurring in the PØD in water-in mode. (a) The nominal MC prediction without any weights applied. (b) Highland2 comparison for (a) without any weights applied using the “NOW” draw option. (c) The flux tuning are applied. (d) The systematic weighting are applied. (e) Both flux and systematic weighting are applied. (f) Highland2 comparison for (e).

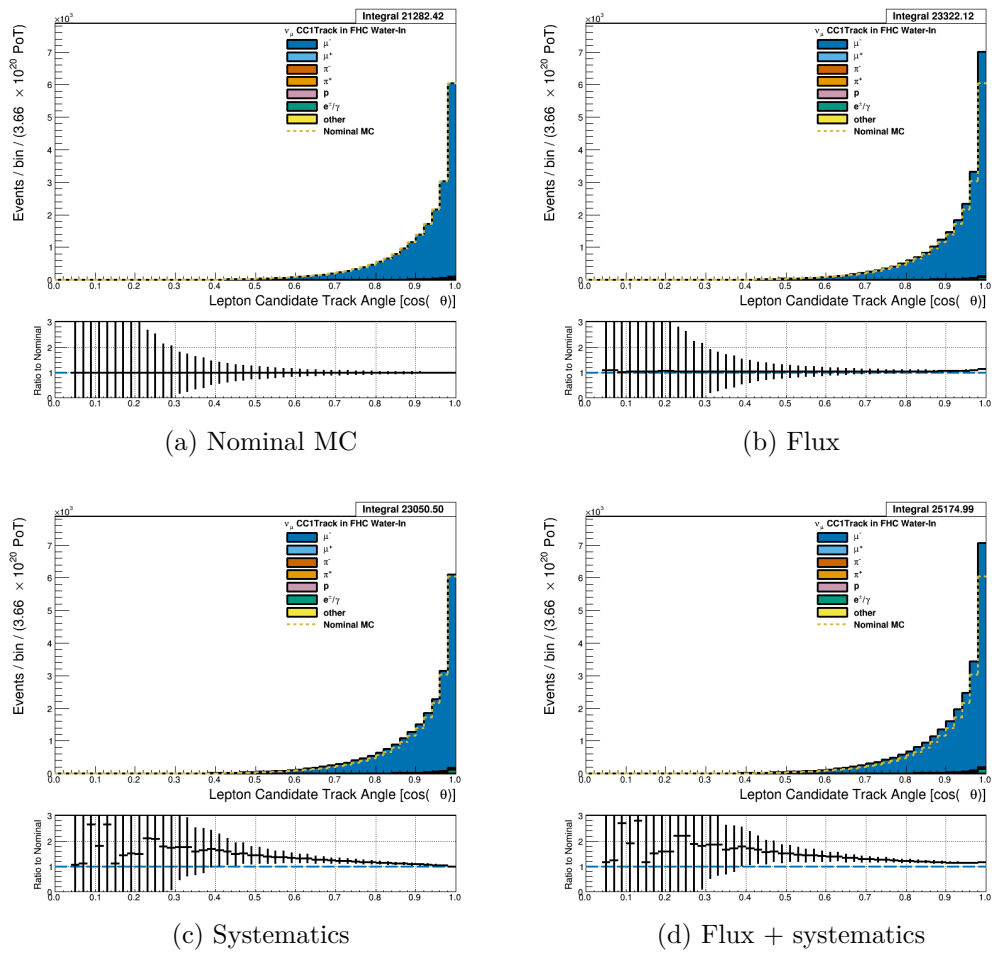


Figure 3.65: Reconstructed lepton candidate angle separated by true particle species for FHC  $\nu_\mu$  CC 1-Track events occurring in the PØD in water-in mode. (a) The nominal MC prediction without any weights applied. (b) The flux tuning are applied. (c) The systematic weighting are applied. (d) Both flux and systematic weighting are applied.

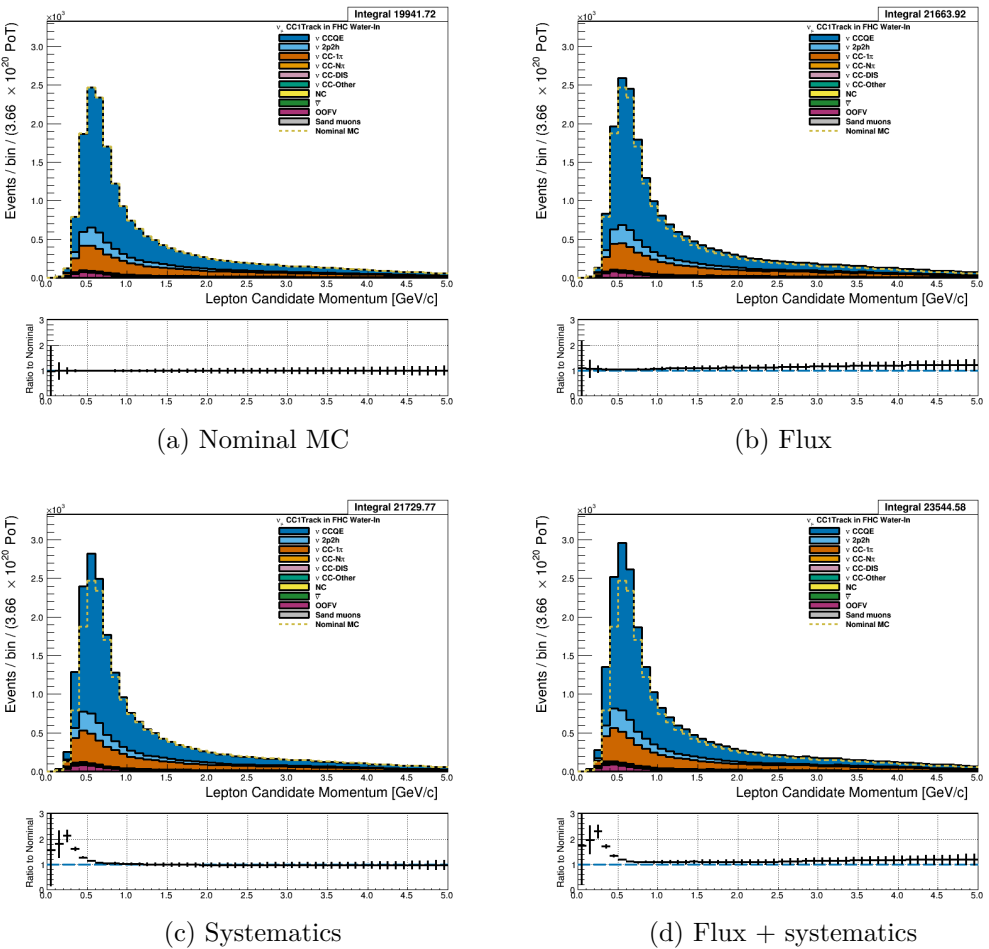


Figure 3.66: Reconstructed lepton candidate momentum separated by NEUT model interaction mode for FHC  $\nu_\mu$  CC 1-Track events occurring in the PØD in water-in mode. (a) The nominal MC prediction without any weights applied. (b) The flux tuning are applied. (c) The systematic weighting are applied. (d) Both flux and systematic weighting are applied.

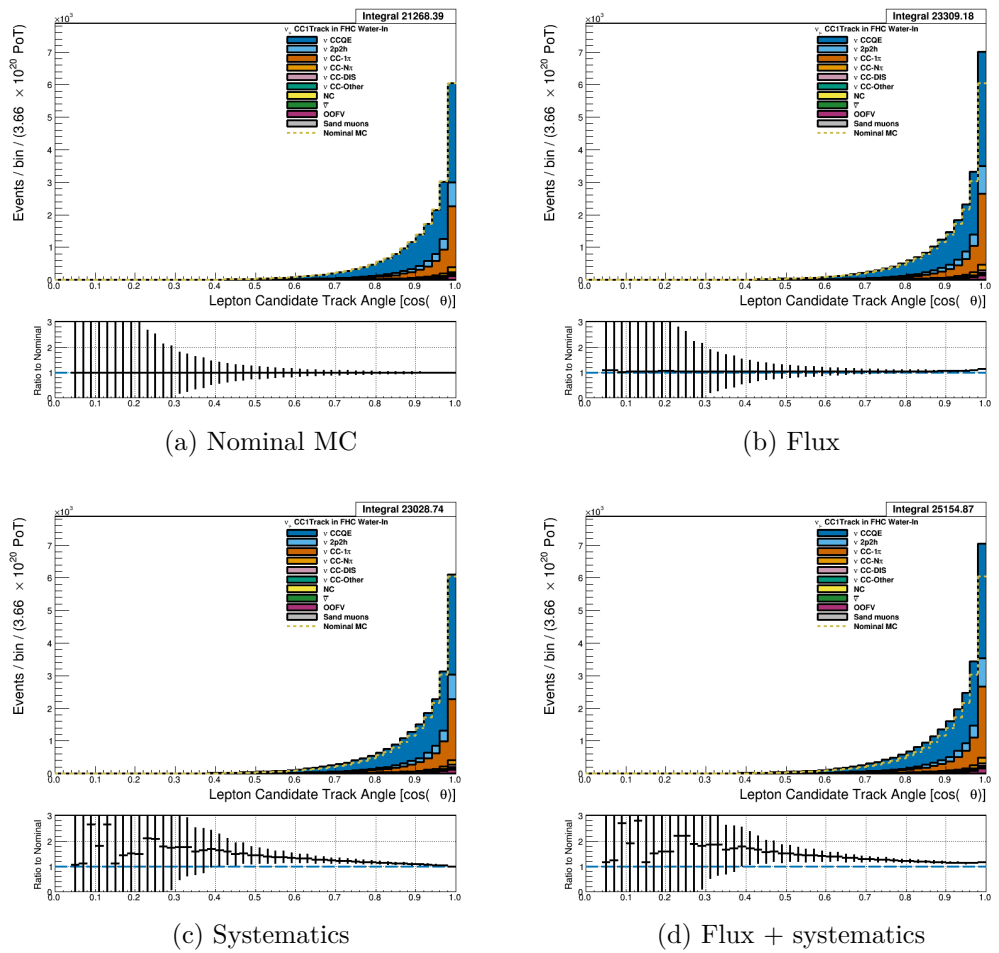


Figure 3.67: Reconstructed lepton candidate  $\cos \theta$  separated by NEUT model interaction mode for FHC  $\nu_\mu$  CC 1-Track events occurring in the PØD in water-in mode. (a) The nominal MC prediction without any weights applied. (b) The flux tuning are applied. (c) The systematic weighting are applied. (d) Both flux and systematic weighting are applied.

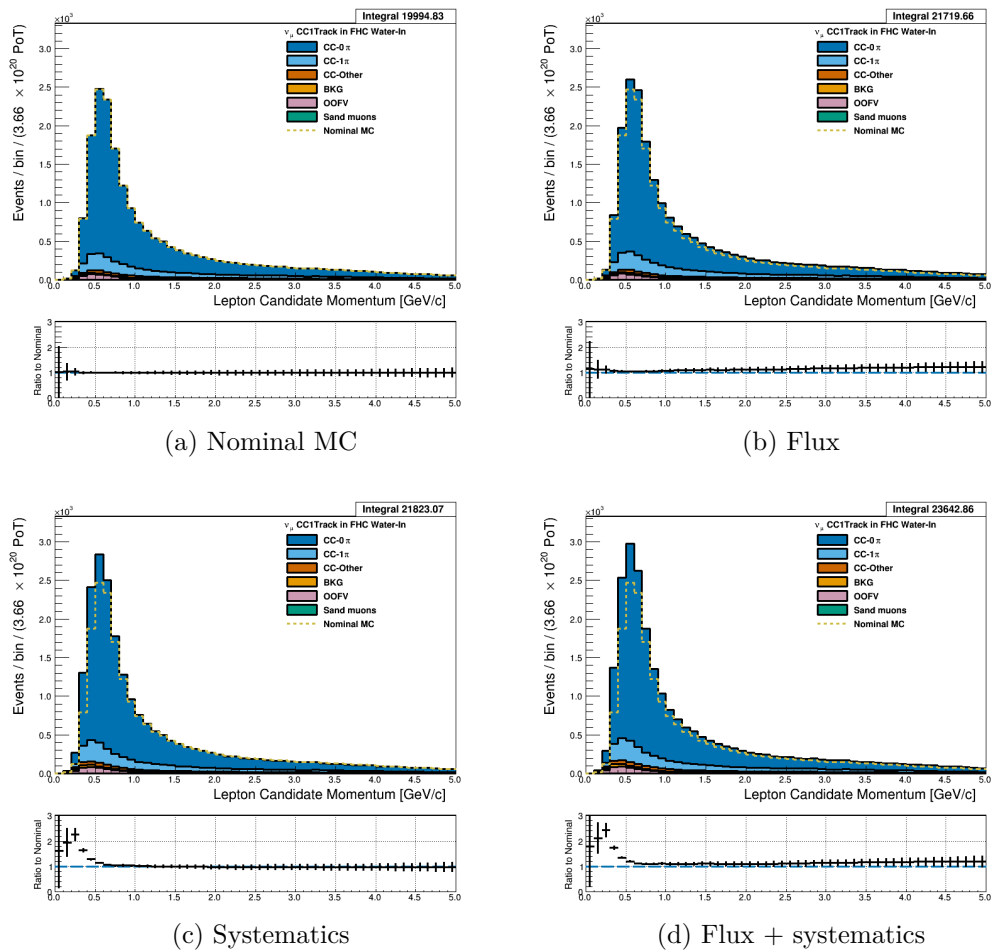


Figure 3.68: Reconstructed lepton candidate momentum separated by topology for FHC  $\nu_\mu$  CC 1-Track events occurring in the PØD in water-in mode. (a) The nominal MC prediction without any weights applied. (b) The flux tuning are applied. (c) The systematic weighting are applied. (d) Both flux and systematic weighting are applied.

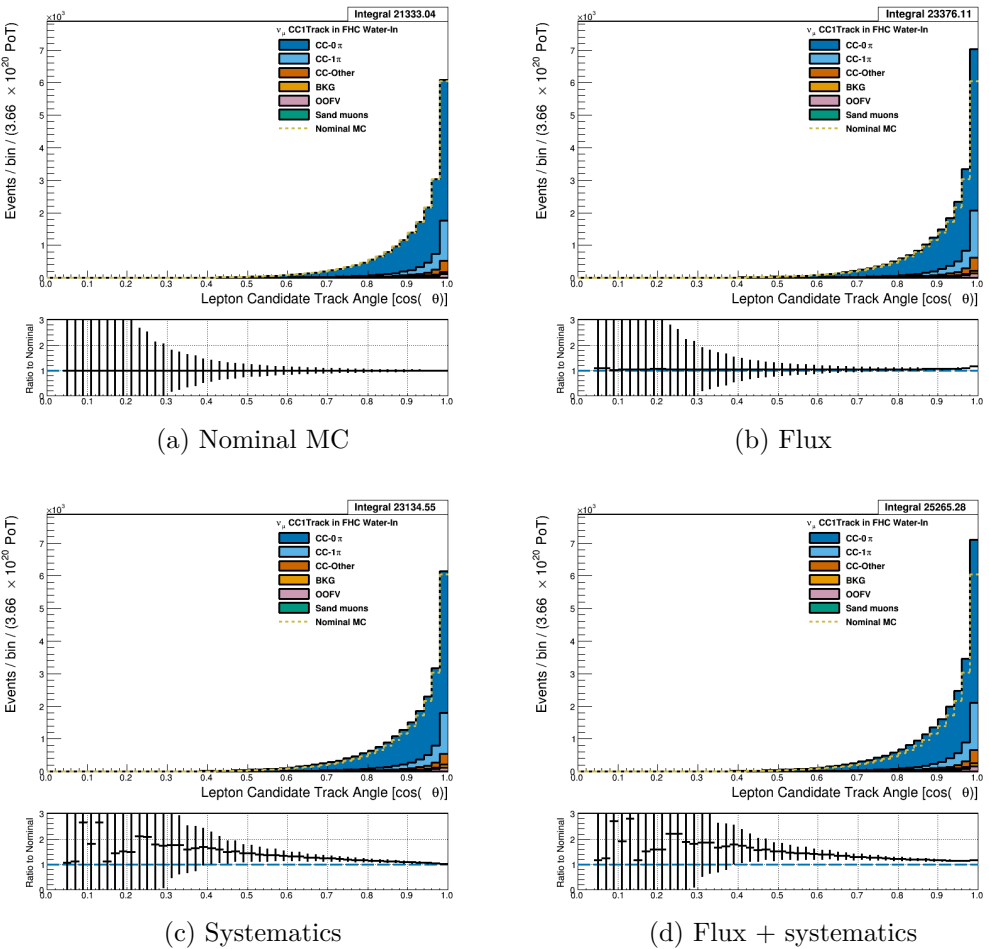


Figure 3.69: Reconstructed lepton candidate  $\cos \theta$  separated by topology for FHC  $\nu_\mu$  CC 1-Track events occurring in the PØD in water-in mode. (a) The nominal MC prediction without any weights applied. (b) The flux tuning are applied. (c) The systematic weighting are applied. (d) Both flux and systematic weighting are applied.

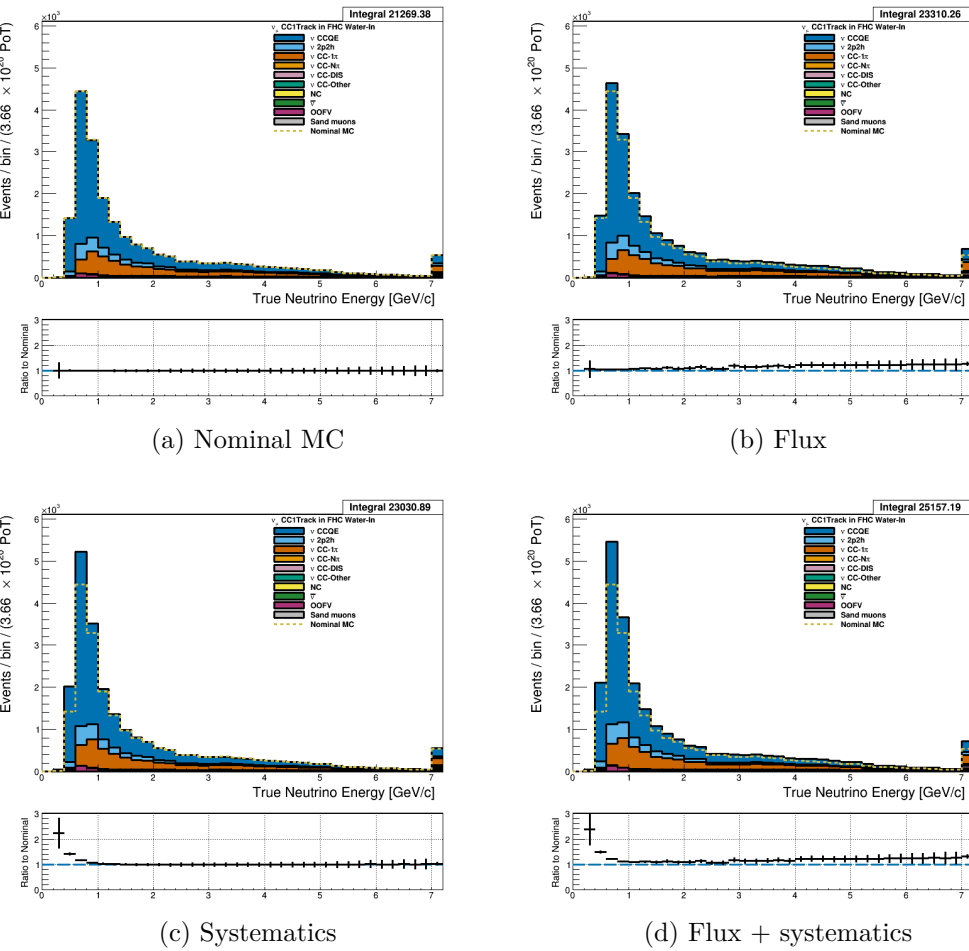


Figure 3.70: True neutrino energy associated with the lepton candidate separated by NEUT model interaction mode for FHC  $\nu_\mu$  CC 1-Track events occurring in the PØD in water-out mode. (a) The nominal MC prediction without any weights applied. (b) The flux tuning are applied. (c) The systematic weighting are applied. (d) Both flux and systematic weighting are applied.

### 3.5.2.2 $\bar{\nu}_\mu$ Selection in RHC Mode: Text

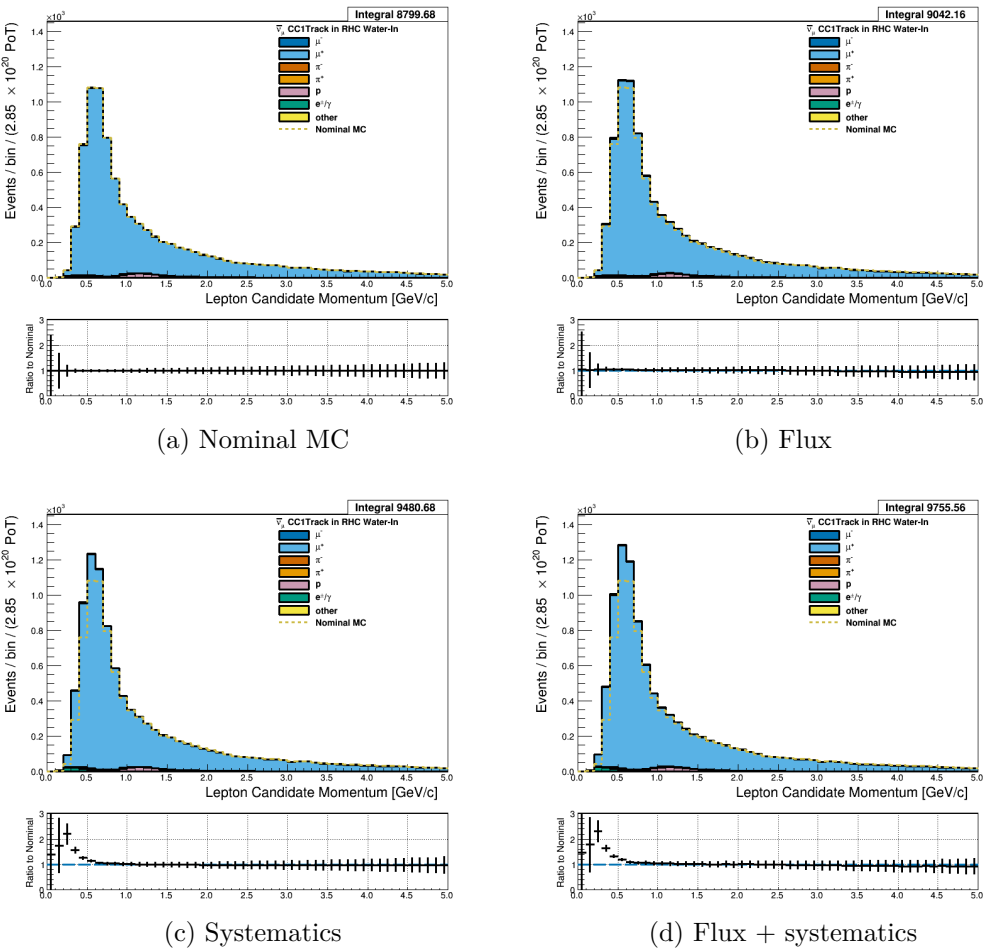


Figure 3.71: Reconstructed lepton candidate momentum separated by true particle species for RHC  $\bar{\nu}_\mu$  CC 1-Track events occurring in the PØD in water-out mode. (a) The nominal MC prediction without any weights applied. (b) The flux tuning are applied. (c) The systematic weighting are applied. (d) Both flux and systematic weighting are applied.

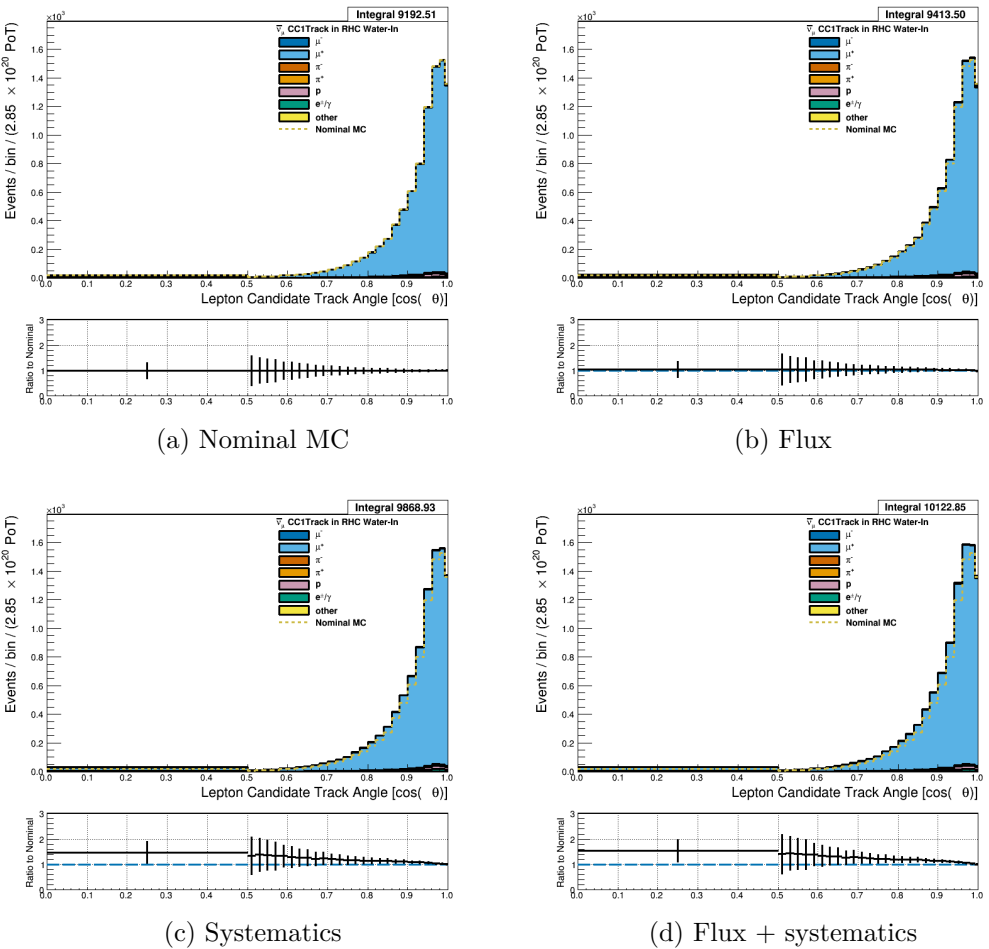


Figure 3.72: Reconstructed lepton candidate angle separated by true particle species for RHC  $\bar{\nu}_\mu$  CC 1-Track events occurring in the PØD in water-in mode. (a) The nominal MC prediction without any weights applied. (b) The flux tuning are applied. (c) The systematic weighting are applied. (d) Both flux and systematic weighting are applied.

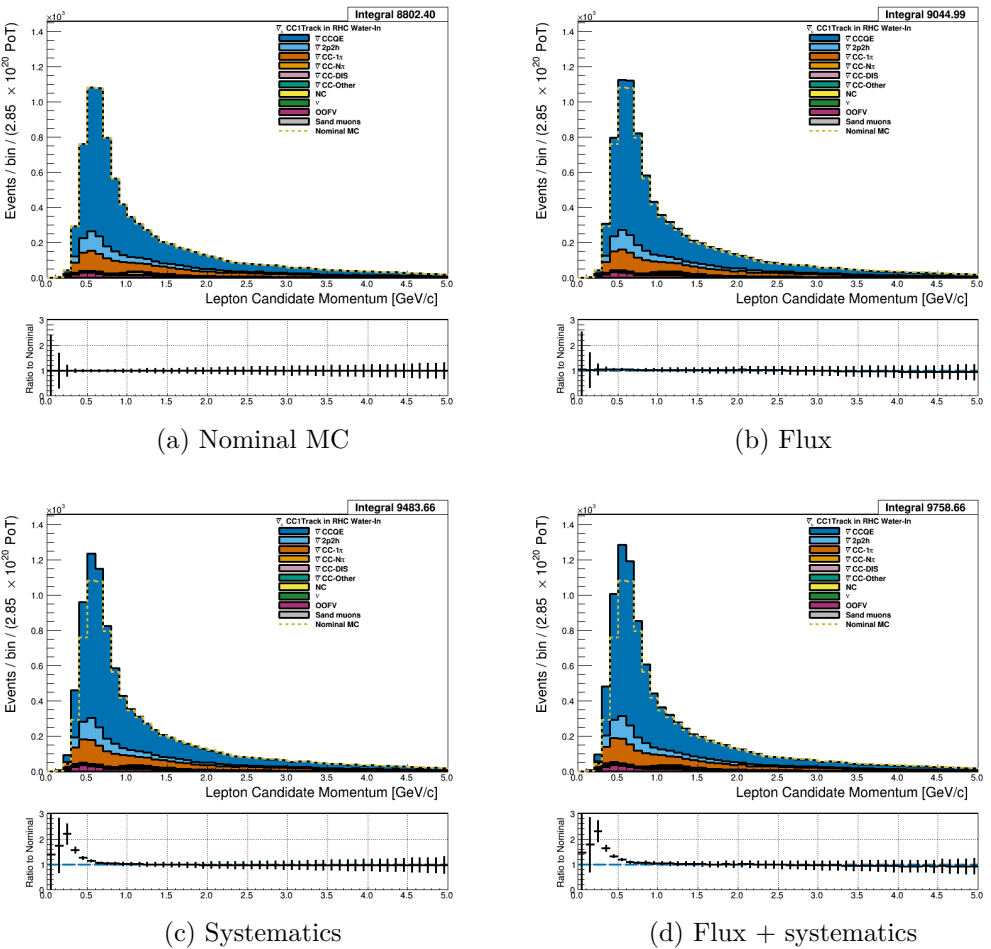


Figure 3.73: Reconstructed lepton candidate momentum separated by NEUT model interaction mode for RHC  $\bar{\nu}_\mu$  CC 1-Track events occurring in the PØD in water-out mode. (a) The nominal MC prediction without any weights applied. (b) The flux tuning are applied. (c) The systematic weighting are applied. (d) Both flux and systematic weighting are applied.

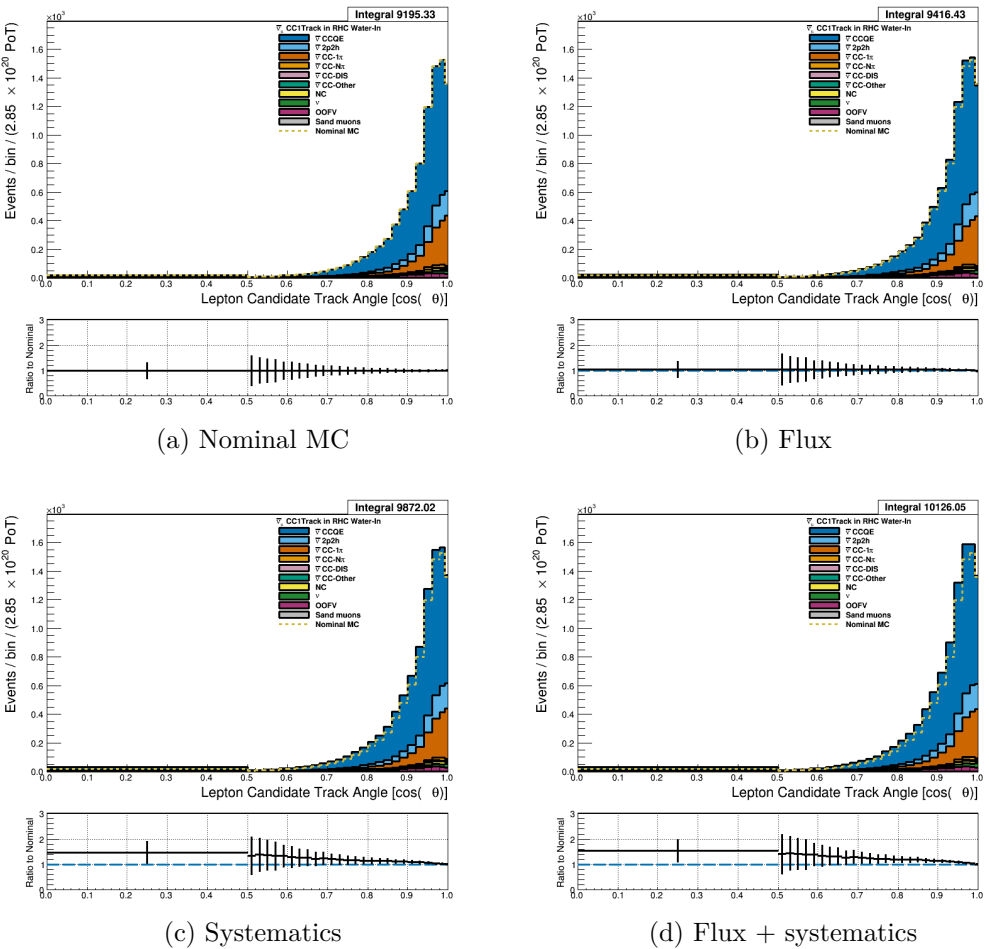


Figure 3.74: Reconstructed lepton candidate  $\cos \theta$  separated by NEUT model interaction mode for RHC  $\bar{\nu}_\mu$  CC 1-Track events occurring in the PØD in water-out mode. (a) The nominal MC prediction without any weights applied. (b) The flux tuning are applied. (c) The systematic weighting are applied. (d) Both flux and systematic weighting are applied.

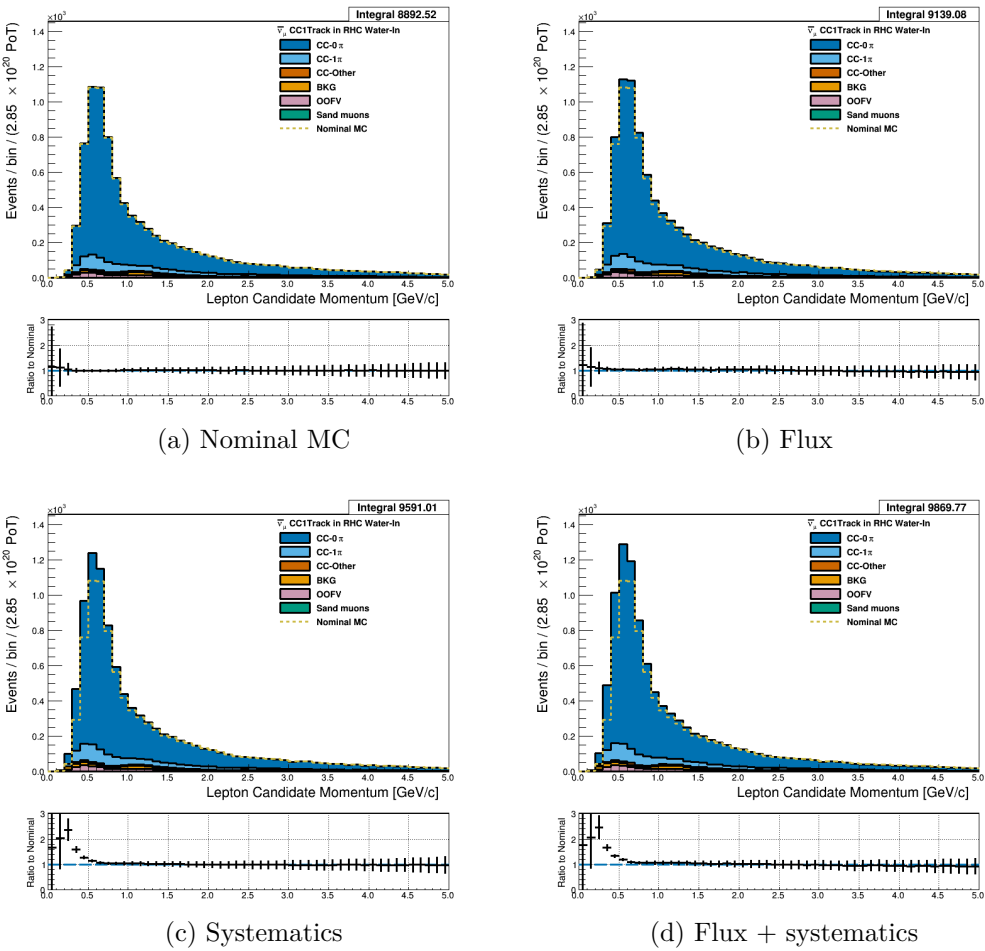


Figure 3.75: Reconstructed lepton candidate momentum separated by topology for RHC  $\bar{\nu}_\mu$  CC 1-Track events occurring in the PØD in water-out mode. (a) The nominal MC prediction without any weights applied. (b) The flux tuning are applied. (c) The systematic weighting are applied. (d) Both flux and systematic weighting are applied.

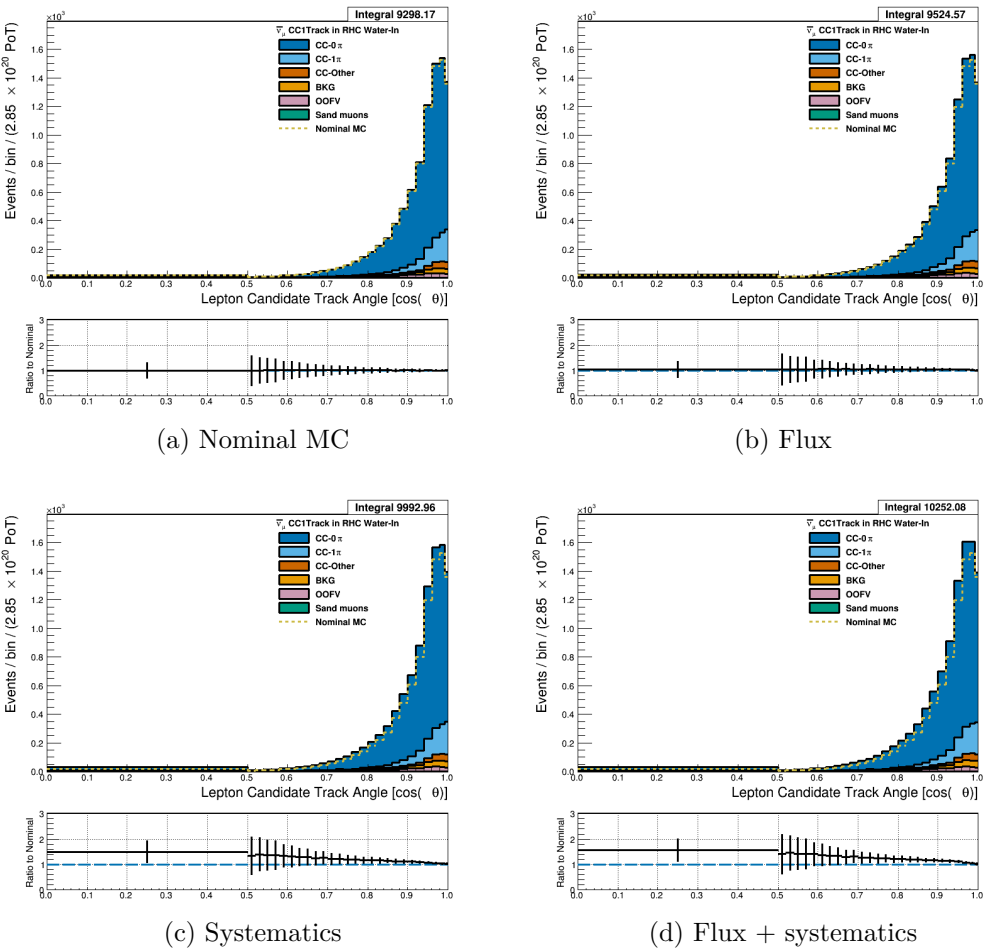


Figure 3.76: Reconstructed lepton candidate  $\cos \theta$  separated by topology for RHC  $\bar{\nu}_\mu$  CC 1-Track events occurring in the PØD in water-out mode. (a) The nominal MC prediction without any weights applied. (b) The flux tuning are applied. (c) The systematic weighting are applied. (d) Both flux and systematic weighting are applied.

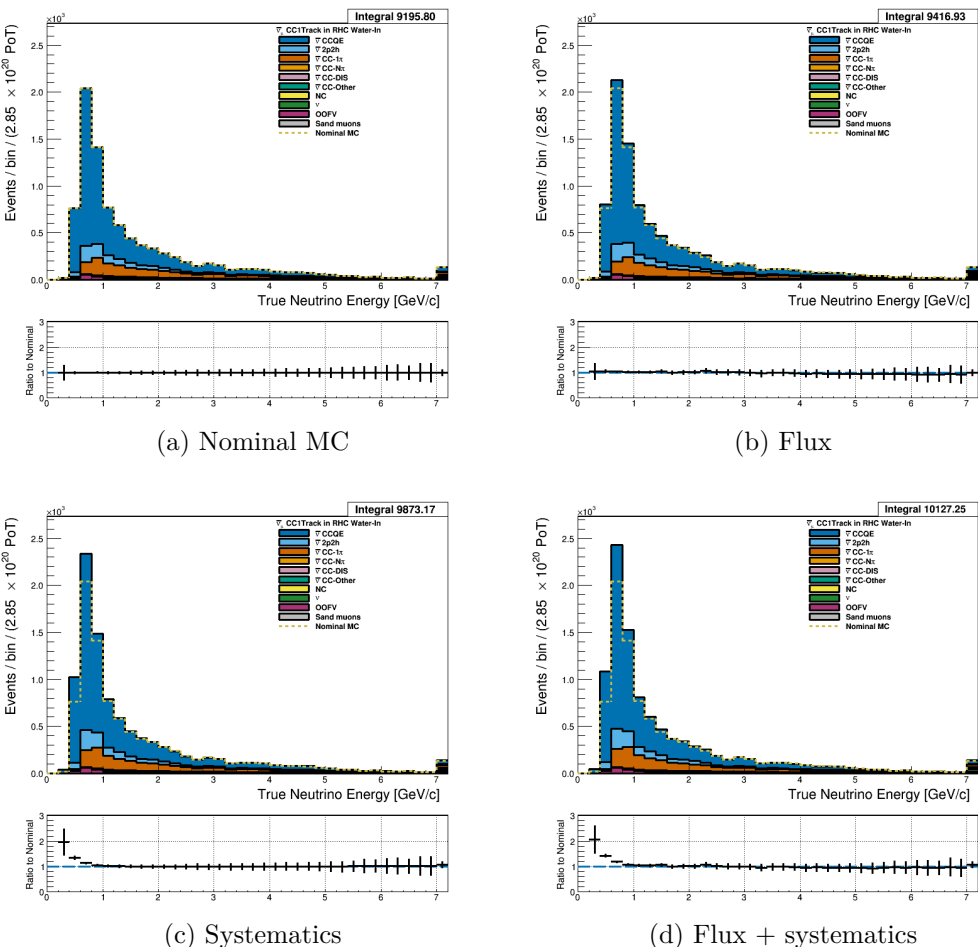


Figure 3.77: True neutrino energy associated with the lepton candidate separated by NEUT model interaction mode for RHC  $\bar{\nu}_\mu$  CC 1-Track events occurring in the PØD in water-out mode. (a) The nominal MC prediction without any weights applied. (b) The flux tuning are applied. (c) The systematic weighting are applied. (d) Both flux and systematic weighting are applied.

### 3.5.2.3 $\nu_\mu$ Background Selection in RHC Mode: Text

### 3.5.3 CC N-Tracks (CCnQE Enhanced)

Text

### 3.5.3.1 $\nu_\mu$ Selection in FHC Mode: Text

587 **3.5.3.2  $\bar{\nu}_\mu$  Selection in RHC Mode:** Text

588 **3.5.3.3  $\nu_\mu$  Background Selection in RHC Mode:** Text

589 **3.5.4 Differences Between Water-Out and Water-In Samples**

590 **4 PØD-Only BANFF Parameterization**

591 **4.1 PØD Samples Fit Binning**

592 The PØD ND280 BANFF fit uses the samples described in 3. The bin edges are tabulated  
593 below.

- 594 • FHC  $\nu_\mu$ CC 1-Track bin edges:

595  $p$  [GeV/c]: 0, 0.3, 0.4, 0.5, 0.6, 0.7, 0.8, 1, 1.25, 1.5, 2, 3, 4, 5.5, 30

596  $\cos\theta$  : -1, 0.7, 0.8 , 0.88, 0.94, 0.96, 0.975, 0.99, 1

- 597 • FHC  $\nu_\mu$ CC N-Tracks bin edges:

598  $p$  [GeV/c]: 0, 0.4, 0.5, 0.6, 0.7, 0.8, 1, 1.2, 1.5, 1.8, 2.2, 2.7, 3.5, 5, 10, 30

599  $\cos\theta$  : -1, 0.65, 0.77, 0.85, 0.9, 0.94, 0.97, 0.99, 1

- 600 • RHC  $\bar{\nu}_\mu$ CC 1-Track bin edges:

601  $p$  [GeV/c]: 0, 0.4, 0.5, 0.6, 0.7, 0.8, 1, 1.25, 1.5, 2, 3, 30

602  $\cos\theta$  : -1, 0.82, 0.87, 0.9, 0.93, 0.95, 0.97, 0.99, 1

- 603 • RHC  $\bar{\nu}_\mu$ CC N-Tracks bin edges:

604  $p$  [GeV/c]: 0, 0.5, 0.9, 1.25, 1.6, 2, 3, 8, 30

605  $\cos\theta$  : -1, 0.8, 0.89, 0.95, 0.97, 0.99, 1

- 606 • RHC  $\nu_\mu$ CC 1-Track bin edges:

607  $p$  [GeV/c]: 0, 0.4, 0.6, 0.8, 1.1, 2, 10

608  $\cos\theta$  : -1, 0.78, 0.84, 0.89, 0.92, 0.95, 0.97, 0.98, 0.99, 1

- 609 • RHC  $\nu_\mu$ CC N-Tracks bin edges:

610  $p$  [GeV/c]:0, 0.4, 0.6, 0.8, 1, 1.5, 2, 3, 10  
611  $\cos\theta$  : -1, 0.7, 0.8, 0.85, 0.9, 0.94, 0.965, 0.98, 0.99, 1

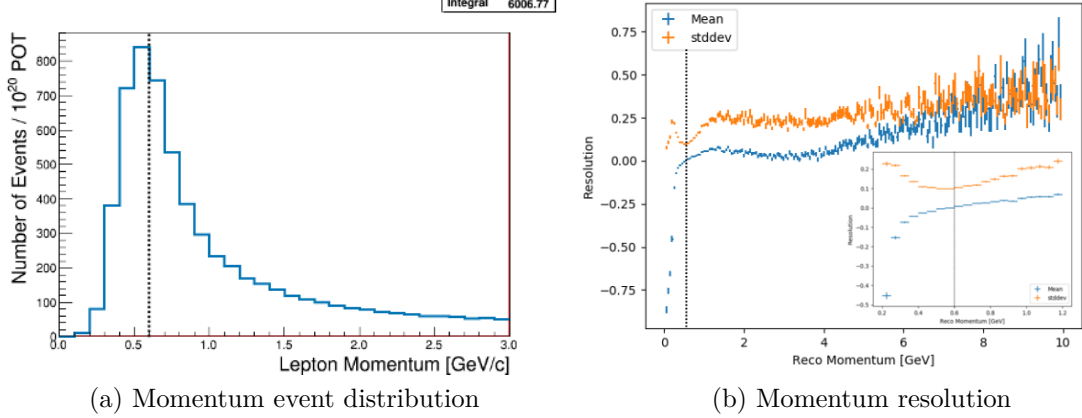
612 **4.1.1 Fit Binning Determination**

613 The fit binning is designed to optimized to ensure at least 1 predicted Monte Carlo (MC)  
614 event in each bin when scaled to the collected data POT. The fit bins must also account  
615 for detector smearing effects. In order to mitigate smearing and event migration, the recon-  
616 structed kinematics were examined to their MC truth value using only correctly identified  
617 leptons in one-dimensional kinematic slices. Since the MC provides about  $10\times$  the data  
618 statistics, the statistical uncertainty for each bin should be negligible for high statistics re-  
619 gions. The kinematics are scanned across their full relevant spaces in order to understand the  
620 needed width for a fit bin. The first fit bin is always defined from the kinematic maximum.

621 For the momentum bins, the momentum resolution is compared to MC truth . The  
622 momentum resolution is defined as

$$R(r, t) = \frac{r - t}{t},$$

623 where  $r$  is the reconstructed momentum and  $t$  is the true value. The momentum was scanned  
624 in finite bin widths with the mean and standard deviation of the resolution  $R$  extracted. The  
625 mean and standard deviation are used as a proxy for the true bias and true resolution, re-  
626 spectively. In addition, a bootstrapping algorithm was employed to understand the accuracy  
627 of the sample estimates. Bootstrapping in this context is sampling over all relevant values  
628 of true momentum and randomly replacing the values. For each scanned bin, at least 1000  
629 bootstrapping sampling with replacement was performed. In the case of large variances in  
630 the bootstrapping samples, additional 10000 sampling with replacement were performed.  
631 The results for analyzing the FHC  $\nu_\mu$ CC 1-Track selection is shown in Figure 4.1 on page



(a) Momentum event distribution

(b) Momentum resolution

Figure 4.1: The momentum event distribution and uncertainty for FHC  $\nu_\mu$ CC 1-Track events is shown above. Only correctly identified muons are shown. (a) The number of events per unit momentum is scaled to  $10^{20}$  POT which is the approximate scale for all the samples in this analysis. A dashed line indicates the maximum of the peak. (b) The resolution of the momentum measurement is shown for a wide region of momenta. In the inset is the resolution zoomed near the momentum distribution maximum. Like in (a), a dashed line shows the momentum maximum.

115.

The angle bins are treated in an almost identical manner. While the fit bins and physics parameterized in  $\cos \theta$ , the angle with respect to the z-axis, the detector smearing is a function of the angle  $\theta$ . In addition, since the angle can be nearly zero for the most forward-going tracks, the resolution was not used to characterize the angular uncertainties. Instead, the difference between the true and reconstructed angle were analyzed as shown in . The mean and standard deviation were studied. Bootstrapping was again used to quantify the accuracy of the mean and standard deviation.

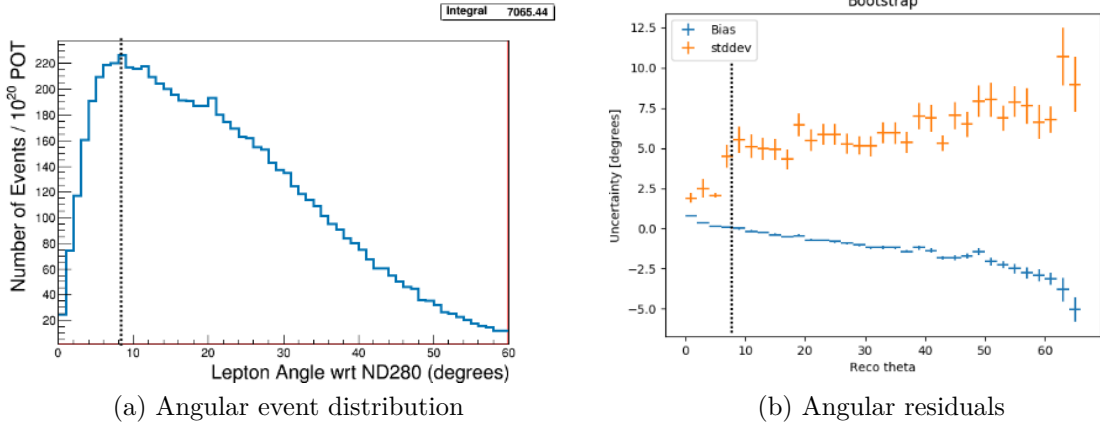


Figure 4.2: The angular event distribution and uncertainty for FHC  $\nu_\mu$ CC 1-Track events is shown above. Only correctly identified muons are shown. (a) The number of angular events is scaled to  $10^{20}$  POT which is the approximate scale for all the samples in this analysis. A dashed line indicates the maximum of the peak. (b) The residual of the angular measurement is shown up to where there are sufficient statistics. Like in (a), a dashed line shows the momentum maximum.

640

## 5 Detector Systematics

641 Sources of systematic uncertainties, hitherto referred to as systematics, must be evaluated in  
642 order to understand their effect on any analysis. The BANFF fit utilizes a set of canonical  
643 systematics

644

### 5.1 Detector Systematic Uncertainties

645 All the detector systematics in BANFF are evaluated as either observable variations or  
646 weights. An observable variation affects the physical observables of selected events. The most  
647 important variation is the energy loss in the PØD of the outgoing muon in CC interactions.

648

#### 5.1.1 Efficiency-like Systematics

649 Efficiency-like systematics are treated as weights to the MC predictions in order to evaluate  
650 the uncertainty the systematic has on an analysis. They are based on studies comparing  
651 data and MC predictions in well known control samples (CS). A CS is designed to provide a  
652 reliable measurement with minimal influence from other dependent and independent factors.

653 An example of a well established CS is a collection of single, isolated cosmic ray (muon) tracks  
654 to measure the energy loss in a detector. In general, a CS may have different properties than  
655 the analysis sample like event topology. In particular the cosmic ray CS cannot account for  
656 efficiency effects of other tracks present. Therefore a model extrapolation is needed to map  
657 the CS to the analysis sample. The model used in psyche/BANFF is that the efficiency of  
658 the data and MC is the same in both analysis sample and CS

$$\epsilon_{\text{Data}}(x) = \left( \frac{\epsilon_{\text{Data}}(x)}{\epsilon_{\text{MC}}(x)} \right)_{\text{CS}} \epsilon_{\text{MC}}(x)$$

659 where  $\epsilon_{\text{MC}} / \epsilon_{\text{Data}}$  denotes the mean efficiency of the MC/data as a function of some observable  
660  $x$ . We need to update this model to account for statistical uncertainties in the CS. The

661 updated model, with  $x$  dependence assumed, is now

$$\epsilon'_{\text{Data}} = \left( \frac{\epsilon_{\text{Data}} + \delta_{\text{Data}} \cdot \sigma_{\epsilon_{\text{Data}}}}{\epsilon_{\text{MC}} + \delta_{\text{MC}} \cdot \sigma_{\epsilon_{\text{MC}}}} \right)_{\text{CS}} \epsilon_{\text{MC}}$$

662 where  $\sigma_{\epsilon_{\text{MC}/\text{Data}}}$  is the standard deviation of the efficiency of the MC/Data and  $\delta_{\text{MC}/\text{Data}}$  is  
663 a random, normally distributed number  $\mathcal{N}(\mu = 0, \sigma^2 = 1)$ .

$$w_{\text{eff}} = \frac{\epsilon'_{\text{Data}}}{\epsilon_{\text{MC}}}$$
$$w_{\text{ineff}} = \frac{1 - \epsilon'_{\text{Data}}}{1 - \epsilon_{\text{MC}}}$$

664 **5.1.2 Observable Variation Systematics**

$$x' = x_{\text{Nom}} + \Delta x + \delta_{\sigma} \cdot \sigma_{\Delta x}$$

665 **5.1.3 Normalization Systematics**

$$w = w_0 (1 + \delta \cdot \sigma_w)$$

Systematic effect	Treatment
TPC cluster eff.	efficiency
TPC tracking eff.	efficiency
TPC charge misassignment	efficiency
TPC particle ID	observable variation
TPC momentum resol.	observable variation
TPC momemtum scale	observable variation
B field distortion	observable variation
FGD “hybrid” tracking eff.	efficiency
Michel election eff.	efficiency
FGD particle ID	observable variation
FGD mass	normalization
Pion secondary interactions	efficiency
Proton secondary interactions	efficiency
TPC-FGD track matching eff.	efficiency
FGD OOFV	efficiency
FGD TOF resol.	observable variation
FGD sand muon eff.	efficiency
FGD event pile up	normalization
PØD energy loss scale	observable variation
PØD energy loss resol.	observable variation
PØD OOFV	efficiency
PØD track veto	efficiency

Table 5.1: [2]

666 **6 Fitter Validation**

667 Fitter validation

668 **7 PØD-Only Fitter Results**

669 Fitter results

670

## 8 FGD-POD Comparisons

671

## 9 Discussion

672

Discussion

673

## References

- 674 [1] K. Abe et al. The T2K Experiment. *Nucl. Instrum. Meth.*, A659:106–135, 2011. 25
- 675 [2] K. Abe and Others. Measurements of neutrino oscillation in appearance and disappearance channels by the t2k experiment with  $6.6 \times 10^{20}$  protons on target. *Phys. Rev. D*,  
676 91:072010, Apr 2015. 9, 119
- 677
- 678 [3] S. Baker and R. D. Cousins. Clarification of the use of Chi-Square and Likelihood  
679 Functions in Fits to Histograms. *Nucl. Instrum. Meth.*, A221:437–442, 1983. 16
- 680 [4] S. Bienstock et al. Assessing the effect of cross-section model uncertainties on the T2K  
681 oscillation analyses with simulated data studies using the BANFF, MaCh3, P-Theta  
682 and VALOR frameworks, May 2018. T2K-TN-331 v5. 14
- 683 [5] S. Bienstock and Others. Constraining the Flux and Cross Section Models with Data  
684 from the ND280 Detector using FGD1 and FGD2 for the 2017 Joint Oscillation Analysis,  
685 August 2017. T2K-TN-324 v3. 14, 21
- 686 [6] S. Bolognesi and Others. Niwg model and uncertainties for 2017 oscillation analysis,  
687 April 2017. T2K-TN-315 v5. 21
- 688 [7] T. Campbell. Measurement of the  $\nu_\mu$  cc-0 $\pi$  double differential cross section on water in  
689 the pød, February 2018. T2K-TN-328. 24
- 690 [8] T. Campbell and Others. Analysis of  $\nu_\mu$  charged current inclusive events in the pød in  
691 runs 1+2+3+4, Mar 2014. T2K-TN-80 v4. 24, 26, 27
- 692 [9] R. Das and Others. Measurement of induced charged current cross section on water  
693 using the pød and tpc, November 2014. T2K-TN-100. 24

- 694 [10] K. Gilje. Geometry and mass of the  $\pi^0$  detector in the nd280 basket, Apr 2012. T2K-  
695 TN-73 v3.1. 27
- 696 [11] M. Hartz and Others. Constraining the flux and cross section models with data from  
697 the nd280 detector for the 2014/15 oscillation analysis, May 2015. T2K-TN-220 v4. 14,  
698 16
- 699 [12] M. Hartz and Others. Constraining the Flux and Cross Section Models with Data from  
700 the ND280 Detector using FGD1 and FGD2 for the 2016 Joint Oscillation Analysis,  
701 June 2016. T2K-TN-230 v3. 14
- 702 [13] A. Hillairet and Others. Nd280 reconstruction, Nov 2011. T2K-TN-72 v1. 27
- 703 [14] T. Koga. Comparison between banff post fit results and on-axis detectors, 2017. 10
- 704 [15] K. Mahn and Others. Implementation of new cross section parameters for the 2017  
705 oscillation analysis, 2017. T2K-TN-307. 21
- 706 [16] G. Wikström and A. Finch. Global kalman vertexing in nd280, Feb 2018. T2K-TN-46  
707 v3. 26
- 708 [17] T. Yuan and Others. Double differential measurement of the flux averaged  $\nu_\mu$  cc0pi  
709 cross section on water, Aug 2016. T2K-TN-258 v4.6.1. 24, 26

710 **Nomenclature**

- 711 BANFF The **beam and near detector task force** is the group responsible for providing near  
712 detector constraints on cross section and flux model parameters.
- 713 CC- $0\pi$  A **charged current zero pion** selection is an exclusive selection that selects neutrino  
714 interaction topologies only one MIP-like particle.
- 715 CC-Inclusive A **charged current event** selection that selects all neutrino interaction topolo-  
716 gies with an outgoing charged lepton.
- 717 FD The **far detector** refers to the particle detector in a long baseline neutrino oscilla-  
718 tion experiment that is located far away from the neutrino production source where  
719 oscillated neutrinos are observed.
- 720 FGD A **fine grain detector** is a detector made of closely spaced, small scintillating bars  
721 designed to provide precise resolution of charged particle tracks
- 722 FHC The **forward horn current** beam configuration that focuses positively charged particles  
723 into the particle decay pipe. This configuration produces a very pure  $\nu_\mu$  neutrino beam
- 724 HMNT The **highest momentum negatively-charged track** in the bunch
- 725 HMPT The **highest momentum positively-charged track** in the bunch
- 726 MIP A **minimum ionizing particle**
- 727 ND280 The **Near Detector** of T2K which is **280** meters away from the neutrino source.
- 728 ND The **near detector** refers to the particle detector in a long baseline neutrino oscillation  
729 experiment that is located close to the neutrino production source before neutrino  
730 oscillations occur.

<sup>731</sup> CECal The **Central ECal** detector which is a part of the PØD inside ND280

<sup>732</sup> PØD The  $\pi^0$  detector (**pi-Ø detector**)

<sup>733</sup> PØDule A collection of two active scintillator bar layers inside the PØD

<sup>734</sup> RHC The **reverse horn current** beam configuration that focuses negatively charged particles  
<sup>735</sup> into the particle decay pipe. This configuration produces a  $\bar{\nu}_\mu$  enriched neutrino beam  
<sup>736</sup> with a significant  $\nu_\mu$  contribution.

<sup>737</sup> FV The **fiducial volume** of a detector is the region where the detector response is well  
<sup>738</sup> understood

<sup>739</sup> TPC A **time projection chamber** is a device that detects and tracks charged particles with  
<sup>740</sup> the application of strong electric fields

<sup>741</sup> Tracker The region of ND280 consisting of two FGDs and TPCs

<sup>742</sup> Global The **Global reconstruction module** responsible for making joined tracks between the  
<sup>743</sup> subdetectors inside ND280

<sup>744</sup> USECal The **Upstream ECal** which is a part of the PØD inside ND280